Researching the impact of wind patterns in urban areas for bladeless wind turbine implementation.

By

Faro, Abdulfatai Ayodeji

In collaboration with

O-Innovations

Thesis for the Degree of Master of Science by Research

14/12/2023

Supervisors: Dr. David Cheneler
Dr. Marianna Cavada

This project was supported by the Centre for Global Eco-Innovation and is part financed by the European Regional Development Fund.

Declaration

The author declares that this thesis has not been previously submitted for the award of a higher degree to this or any University and that the contents, except where otherwise stated, are the author's work.

Abstract

The aim of this research is to understand the urban wind flows for the implementation of bladeless wind turbines named O-wind turbine by carrying out research from existing sources, which will allow conclusions to be drawn on how buildings can manipulate the flows. The novelty introduced by the present research is the development of a methodology, focusing on creating a guide on where and how to look for ideal locations for implementing the O-Wind turbine to harness these unique winds and generate clean electricity in dense urban environments. The Installation of wind turbines to all possible extents has contributed to meet the ever-increasing energy demand. Technologically Developed areas have a high potential for wind energy, including the rooftop of high-rise buildings, railway tracks, the region between or around multi-storeyed buildings, and city roads. Harnessing wind energy from these areas is quite challenging since it has a dramatic nature being chaotic and turbulent on urban surfaces. An O-Wind turbine is a new form of blade-less wind turbine that can harness winds from any direction.

The method used was a systematic approach consisting of the following studied site, field measurement, wind data analysis, wind direction study, and computational fluid dynamics which comprises turbulence modelling, boundary conditions, and sensitivity studies. This study developed computational fluid dynamics (CFD)-based evaluation procedures to determine potential implementation sites of wind turbines and obtain estimates of wind velocity and wind power by taking into consideration the details of the local urban topography and boundary conditions of the objective buildings.

Parameters such as the wind velocity, direction as well and turbulence intensity, are compared with field measurements via anemometers and analytical methods at different floors of our building of interest to validate the computational model as well as attain a better understanding of the interaction of the wind with buildings in complex terrain. The grid-independent study, analytical method (accuracy), sensitivity study, and best urban settings that favour the use of this turbine using CFD for wind turbines on the studied site are different from those suggested in the literature and their deficiency in providing optimum mounting sites in micro-environments. Moreover, an improved roof design with a rounded shape is proposed for the enhancement of wind power density with relatively lower turbulence intensity.

Acknowledgment

I would like to thank Almighty Allah, the most beneficent, the most merciful for making this a success.

I would like to thank my supervisors, Dr. David Cheneler and Dr. Marianna Cavada for their highly supportive roles. They ensured and guided me adequately for the success of this research.

I would like to give special thanks to the O-Innovation team; Nicolas Orellana and Dominic Chippendale for collaborating with the Centre for Global Eco-Innovation (CGE) to provide funding for the research and also providing necessary support when requested.

I would also like to appreciate the awesome support I received from the CGE team; From Andy to Janine to Rachel and the whole administrative staff member. They gave me all the necessary support to settle quickly as an international student. The best way to get through graduate school is to embrace your goofy side and have fun with your work. And if you start feeling stressed, take a day off to relax; CGE provided an atmosphere for relaxation and it's quite amazing.

Finally, I would like to thank my parents, my siblings, and my Lovely wife, Olaitan for their care and support throughout this programme.

Contents

List of Figures

List of Tables

Nomenclature

U_i	Velocity component in the i direction	$[ms^{-1}]$
U_j	Velocity component in the j direction	$[ms^{-1}]$
ρ	Density	$[kgm^{-3}]$
P	Pressure	$[Nm^{-2}]$
μ	Laminar viscosity	$[Nm^{-2}]$
μ_i	Turbulent viscosity	$[Nm^{-2}]$
ρg_i	Gravitational force	[N]
K	Turbulent kinetic energy	$[Jkg^{-1}]$
ε	Turbulent dissipation rate	$[m^2/s^3]$
t	Eddy viscosity	$[Pa.s]$
S_{ij}	Average strain rate tensor	$[s^{-1}]$
$C_{1\varepsilon}$	Constant	[-]
k	Von Karma constant	[-]
U^*	Friction velocity	$[ms^{-1}]$
z	Height which the velocity is calculated	[m]
z_0	Aerodynamic roughness length	[-]
V	Instantaneous velocity	$[ms^{-1}]$
I	Turbulence intensity	[-]
P_A	Wind Power	$[W]$
ω	Specific turbulent dissipation rate	$[1/s]$

Acronyms

CFD	Computational Fluid Dynamic
WEB	Wind Energy for the Built Environment
UWECS	Urban Wind Energy Conversion Systems

BUWTs	Building Mounted/Integrated Wind Turbines
WINEUR	Wind energy integration in the urban environment
VIV	vortex-induced vibration
LIDAR	Light direction and ranging
3D	three-dimensional
CEDA	Centre for Environmental Data Analysis
N	North
NE	Northeast
E	East
SE	Southeast
S	South
SW	Southwest
W	West
NW	Northwest
WNW	West-northwest
NNW	North-northwest
NNE	North-northeast
ENE	East-northeast
ESE	East-southeast
SSE	South-southeast

Chapter 1 Introduction

Energy is an inseparable part of our life. Energy is necessary for the daily needs of our society, we can imagine how difficult our lives without mobile phones, computers, microwaves, and other electric devices. The adverse impacts of fossil and nuclear fuel-based power generation have increasingly made the world more enthusiastic about renewable power generation(Park and Kim, 2019). According to the International Energy Agency, by 2040, there will be an increase of 69% in electric power compared with 2016 (Burton *et al.*, 2011). Renewables play such a big role in society today. There are several reasons renewable energy is essential: a cleaner environment from carbon emission, good health, abundant energy, and cheaper to run. One of the main reasons why the forecast energy growth is so high is the ever-increasing number of inhabitants in urban areas. At the same time, population growth in cities will cause increased energy demand for heating and cooling (Venditti, 2022). For this reason, paying attention to clean and environmentally friendly resources such as renewable energy is very necessary. Renewable energy sources are generally intermittent in nature and location-specific. They are those natural sources that replenish themselves over a short period. Since they are location-specific, power generated from such sources is highly dependent on environmental conditions. Due to such environmental constraints, renewable energy sources can only provide energy with interruption, unlike fossil fuels. However, more work such as the improvement of existing sources of renewable energy sources to harvest maximum energy has been done in harnessing renewable energy, especially wind.

There is a need for special attention to be paid to wind power because wind technology prices are very reasonable compared to other sources of energy, at the same time electric power made in wind turbines is becoming cheaper and more competitive with electricity produced by using other resources. The global weighted-average cost of electricity of new onshore wind farms in 2019 was USD 0.053/kWh with country/region values of between USD 0.051 and USD 0.099/kWh depending on the region. Costs of the most competitive projects are now as low as USD 0.030/kWh, without financial support (IRENE, 2022). The average electricity price for 1 kWh produced by a wind turbine in some European nations such as Lithuania in 2016 was 0.075 euro/kWh; produced by the solar panel - 0.142 Euro/kWh. At the same time, the average electricity price for 1 kWh in the market in 2015 was 0.042 euro/kWh. One of the attractive things about installing a renewable energy source is the chance it gives you to sell your excess electricity to the power companies and make a decent return on investment. The Feed Tariff for wind turbines varies according to the size of the array and how much power it produces. A 1.5 kW turbine would attract a Feed Tariff of 8.53 pence per kWh whilst one that produced over 50kW but less than 100kW would earn you 8.53 pence per kWh and for 100kW to 1.5MW 5.46p and for over 1.5MW its only 0.86p (Hub, 2022). (Haas, 2019) reported the European Wind Energy Association has taken a target to generate 320 GW of wind power by the year 2030 and initiated renewable-friendly policies across its member states to accelerate the installation of renewable power plants. In addition to that, some countries such as UK, Germany, Canada, and the U.S.A have added wind energy as additional options to diversify their energy source, which could enhance the safety of their energy supply.

The global trend of increasing urbanisation and industrialization in recent times has resulted in a corresponding rise in energy demand. It is anticipated that a greater number of people, particularly in

developing nations, will relocate to cities over the course of the next few decades, which has raised the demand for more economical, environmentally friendly, safe, and secure energy sources to meet the needs of the expanding population (Bahaj, Myers and James, 2007). According to reports from recent years (Saidur *et al.*, 2011), cities use about 75% of the power that is produced. In order to lower the transmission infrastructure and the generation load, municipal power generation may be crucial. It might help lessen transmission losses as a result of consumers being closer together. The demand for energy worldwide is estimated to increase by about 30% by 2040 compared to 2010, it is predicted that more challenges such as increased environmental problems, depletion of fossil fuels and unstable oil prices will intensify. These factors make it imperative that energy-saving techniques and alternative energy sources be included in urban design and development. Given its affordability, safety, cleanness, and long-term availability, wind energy has been widely predicted to rank among the greatest alternative energy sources required for metropolitan environments in recent years(Al-Mulali *et al.*, 2013).

Wind energy has a lot of potential in urban areas in the capacity of shapes (gabled, pyramidal, barrel vaulted), configuration (Urban Canyon, staggered Urban Canyon), and height and size (Campus, Business district, and Residential)(see Figure 6-7) It was shown that urban obstacles like high buildings could increase wind speed and also could help to increase the performance of small-scale wind turbines (Razak et al., 2013). However, at the same time, those obstacles increase turbulence intensity. Wind energy is one of the best choices for trying to reduce dependence on fossil fuels. Due to the drawbacks, they have been alternatives addressed so far such as vortex-induced vibration (VIV) -based piezoelectric energy harvesters. The kinetic energy of this harvester stems from wind-induced vibrations of a circular cylinder mounted on an orthogonal bibeam system, rather than a traditional single beam (Shi *et al.*, 2021), and vortex wind generation showed distinct outcomes (Ren *et al.*, 2021), insect-inspired kites; This research used the concept of nature to establish durability and load-bearing are difficult to be combined in engineering systems. Hence, in majority of man-made structures, the two characteristics are typically mutually exclusive. Nature, however, has provided us with design strategies, through which many biological systems have overcome this conflict. Insect wings represent a striking example of such a combination (Khaheshi *et al.*, 2021), various subsystems for drag power kites (Bauer. F et al., 2019), power kites with inflatable wings (Rushdi et al., 2020), analysis of LIDAR (light direction and ranging) and mesoscale models (Sommerfeld *et al.*, 2019), filtration method of analysing tethered kite wings (Schmidt *et al.*, 2020). However, some limitations have been observed from an environmental perspective in the current alternatives. Furthermore, many reviews have been done on the impacts of wind turbines in recent times. Some of them are regarding the health hazards that the wind turbines employees might be exposed to (Karanikas *et al.*, 2021), the impact of wind turbines on airport facilities , effects of wind turbines on wildlife (Schöll and Nopp-Mayr, 2021) and impacts on surface temperatures of downwind locations (Moravec. D et al., 2018). Whereas, reviews like (M.S. Nazir, A.J. Mahdi, M. Bilal, H.M. Sohail, N. Ali, 2019), focused on a very narrow geographical region. To maximize the usage of wind energy potential more, wind speed parameter measurements should be taken; and more attention should be paid to wind turbine implementations in urban areas.

O-Wind is the first truly omni-directional wind turbine, designed by O-Innovations; based in Lancaster and the O-Wind turbine (O-Innovation, 2022) is a new form of blade-less turbine that can harness winds from any direction including vertical winds. This new unique design can be applied in urban areas where buildings create complex and powerful wind patterns, channelling winds through effects such as the Downdraft, Updraft, and Venturi effects. O-Wind's ability to harness chaotic winds i.e., the

dynamic behaviour of short-term wind speed time series found in urban areas, coupled with its being a blade-less turbine making it quieter and safer than existing bladed technology, provides significant implementation opportunities in urban areas. For those living in dense urban areas, it is difficult to find the required space to install other renewable options such as solar panels, it is also difficult to find areas where these technologies will receive access to enough sunlight to be efficient due to narrow and compact streets.

It is the influence buildings have on urban wind flow that creates a real opportunity for an omni-directional wind turbine such as O-Wind, that is capable of harnessing both vertical and horizontal winds simultaneously. This research will attempt to explain these complex wind patterns in more detail and highlight how the unique design of O-Wind is ideal for harnessing this turbulent, yet powerful resource. By having a blade-less turbine that can harness chaotic winds and that is also safe and quiet, O-Wind can become the renewable energy option for individuals living in apartments; the same way solar panels have become the renewable option for those living in the countryside and suburbs. O-Wind's ability to be installed on apartment balconies and building facades open up a brand new and significant innovation, allowing those living and working in the areas of highest energy consumption to become one of its greatest renewable energy generators.

1.1 Aim and Objectives

This discussion here emphasizes the critical importance of developing accurate models that can be used to quickly estimate wind resources and are easily accessible to potential O-Wind turbine implementation.

As a result, the fundamental objective of this research is to establish the impact of wind patterns in urban areas using Computational Fluid Dynamics (CFD) and to utilize the results to investigate the extent of untapped wind energy potential in UK cities, which reduces the necessity for onsite meteorological measurements. Using unique modelling tools, this methodology will address some of the most significant challenges that arise when projecting urban wind resources. For the best result, the study focused on the following five directions:

1. Critical analysis (literature review) of the impact of wind patterns in urban areas for bladeless wind turbine implementation.
2. Development of novel analytical and computational models of wind interaction with urban structures.
3. Collection of data from field measurement for comparison study with the numerical modelling.
4. Creation of new holistic models of wind-structure interactions, where the structural component is embedded.
5. Wind loads and Turbulence predictions modelling using Computational Fluid Dynamics (CFD).

1.2 Structure of the Thesis

The thesis is structured as described in the following outline.

Chapter 2 – Literature Review. Introduces existing knowledge on the topic of study that was gathered through comprehensive research in the public domain during this study. The work of a number of researchers is presented in the areas of wind energy, urban and regional planning, wind turbine designs, CFD and turbulence modelling which guided me to the study gaps.

Chapter 3 – Methodology. The established methodology explained in detail the capturing of the wind data, wind data analysis, and also the CFD and its properties to systematically address the objectives of the research.

Chapter 4 – Numerical Modelling/CFD. The developed numerical model is described in detail with the mathematical background and the steps of the algorithm. A few computational issues are discussed like the effect of the meshing in computational time and accuracy of the main variables.

Chapter 5 – Analytical method of Atmospheric Boundary Layer, Turbulent Intensity, Turbulent Kinetic Energy, Turbulence Dissipation, Specific Turbulent Dissipation Rate, and Wind Power Distributions were carried out and the results are presented.

Chapter 6 – Results. The results of the simulations were comprehensively reported and analysed.

Chapter 7 – Validation and Verification of Results. Lancaster's data from the building of interest which was used as a case study was adopted for the analytical analysis and is compared with the results of the simulation using the developed model under the same circumstances and the results are presented and discussed.

Chapter 8 – Conclusion and Recommendation.

Chapter 2 Literature Review

The aim of this chapter is to review the literature pertaining to renewable energy sources, wind energy specifically and its patterns in urban areas. This review considers the case for wind turbine capabilities in urban areas and their potential vis-à-vis national and international energy policies. This consideration, therefore, is regarding the international uptake of renewable energy and more specifically, small wind energy, the drivers towards increasing the impact of such renewable energy, and the impact of the wind flows pattern around buildings.

2.1 Renewable Energy: An International Perspective

The Renewables 2022: Global Status Report (Programme, 2022), presented a very positive picture of 'sustainable' renewable energy development across the world. This report highlighted a number of key statistics, which are summarised below:

- As in previous years, the greatest success for renewables was in the power sector. After largely withstanding the impacts of the COVID-19 pandemic, growth in global renewable power capacity accelerated in 2021, adding more than 314 gigawatts (GW), with wind contributing 30%)

- The market also diversified geographically, with the top five countries accounting for 71% of all capacity added (down from 75% in 2020, but still less diverse than in 2019 and 2018). Overall, the renewable power capacity additions reflected market growth of 11%; however, they still represented only a third of the additions needed annually to achieve the world's major goals for net zero carbon emissions.

- Renewable energy comprised 28.3% of the global electricity mix in 2021, roughly on par with 2020 levels. The growth in renewable energy penetration was mitigated by the overall rise in electricity demand and by drought conditions that greatly reduced global hydropower generation

- In the EU, renewables account for 71% of total electric capacity additions, which brings the renewable share of total electricity capacity to 31.1% (contributing 19.8% toward total electricity consumption)

- For the first time in the history of UN climate agreements, the Glasgow climate pact explicitly acknowledges the need to reduce the use of fossil fuels. During the meetings, 140 countries agreed to "phase down" unabated coal power, while numerous businesses, nations, and public financial institutions committed to ending public support and funding for unabated fossil fuels.

From a European perspective, as a result of the Kyoto Protocol, which established legally binding targets for each signatory nation to limit its emissions of greenhouse gases to 8% above the baseline level in 1990, there are a number of important obligations for European legislation. The European Commission raised its 2030 target for renewables in total final energy consumption (TFEC) first to 40% in 2021, then to 45% in early 2022. Also in the lead-up to COP26, 151 countries submitted new or updated Nationally Determined Contributions (NDCs) towards reducing their greenhouse gas emissions under the Paris Agreement Under guidelines agreed at the conference, richer nations could

be financially responsible to other nations for their failure to reduce carbon emissions (UN Climate Change, 2022).

The European Environment Agency's Greenhouse gas emission trends and projections in its most recent report suggest that almost all European countries are on track toward their Kyoto targets. As of 28 October 2020, 147 Parties deposited their instrument of acceptance, therefore the threshold of 144 instruments of acceptance for entry into force of the Doha Amendment was achieved. The amendment entered into force on 31 December 2020. Between 2020 and 2021, renewable energy-generated electricity decreased by 9.3% to 122.2 TWh, but it remains the second-highest annual figure ever recorded. Renewable energy generation set a new record in 2020. The majority of the decrease can be attributed to less favourable weather. Limit developed by 3.7%, a higher development rate than in 2020 (where the new limit was hampered by the Coronavirus pandemic) however more slowly than in earlier years. Due to exceptionally strong wind speeds in 2020, total wind generation decreased by nearly 15% to 64.7 TWh.

In 2020, hydro generation decreased by nearly 20%, largely as a result of lower average rainfall. A small increase in capacity was offset by a decrease in the average number of hours of sunlight, resulting in a 5.9% decrease in solar PV generation. The amount of bioenergy produced rose by 1.3%. Within this, generation from anaerobic digestion increased significantly, but in 2020, outages reduced it. In 2021, renewable electricity accounted for a record 39.7% of the UK's electricity production—3.5 percentage points less than in 2020 but higher than in any year before that.

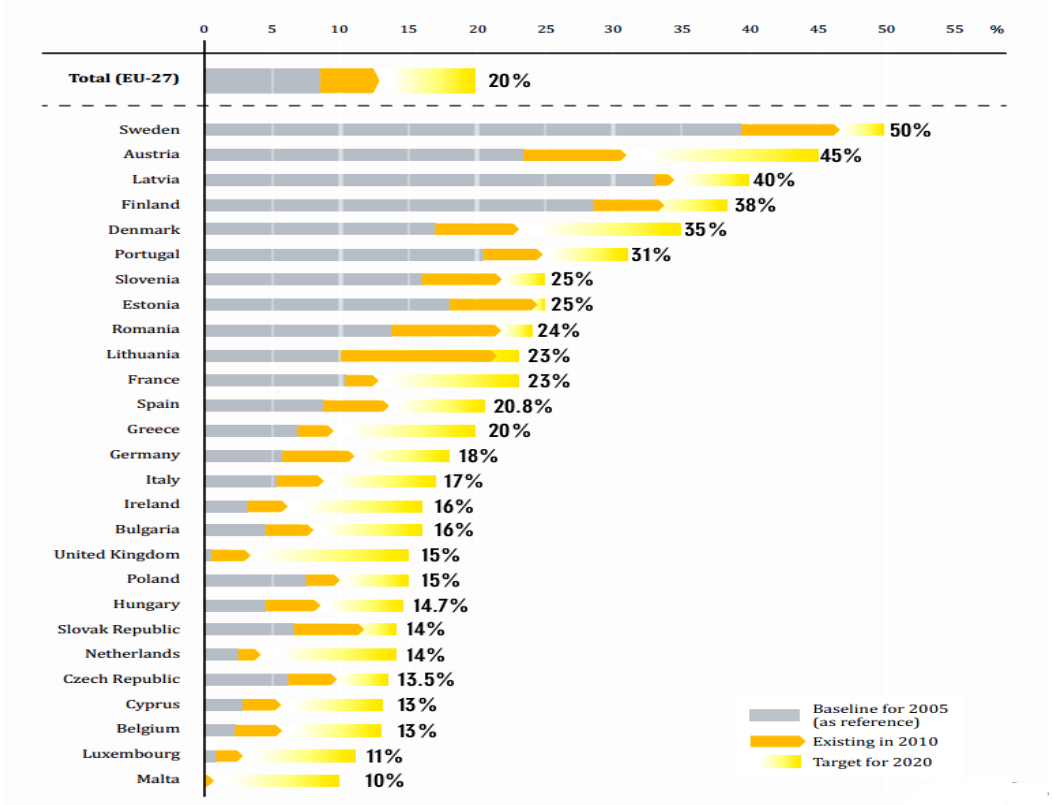

Figure 2-1 EU Renewable Shares of Final Energy, 2005 and 2010, with Targets for 2020 (Extracted from European European Renewable Energy Council, 2011)

2.2 Global Wind Energy

The Global Wind Report 2022, shows the trend of the wind industry in 2021. Several points have been emphasized: The wind industry had its second-best year ever, with 2021 growth only 1.8% behind 2020's record. Global cumulative wind power capacity increased by 12% year-over-year (YoY) by nearly 94 GW, bringing it to 837 GW. Europe has contributed significantly to this expansion, with a 19% increase in new onshore installations. In 1998, a European Commission project named WEB (Wind Energy for the Built Environment) was launched and a new architectural and aerodynamic model was invented as the prototype of UWECS (Urban Wind Energy Conversion Systems)(Stankovic, 2001). Later, the UK looked into the feasibility of the BUWTs (Building Mounted/Integrated Wind Turbines) project in 2003–2004 (Dutton, A. G., Bonnet, P. A., Hogg, P., & Lleong, 2005). BUWTs and another European Commission project named WINEUR (Wind energy integration in the urban environment, from 2005 to 2007) were elected for more detailed investigation of wind energy development in an urban environment: suggestions for turbine installation, economic analysis and detection of potential social problems associated with the implementation of small wind generators in urban areas (WINEUR, 2005).

The wind industry (Department of business, 2022) has demonstrated that it is the best technology that can guarantee the respect of international climate targets and, more than ever, the reduction of dependence on fossil fuels like gas and oil, confirming its central role as a custodian of the energy transition. The issue of energy security has made it even more important to boost new wind power installations all over the world, particularly in Europe, where the report emphasizes the difficulties in permitting and regulation-related areas, a real obstacle to wind growth, and the urgent need to invest in electricity networks and grid connections. As a result, wind power has the potential to significantly accelerate the global energy transition, ERG reportedly intends to maintain the expansion of its renewable portfolio from 2022 to 2026 by increasing the installed capacity to 4.6 GW, 3.8 GW of which will come from wind assets, with a strong emphasis on innovation: In this regard, the group is carefully evaluating repowering projects that will enable us to rejuvenate our Assets by utilizing superior wind locations and cutting-edge technologies like energy storage, floating wind power, green hydrogen, and the circular economy—where it is also engaged in an ESG perspective—to seek novel opportunities for the large-scale recycling of blades from wind turbines that are no longer in use.

Country/Region	2021	New Capacity 2021	Growth Rates 2021	2020	2019	2018
China*	343'829	55'800	19.4%	288'029	236'029	209'529
United States***	134'846	12'518	10.2%	122'328	105'433	96'363
Germany	63'924	1'716	2.8%	62'208	61'357	59'313
India	40'100	1'475	3.8%	38'625	37'529	35'129
Spain	28'196	750	2.7%	27'446	25'808	23'494
United Kingdom	26'812	2'645	10.9%	24'167	23'515	20'743
Brazil**	21'365	3'355	18.6%	18'010	15'452	14'707
France	19'081	1'132	6.3%	17'949	16'646	15'313
Canada	14'304	677	5.0%	13'627	13'413	12'816
Sweden	12'097	2'175	21.9%	9'922	8'985	7'406
Rest of the World*	135'166	15'019	12.5%	120'147	105'618	94'719
Total*	**839'730**	**97'272**	**13.1%**	**742'458**	**649'785**	**589'547**

* Preliminary, ** By November 2021, ***excl. Puerto Rico

©WWEA.2022

Figure 2-2 International wind installed capacity (WWEA,2022)

Figure 2-2 further illustrates that as of 2021, Germany and Spain had by far the largest installed capacities in Europe with 63.9GW and 28.1GW capacities respectively. This is compared to the remaining leaders, the UK, Italy, France, Portugal, Sweden, and Denmark, which collectively had 39.8GW with capacities ranging from 4.2-8.5GW. That said, the significance that wind energy plays in the UK is quite evident in Figure 2.1, where it is seen to account for Wind power contributing 26.8% of the UK's total electricity generation. UK ranks 3rd in the EU15 in this regard (Department of business, 2022).

2.2.1 Wind Energy In the UK

The United Kingdom boasts the largest offshore wind capacity in the world, making it one of the world leaders in wind generation. The three largest offshore wind farms in the world at the moment are Hornsea One, walney extension, and London array. Regarding european examinations, in 2017, there were five nations detailing a higher portion of their power creation from wind, as displayed in Figure 2.3. In 2018, (Department for Energy Security and Net Zero, 2022) the UK was the second biggest generator of wind-fueled power in Europe (behind Germany) with the third biggest limit (with Germany also, Spain first and second separately). From 2010 to 2017, the United Kingdom's share of the OECD Europe's total wind generation, excluding 2016, was 13.3%. Wind technologies were responsible for one-tenth of all electricity produced in OECD Europe. The UK also benefits from favourable wind speeds; load factors for onshore and offshore were reported in 2018 for the United Kingdom. (Department for Business, 2022) commercial wind farms containing a progression of wind turbines at a solitary site were presented in the UK in 1991 with the kick-off of the delabole wind ranch. Ten 50-metre wind turbines with a combined capacity of 4 MW were located on the site. The growth of wind-powered electricity generation was sluggish throughout the 1990s, but momentum gradually increased. Rapid expansion was made possible by government subsidy programmes and technological advancements that began in the early 2000s. The appropriation plans were the Renewables Commitment (RO, 2002-2017), Feed in Duty plot (FIT, 2010-2019), and Agreements for Contrast (CFD, 2015-). In 2001, offshore wind development began.

In 2019, England produced 52% of the UK's total wind generation and was the four-country UK's largest generator of wind-powered electricity. Scotland, Ribs, and Northern Ireland gave 35, 8.0, and 5.0 percent separately. From 5.4 GW in 2010 to 24 GW in 2019, total wind generation capacity increased by 19 GW. This is because both onshore and offshore capacity have increased significantly, by 10 GW and 8.5 GW, respectively. Following the opening of Hornsea One, the Beatrice extension (partially operational in 2018), and East Anglia One (partially operational), the UK's offshore wind capacity increased by 1.6 GW in 2018. With a capacity of over 1.2 GW, Hornsea One is now the largest offshore wind farm in the world. With 64 TWh, wind generators took over as the second largest source of electricity in the UK in 2019; almost a fifth of the total generation in the UK. This was accomplished despite wind conditions that were suboptimal, with 2019 reporting the lowest average wind speeds since 2012 (Department of business, 2022). From 2010 to 2019, offshore generation outpaced onshore generation, but the gap narrowed each year. (Department for Business, 2022) With each providing 32 TWh of electricity and 9.9% of the UK's total generation in 2019, the disparity was minimal; because the wind speed and direction are more constant offshore, offshore sites typically have more capacity for a generation. The load factor, or proportion of maximum generation achieved, is used to measure this. From 2010 to 2019, offshore load factors averaged 38%, while onshore load factors averaged 26%. Onshore and offshore, UK wind farms achieved higher load factors in 2018 than the global average. From 2010 to 2017, the UK's share of total wind generation grew almost every year among OECD European nations with the third-largest capacity in 2018, the UK was the group's second-largest generator of wind-powered electricity, following Germany; Germany and Spain came out on top.

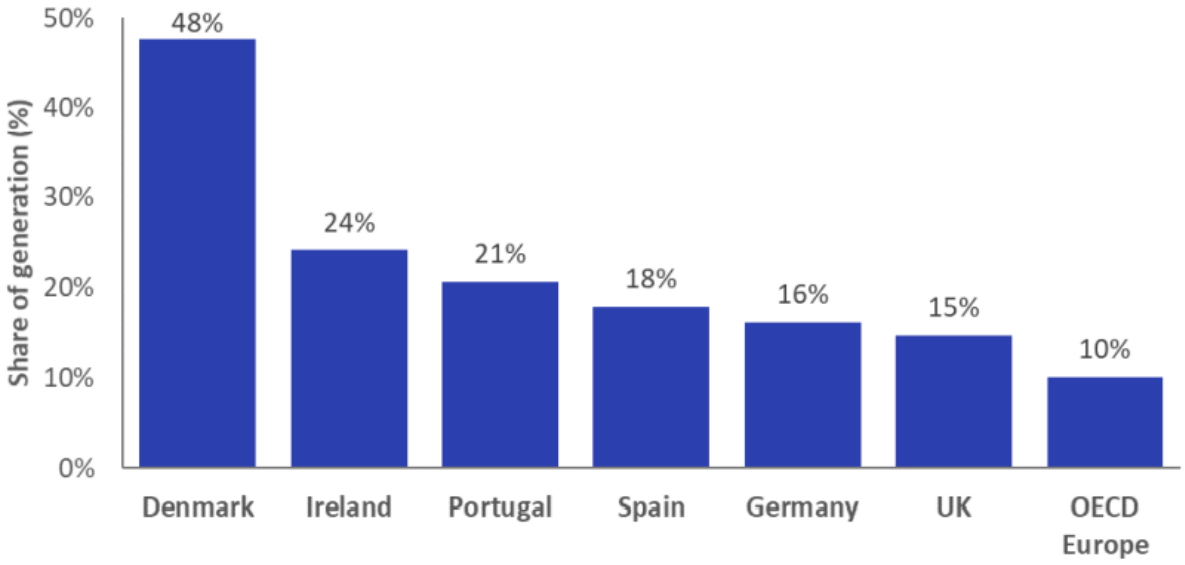

Figure 2-3 Wind share of total electricity generation - OECD Europe countries in 2017 (Alonso et al., 2017)

2.2.2 Onshore and offshore wind in the UK

Figures 2-4 and 2-5 describe the UK’s onshore and offshore wind capacity and generation in the period from 2010 to 2019.

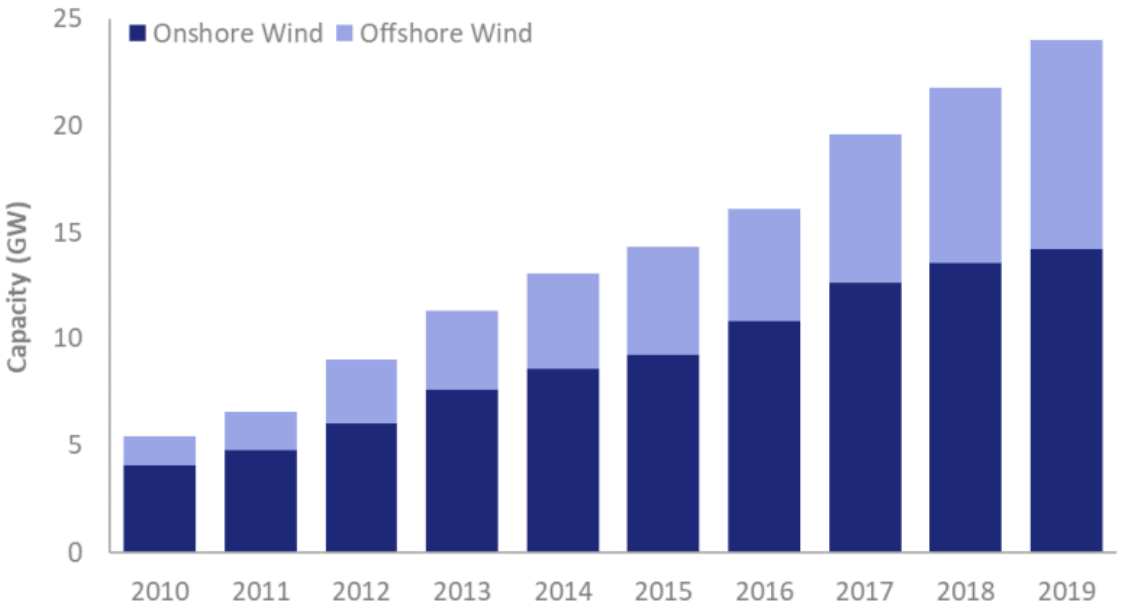

Figure 2-4 UK onshore/offshore wind capacity 2010 to 2019 (UK Energy brief 2021)

The UK had 5.4 GW of total wind capacity in 2010. This capacity has more than quadrupled in the past ten years, reaching 24 GW as a result of significant increases both onshore (from 4.1 GW to 14.2 GW) and offshore (from 1.3 GW to 9.8 GW). Onshore wind capacity increased more rapidly than offshore capacity between 2010 and 2017. However, as major offshore wind sites came online and the growth of onshore wind slowed, the trend reversed in 2018 and 2019. Throughout recent years, prominent openings seaward include Beatrice (0.6 GW), Walney expansion (0.7 GW), East Anglia One (0.2 GW of its 0.7GW limit is functional), and Hornsea One (1.2 GW). Hornsea One is currently the largest offshore wind farm in the world, with 1.2 GW of operational capacity. There are 174 190-metre-tall turbines on the 407-kilometre-square site, which is larger than the Isle of Wight. Over half of the UK's new renewable capacity in 2019 came from offshore wind (+1,6 GW), and onshore wind contributed 21% of the growth (+1,6 GW).

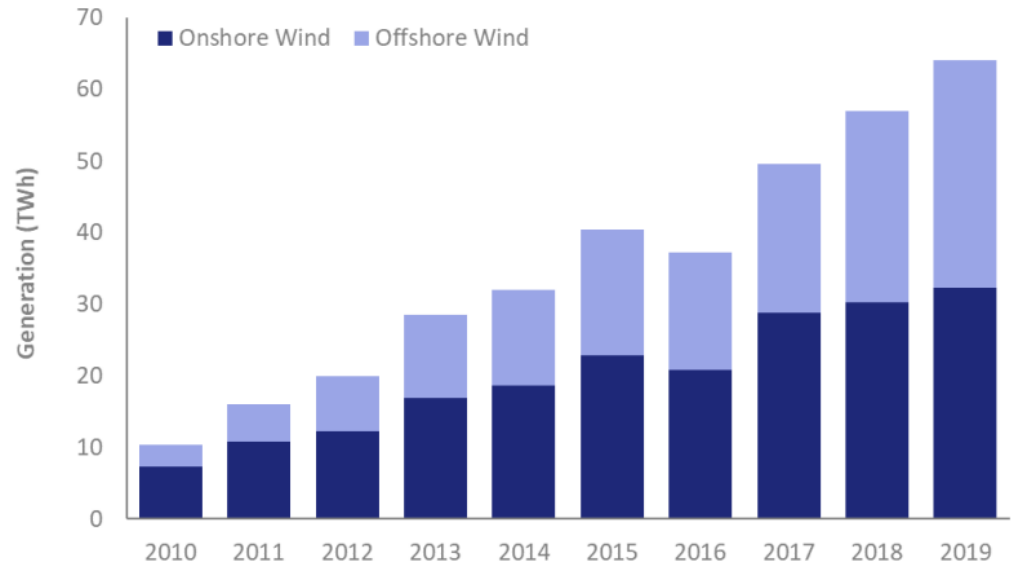

Figure 2-5 UK onshore/offshore wind generation 2010 to 2019 (UK Energy Brief 2022)

In 2010, wind (both coastal and seaward) created 10.3 TWh of power; 2.7% of the UK's total generation. In the context of wind, "coastal" refers to areas near or along the coast, usually within a certain distance from the shoreline. When discussing wind patterns, coastal areas often experience specific wind patterns influenced by their proximity to the sea or ocean. These areas might encounter winds influenced by the temperature gradients between the land and the water or by local geographic features. "Seaward," on the other hand, refers to the direction towards the sea or ocean. When wind is said to be blowing seaward, it means the wind is traveling from inland areas toward the sea or ocean. Wind directions are often described in terms of where they come from, such as an onshore wind blowing from the sea toward the land or an offshore wind blowing from the land toward the sea. Understanding these terms in the context of wind helps in describing wind patterns, especially in relation to coastal regions and their interactions with the nearby bodies of water. The increases in onshore and offshore wind capacity have correlated with generation records year over year, with the exception of 2016, when average wind speeds decreased by 11% from the previous year. Generation reached 64.1 TWh in 2019, more than six times the figure reported at the beginning of the decade (Department for Business, 2022).

For every year from 2010 to 2019, onshore generation has outperformed offshore, but in 2019, the gap between the two was only slight, with each producing 32 TWh of electricity and 9.9% of the UK's total generation. For the years 2010 to 2019, the percentages of annual electricity produced by onshore and offshore wind are shown in Table 1-1. Offshore generation surpassed onshore generation for the first time in 2019's third and fourth quarters. This was in spite of the coastal breeze's bigger limit (+4.4 GW) also, is on the grounds that seaward wind benefits from more reliable breeze rates and headings. As a result, offshore generators typically have the ability to generate more electricity by using more of their available capacity, resulting in higher load factors (the total electricity generated as a percentage of total potential generation for a given capacity). From 2010 to 2019, offshore generation had an average load factor of 38%, while onshore generation had an average load factor of 26%.

2.3 Wind Energy Fundamentals

One of the fastest growing sources of power generation in the world is wind energy and they have been public and political support for it such as wind is a renewable & clean source of energy, it requires low operating costs, efficient use of land space, wind energy is a job creator (Graham, 2009). Even while wind energy is still a more reliable and developed technology to offset a significant amount of power, more work needs to be done to fully realize its potential (Pasquay, 2004), especially in urban environments. Urban wind characteristics are currently the subject of many research, with many of them concentrating on the construction of mounted turbines. According to the World Wind Energy Report from 2011, improvements in wind turbine aerodynamics, structural dynamics, and micrometeorology have increased the turbines' ability to produce energy by 5% annually over the previous two to three decades. Over the past few years, the turbines' weights and noise levels have decreased by half in addition to their increased energy output. The construction of wind farms can also disrupt natural habitats of local species if not conducted in a sustainable manner. However, these problems can be solved to some extent with technological advancements and properly-siting wind farms (Devine-Wright, 2012), particularly, turbine-related impacts on homes located a short distance away (Hoen, 2006). If such discomfort is reportedly created by wind turbines, then the prices of the house closer to the turbine would be expected to decline (all things being equal). For acceptability and urban planning, the aforementioned pros and cons of the wind turbines' impact can be examined by investigating nearby house prices after the facility has been erected compared to their values before

the turbine was installed while taking into account the prices of houses farther away from that sold during the same period. The discussion here are around wind energy fundamentals.

The viability of wind resources and their utilisation techniques in the urban environment becomes a timely choice as wind energy resources, exploration, and utilisation in urban settings come under increased examination as part of renewable energy solutions (Grant, Johnstone and Kelly, 2008). A thorough analysis of the key developments, opportunities, and paths for future research and development in wind turbine technology was conducted by (Kaldellis and Zafirakis, 2011). They reviewed the most significant research projects connected to the development of wind energy and looked into the key technological advancements during the course of the industry's expansion.

2.3.1 Extracting energy from the wind

The fundamental idea behind the production of wind energy is to convert any kinetic energy that is present in the wind into energy that can be used. Calculating the total amount of available wind power passing through an area (A) that is perpendicular to the wind direction is simple using fundamental physical principles. According to (James and Earthscan, 2004), this can be expressed in terms of the air density (ρ) and the speed of the wind (U).

$$\text{Wind power} = \frac{1}{2}\rho A U^3 \qquad 1$$

Here, on a very basic level significant perception can be made: according to Equation 1, the wind's power is directly proportional to the wind speed's cube. This relationship emerges due to the way that the dynamic energy in a specific mass (m) of air is ½mU^2, while the mass of air going through a turbine's cleared region in one moment is ρAU. As a result, estimates of energy yields can be significantly miscalculated when estimating the wind resource at a potential turbine site due to even minor errors in wind speed predictions. In addition, it mandates that the site-specific wind speed distribution, as opposed to just the mean wind speed, must be known.

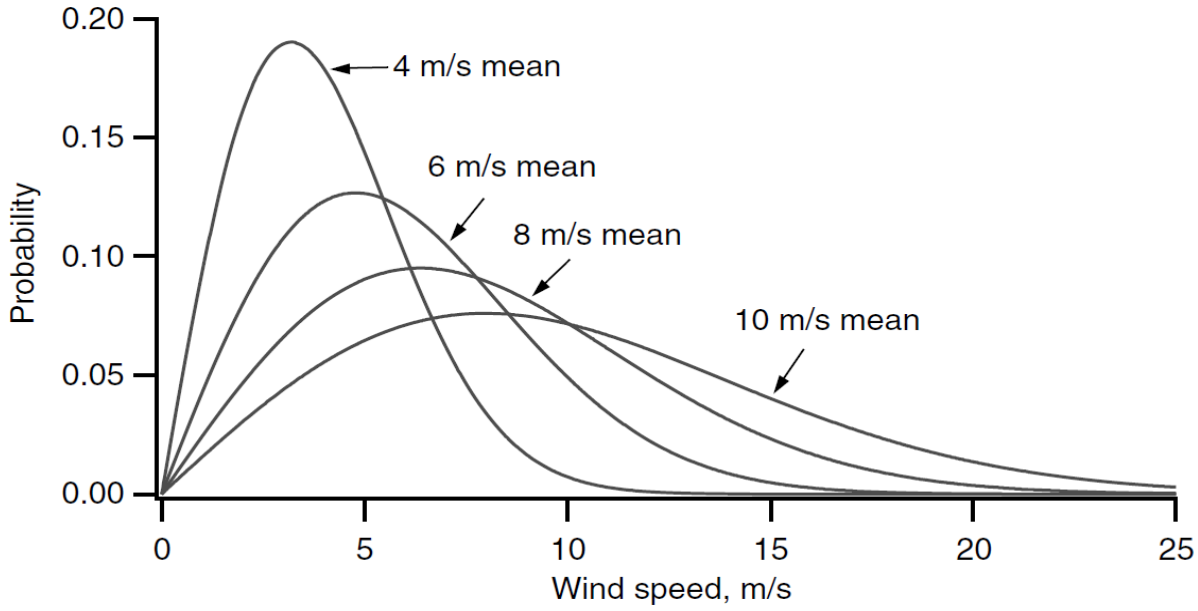

Figure 2-6 Examples of Weibull distribution typically used to represent wind speed distribution (Burton et al., 2011).

if it is to be estimated how much wind power is available. A weibull distribution, which is controlled by two parameters known as the 'shape' (β) and 'scale' (η) factors (Burton, 2001), is typically used to estimate this. The probability density function (PDF) of this distribution is given by:

$$\text{PDF} = \frac{\beta}{\cap}\left(\frac{V}{\cap}\right)^{\beta-1} e^{\left(\frac{V}{\cap}\right)^{\beta}} \qquad 2$$

As shown in Figure 2-6, specific values of these parameters can be chosen to best represent the available wind speed distribution at a specific location. In metropolitan regions, this cubic relationship of wind power with wind speed is especially critical, as winds speeds close to rooftop level where turbines are regularly sited are profoundly spatial factors due to the complex influence of building aerodynamics and the high roughness of urban surfaces, this variation occurs horizontally and vertically. This means that even a small increase in a turbine's mast height can have a significant impact on power output (James and Earthscan, 2004).

2.3.2 Environmental and financial viability

Urban planning encompasses the preparation of plans for and the regulation and management of towns, cities, and metropolitan regions (Millward-hopkins, 2013). It attempts to organize sociospatial relations across different scales of government and governance. Urban planning is concerned with the social, economic, and environmental consequences of delineating spatial boundaries and influencing spatial distributions of resources. Increasingly, debates about space, the social, the subject, and postcoloniality illuminate how present sociospatial configurations have come about, what might or might not need to change, and what planning might or might not contribute in any particular instance (Margo Huxley, 2020). Cities are made and grown by people; however, it is difficult to predict city living and city expansion that proves to be not harmful, but courteous to humans. Therefore, rapid urbanization and fast developing technology have created problems in the past. Even more nowadays, cities face problems such pollution, illness, crime and others that demand human response. Smart cities could be part of the response for the betterment of life in cities (Cavada, Hunt and Rogers, 2014). (Sims, Dent and Oskrochi, 2008; Hoen *et al.*, 2009, 2015; Lang, Opaluch and Sfinarolakis, 2014; Vyn and Mccullough, 2014). These peer-reviewed, published studies that used hedonic modelling have generally found non-significant post-construction effects or relatively small impacts, Five academic studies found similarly non-significant results, which implies that average impacts in their study areas were either relatively too small or sporadic near existing turbines. (Hoen *et al.*, 2009; Hinman, 2010; Carter, 2011; Schöll and Nopp-Mayr, 2021), while two found relatively small effects and one found a substantial effect (Stankovic, Campbell and Harries, 2015)

(Carter, 2011; Lang, Opaluch and Sfinarolakis, 2014; Vyn and Mccullough, 2014; Hoen *et al.*, 2015) gave an interesting insight into the geographic extent of the American studies; specifically, North America varied from a single county to eight (Hoen *et al.*, 2009) or nine states (Heintzelman and Tuttle, no date; Hinman, 2010; Hoen *et al.*, 2015) found evidence of pre-construction yet post-announcement impacts, showing that results have been robust to geographic scale and sample selection. (Hinman, 2010) gave the ''*anticipation effect*'' which correlates with surveys of residents living near wind turbine facilities finding that residents are more supportive of the facilities after they have been built than they were when the construction of that facility was announced (Wolsink, 2007). There is a constituency in the effect with analyses of home prices related to other disamenities (e.g., incinerators), which have also shown anticipation effects and post-construction rebounds in prices in

according to (Kiel, 1995; McKenna *et al.*, 2022). Wind turbines are typically limited to high-wind-resource areas but disamenities such as highways, overhead electricity transmission lines, power plants, and landfills are ubiquitous in urban and semi-rural areas and have been well studied.

This more established ‘‘disamenity literature’’ (e.g., (Jackson, 2001; Simons and Saginor, 2006) helps both to frame the expected level of impact around turbines and validate whether the coefficients for the amenities and disamenities included in our model are reasonable. For example, adverse home-price effects near electricity transmission lines, a largely visual disturbance, have ranged from 5% to 20%, fading quickly with distance and disappearing beyond 200 to 500 ft according to (Grant, Johnstone and Kelly, 2008). Landfills, which present smell and truck activity nuisances and potential health risks from groundwater contamination, have been found to decrease adjacent property values by 13.7% on average, decreasing by 5.9% for each mile home is further away for large volume operations. Lower-volume operations decreased adjacent property values by 2.7% on average, decreasing by 1.3% per mile (Ready, 2005). While thinking about the reasonability of a potential turbine establishment the essential contemplations are the natural and monetary restitution time frames. There are different elements affecting the length of these periods, for example, the specific turbine model, the monetary endowments that are accessible, and the carbon force of the power which is counterbalanced by that delivered by the turbine. The site's wind resource, on the other hand, may be the most significant determinant (Davidovic *et al.*, 2014)

An audit of the environmental impacts caused by a turbine's production, transportation, and upkeep (a life cycle analysis;) must first be carried out before the turbine's environmental viability can be determined. LCA). The emissions that could be avoided by producing renewable energy rather than importing electricity from the grid can then be compared. The on-site wind speed distribution and the power curve of the turbine can be used to estimate the amount of electricity produced (Rankine et al., Allen et al. 2006, 2008). However, the degree to which the onsite wind conditions are anticipated to change in the future determines how accurate this estimate is. Additionally, it is difficult to trace the "cradle to grave" effects of any complex goods during an LCA, so estimates of the turbine's environmental impacts are inherently uncertain (Allen et al., 2008).

By and large, in any case, concentrates on examining the feasibility of little wind turbines from a natural point of view has viewed compensation times as well inside the normal turbine lifetime, in any event, for destinations with moderately low mean breeze speeds. (Allen S.R, Hammond G.P, 2008), Allen and Hammond modelling studies have suggested that the installation of a turbine may be harmful to the environment at locations with low mean wind speeds and high levels of turbulence (5ms-1 and 50%, respectively). However, when more complex environmental impacts (such as heavy metal pollution and the production of chemicals related to smog, for example) are considered, the balance shifts back in favour of installation. Additionally, other authors have demonstrated that the use of recycled materials in turbine manufacturing can significantly shorten environmental payback times (Rankine et al., 2006). According to Allen et al., financial payback times typically last significantly longer than environmental payback times. Peacock et al., 2008, 2008), even though that the feed-in tariff subsidies available in the UK can significantly shorten financial payback times (Energy Savings Trust, 2006). This indicates that the most purchase turbines solely on the basis of financial considerations. According to Energy Saving Trust (2006), a site's estimated mean wind speed calculated using the Carbon Trust online wind estimator should be at least 5 ms-1 for it to be worthy of further investigation via onsite measurements. However, the fact that some turbine models are specifically designed to operate in lower, more turbulent winds (such as www.hi-vawt.com.tw) is not

taken into account by this proposed wind speed; consequently, these designs may be suitable for installation at locations with low mean wind speeds (less than 5 ms-1).

In a nutshell, previous research into the financial and environmental advantages of small-wind energy has demonstrated that the technology can be implemented in locations with sufficient wind resources. However, it is abundantly clear that the tools that are at this time available to estimate this resource are insufficient, particularly in urban areas. The lack of sufficiently accurate methods to estimate mean wind speeds at potential locations is a fundamental problem; these estimates serve as the foundation for any viability study. The absence of a reliable method for selecting the turbine model that is most suitable for a particular site, given the characteristics of the, is also significant, albeit to a lesser extent.

2.4 Wind characteristics

The weather, local landforms, the time of day, the season, the elevation above the earth's surface, and the geographical locations all influence wind variations. Understanding the characteristics of the wind will assist in the development of wind measuring methods, the selection of wind farm locations, and the optimization of the design of wind turbines.

2.4.1 Wind speed

One of the most important aspects of producing wind power is the speed of the wind. Wind speed fluctuates and is not entirely set in stone by many elements like geographic and atmospheric conditions. Measured wind speed data are typically processed using statistical techniques because the wind speed is a random parameter. Sinus waves are frequently used to describe the diurnal variations in average wind speeds. For instance, the wavy pattern can be seen in the diurnal variations of hourly wind speed values at Dhahran, Saudi Arabia, which are the average values derived from data collected between 1970 and 1984. The fact that the maximum wind speed occurs around 3 p.m. during the day indicates that the daytime wind speed is inversely proportional to the intensity of the sun. George and others (Csavina *et al.*, 2014) reported that the wind speed in Lubbock, Texas, is nearly constant at night and curvilinear during the day. George et al. have demonstrated that there is a pattern in the diurnal wind patterns at several locations across the Great Plains that is comparable to that found in.

(Sinden, 2007) came to the conclusion that the monthly average wind speed is inversely proportional to the monthly average temperature, i.e., it is higher in the winter and lower in the summer, based on data from up to 66 onshore locations across the UK from 1970 to 2003. The month of January sees the highest wind speed, while August sees the lowest. According to Hassanm and Hill, the wavy pattern was observed in the month-to-month variation of mean wind speed values at Dhahran, Saudi Arabia, from 1970 to 1984 (Hassanm, Y.H. & Hill, 1986). However, there is not a clear correlation between wind speed and temperatures due to the small annual temperature variation at Dhahran. The year-to-year variety of yearly mean breeze speeds depends profoundly on chosen areas and consequently, there is no normal connection to anticipate it. For instance, except for a few years, the annual mean wind speeds at Dhahran, Saudi Arabia, decrease all the way down to zero from 1970 to 1983. For the years 1970–2003, this variation is more pronounced in the United Kingdom (Siddiqi A H, Khan S and Rehman S, 2005). In a similar vein, the annual mean wind speed showed significant variation over a 20-year period (1978–1998) in (European Wind Energy Association., 2009), with maximum and minimum values ranging from less than 7.8 m/s to nearly 9.2 m/s. Ko et al. analysed and reported on the long-term wind data from the automated synoptic observation system of meteorological observatories from 1978 to 2007 (Müller, Jentsch and Stoddart, 2009). The findings indicate that the

observed locations experience fluctuation in annual average wind speed; It tends to decrease slightly at Jeju Island, whereas the other two locations exhibit erratic trends.

2.4.2 Wind turbulence

The fluctuation in wind speed over short time scales, particularly for the horizontal velocity component, is known as wind turbulence. There are two parts to the wind speed u (t) at any given point in time: the instantaneous speed variation u'(t) and the mean wind speed u, i.e.:

$$u(t) = u'(t) + u \qquad 3$$

Wind turbulence unequivocally affects the power yield fluctuation of wind turbines. Large dynamic fatigue loads acting on the turbine caused by heavy turbulence may reduce the expected lifespan of the turbine or cause its failure. In selection of wind farm sites, the knowledge of wind turbulence intensity is crucial for the stability of wind power production. The wind turbulence intensity I is defi ned as the ratio of the standard deviation δ to the mean wind velocity u;

$$I = \frac{\delta}{U} \qquad 4$$

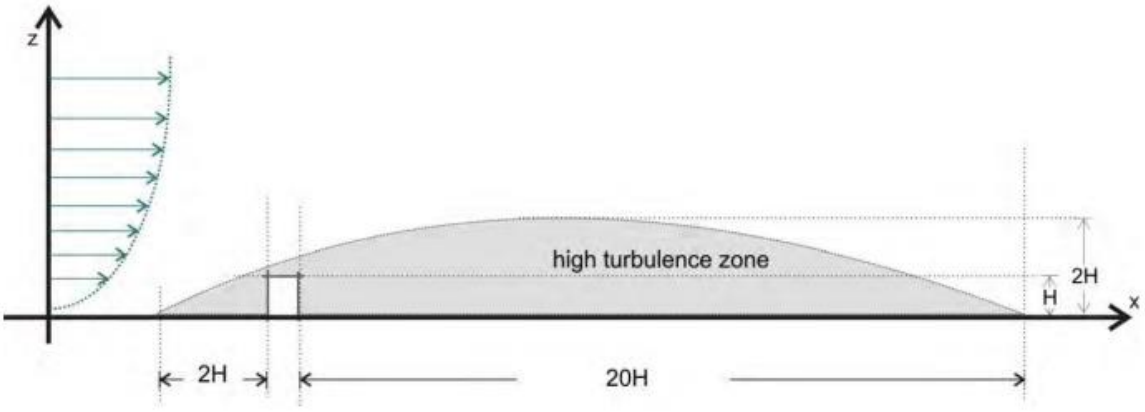

Figure 2-7 Turbulence from obstacle (Ricardo Gasparini, 2020)

2.4.3 Wind gust

The term "wind gust" refers to the phenomenon of a sudden increase in wind speed over a short period of time. Wind speed, turbulence, and wind shear may drastically alter in the event of sudden turbulent gusts. During such sudden, turbulent gusts, relatively rapid changes in the pitch angle of the blades are required to reduce rotor imbalance while preserving the generator's power output. Notwithstanding, there is ordinarily a delay between the event of a tempestuous blast and the genuine pitching of the cutting edges in light of elements of the pitch control actuator and the enormous idleness of the mechanical parts. Thus, Wind gusts can have several effects, impacting various aspects of the environment, structures, and human activities. Understanding the potential effects of wind gusts is crucial for preparedness and taking appropriate safety measures to minimize risks to life and property. During periods of high winds or gusty conditions, staying informed through weather forecasts and taking precautions can help mitigate the impact of these weather events.

Predictions of wind gusts are highly desired in order to guarantee the safe operation of wind farms. A few different blast expectation techniques have been proposed. In opposition to most strategies utilized in functional weather conditions determining, (Barbu, C. & Vyas, 2009) fostered a new wind blast forecast strategy in light of actual thought. Using a gust factor, defined as peak gust over mean wind speed, could accurately predict wind gust speeds, according to another study. These findings are consistent with previous research by other researchers.

2.4.4 Wind direction

One of the characteristics of the wind is its direction. When choosing a location for a wind farm and arranging its wind turbines, statistical data of wind directions over a long period of time are crucial. Analysing wind data related to wind directions at a specific location over a specific time period (year, season, month, week, etc.) can be done with ease using the wind rose diagram. The relative frequency of wind directions in eight or sixteen principal directions is depicted in this circular diagram. As an illustration, see Fig. 2.8, The wind rose diagram has 16 radial lines that are separated by 22.5 degrees. The frequency of wind direction is directly proportional to the length of each line.

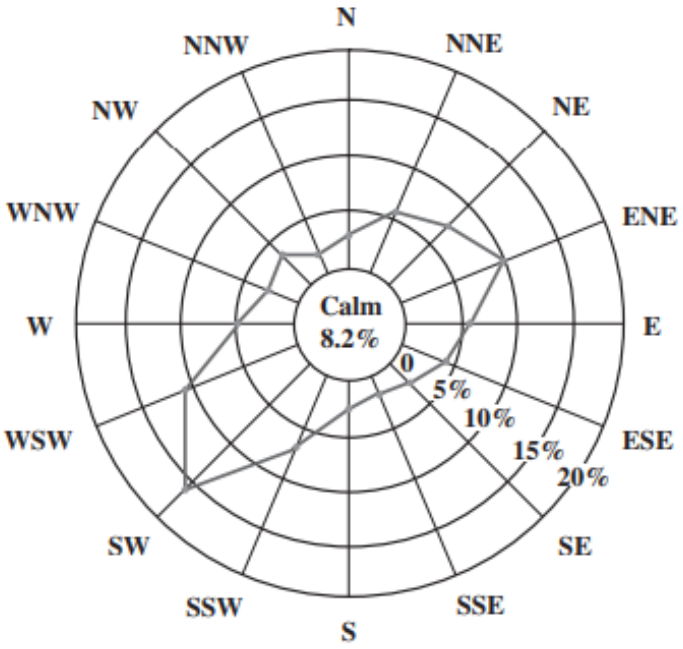

Figure 2-8 Wind rose diagram for wind directions (Wind generation by Wei Tong)

In the centre circle, a number indicates the frequency of air that is calm or near calm. Wind speeds may also be included in some wind rose diagrams.

2.5 Wind Turbine Basics

A modern wind turbine is a machine that converts energy from wind kinetic energy into mechanical energy and electrical energy. In the ongoing thirty years, wonderful advances in wind turbine configuration have been accomplished alongside current mechanical turns of events. The energy yield of wind turbines may have increased by 5% annually as a result of advancements in aerodynamics, structural dynamics, and micrometeorology, according to estimates. For the purposes of maximizing

wind energy output, reducing turbine costs, and improving turbine efficiency and dependability, a number of different concepts for wind turbines have been developed and constructed.

2.5.1 Wind turbine classification

The capacity of the turbine, the generator-driving pattern, the power supply mode, the location of the turbine installation, and the airflow path in relation to the turbine rotor are all factors that can be used to classify wind turbines.

2.5.1.1 Horizontal-axis and vertical-axis wind turbines.

Horizontal-axis wind turbines (HAWTs) and vertical-axis wind turbines (VAWTs) are two primary designs used for harnessing wind energy. HAWTs are the most commonly used wind turbines. They have a horizontal rotor shaft and blades similar to an airplane propeller, with the main rotor shaft placed parallel to the ground. The blades of HAWTs typically rotate facing the wind, and they are adjustable to capture the maximum amount of wind energy efficiently. HAWTs are more prevalent in large-scale wind farms and are effective in areas with consistent and unobstructed wind flow.

VAWTs have a vertically oriented rotor shaft and blades that rotate around a vertical axis. They can have various designs, such as Savonius, Darrieus, or helical. These turbines can capture wind from any direction as they are omnidirectional, meaning they are not required to constantly face the wind to generate power. VAWTs are often smaller and more compact, making them suitable for urban or residential areas where space may be limited. They are also less sensitive to changes in wind direction and can be positioned closer to the ground, which simplifies maintenance. Each type of turbine has its advantages and disadvantages, and the choice between HAWTs and VAWTs depends on various factors like wind conditions, available space, cost, and intended application.

HAWTs are more commonly seen in large-scale wind farms due to their higher efficiency and power generation capabilities, while VAWTs might be used in smaller installations or urban settings where their unique design features offer advantages in certain conditions. The majority of commercial wind turbines in use today have a horizontal axis, with the blades rotating parallel to the wind stream. High turbine efficacy, high power density, low cut-in wind speeds, and low cost per unit of power output are some of the benefits of this type of wind turbine. A few regular vertical-hub wind turbines are displayed in Fig. 2-9 Wind turbines with a vertical axis rotate their blades in relation to their vertical axes, which are perpendicular to the ground. The fact that a vertical-axis wind turbine can accept wind from any direction without the need for yaw control is a significant advantage. The wind generator, gearbox, and other important parts of the turbine can be set up on the ground, making the design and construction of the wind tower much simpler. This lowers the cost of the turbine. During initialization, however, vertical-axis wind turbines must utilize an external energy source to rotate the blades. The wind turbine's maximum practical height is limited because only one end is supported at the ground by the axis. Vertical-axis wind turbines only make up a small portion of wind turbines today due to their lower wind power efficiency.

2.5.1.2 Upwind and downwind wind turbines

In light of the configuration of the breeze rotor as for the breeze flowing heading, the flat pivot wind turbines can be further classified as upwind. furthermore, downwind wind turbines. The wind rotors on the majority of current horizontal-axis wind turbines face the wind, making them upwind turbines. The primary advantage of upwind designs is that they prevent the wind field from being distorted as it passes through the wind tower and nacelle. Wind first blows through the nacelle and tower of a downwind turbine, then the rotor blades. The rotor blades can be made more flexible without

considering tower strike thanks to this confirmation. However, the wind power output is affected by the influence of the distorted and unstable wakes behind the tower and nacelle.

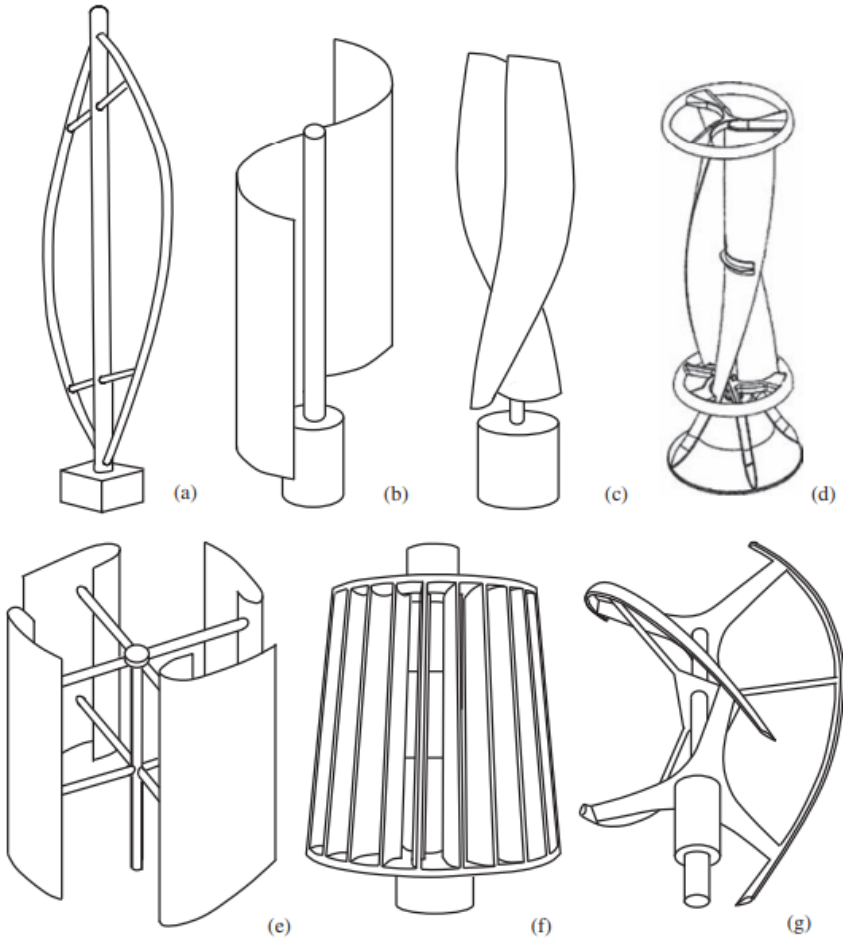

Figure 2-9 Several typical types of vertical-axis wind turbines: (a) Darrius; (b) Savonius; (c) Solarwind™; (d) Helical (e) Noguchi (f) Maglev (g) Cochrane (James and Earthscan, 2004)

In light of the configuration of the breeze rotor as for the breeze flowing heading, the flat pivot wind turbines can be further classified as upwind furthermore, downwind wind turbines. The wind rotors on the majority of current horizontal-axis wind turbines face the wind, making them upwind turbines. The primary advantage of upwind designs is that they prevent the wind field from being distorted as it passes through the wind tower and nacelle. Wind moves first through the nacelle and tower of a downwind turbine, then the rotor blades. This arrangement empowers the rotor cutting edges to be made more adaptable disregarding tower strike. However, a downwind turbine's wind power output fluctuates significantly due to the influence of the distorted, unstable wakes behind the tower and nacelle. Additionally, the unstable flow field may increase fatigue loads on the turbine and cause additional aerodynamic losses. Additionally, a downwind wind turbine's blades may produce more impulsive or thumping noise.

2.5.2 Small and Micro wind generation

Wind turbines can be separated into various general classifications considering their evaluated limits: wind turbines in the micro, medium, large, and extremely large sizes. It is accepted that a turbine with a rated power of less than several kilowatts can be considered a micro wind turbine, despite the lack of a restricted definition. Micro wind turbines are especially useful in places where there is no access

to the electrical grid. They can be utilized per structure, such as for water pumping, street lighting, and residents in remote areas, especially in developing nations. Micro wind turbines can be widely installed to fully utilize wind resources and significantly increase the availability of wind power generation because they require relatively low cut-in speeds at start-up and operate at moderate wind speeds. The term "small wind turbine" typically refers to turbines that produce less than 100 kW. Small wind turbines have been used a lot in homes, farms, and other isolated applications like telecom sites, water pumping stations, and so on. in country areas. Small, distributed wind turbines have the potential to boost regional electricity supply while delaying or avoiding the need to expand transmission lines' capacity. Most wind turbines have power ratings ranging from 100 kW to 1 MW and are medium-sized. These wind turbines can be used in village power, hybrid systems, distributed power, wind power plants, and other off-grid systems. Large wind turbines may include those with a megawatt of up to 10 megawatts. Multi-megawatt wind turbines have emerged as the mainstay of the global market for wind power in recent years. Most wind cultivates by and by use megawatt wind turbines, particularly in seaward wind ranches. Wind turbines with a capacity greater than 10 MW are referred to as ultra-large. The development of this kind of wind turbine is still in its early stages. The use of small-scale wind turbines (SWTs) with less than 100 kW is growing worldwide; driven by the need for electricity in rural areas, the availability of grid-connected inverters at a lower cost, and incentives from the government. The ability of small wind to produce a small amount of electricity for household appliances or to meet a variety of household-based electricity requirements was the original definition of the term.

Figure 2-10 O-wind bladeless turbine Courtesy: O-Innovation.

The effective deployment of micro-wind turbines around urban areas has a major difficulty, which is the lack of accurate means to estimate the wind speed and energy yield at the potential mounting

sites of these turbines. In earlier studies, however, some approaches such as the Weibull analysis, micrometeorology data, experimental measurements and computational fluid dynamics (CFD) have been applied to evaluate the wind power available for energy production(Mertens, 2002; Chandel, Ramasamy and Murthy, 2014). (Dahbi, Benatiallah and Sellam, 2013) collected long-term monthly wind speed data through the local meteorological office over a period of 12 years and wind power density and used it to evaluate the wind power potential for the Sahara site of Algeria. The power generation was also determined by generating a power curve from the turbine of a BWC XL1 wind generator (1-kW). (Olaofe and Folly, 2013) had a wind power curves derivation from time series weather data (5-min) measured at a height of 10 m for 24 months in Darling, South Africa, and used them to simulate wind resources for predicting the long-term energy output of wind turbines for various weather conditions.

2.6 Predicting the Wind Resource and impact of the wind pattern in Cities – the knowledge gap.

Estimating the available wind resource and determining whether a potential site for a wind turbine is suitable can be done in a variety of ways. These range in complexity from "folklore," which is based solely on the subjective knowledge of locals, to more in-depth computational methods that combine large-scale (5-10 km) mesoscale modelling with micro-scale (1 m) flow models, such as CFD (Landberg *et al.*, 2003). When it comes to urban sites, direct wind speed measurements, analytical models, or a hybrid approach are typically the best methods for predicting wind resources.

2.6.1 Three different approaches

2.6.1.1 Analytical Model

Insightful models for anticipating the breeze asset accessible to limited-scope wind turbines commonly follow a 'wind chart book strategy' (Landberg *et al.*, 2003). The software package "WASP" and the UK Meteorological Office's is other prominent model, and, even though it has a comparative hidden technique to that of the Met Office, it was created explicitly for metropolitan regions. A dataset consisting of long-term wind measurements taken at a local reference site serves as the foundation for the WASP method. These are then adjusted to eliminate any impact of shielding furthermore, neighbourhood surface unpleasantness, to give the 'provincial breeze climate'. The regional wind climate is then adjusted to estimate the available wind resource by considering the surrounding topography, surface roughness, and the sheltering of nearby obstructions at the potential turbine location. The strategy of the Met Office is extensively like that of WASP, although its beginning point is the NCIC data set. This data set gives wind speeds over the entire of the UK (at a goal of 1 km) that are legitimate at a level of 10 m over a smooth surface, and which additionally considers the impact of the nearby geography (on scales more noteworthy than 1 km) as a result, only the last half of WASP's methods are followed by the Met Office methodology.

2.6.1.2 Measurement-based approaches

For small-scale installations, it is generally impractical to conduct measurements over extended periods of time (up to three years, as is typically done during site assessments for wind farms). Alternately, shorter-term measurements can be taken and extrapolated to estimate the future wind resource using long-term measurements from a local reference site in a method known as a "measure-correlate-predict" strategy. Nonetheless, this approach can in any case cause a huge monetary expense. According to (Cook, K.R. & Gruenbacher, 2008), small-scale wind energy applications particularly benefit from the availability of inexpensive, accurate analytical models.

2.6.1.3 Computational Fluid Dynamics

The fact that the analytical approaches fail to consider the intricate flow patterns created by nearby buildings and other obstructions is a problem. CFD simulations are required to accurately model these complexities. Navier-Stokes equations, the fundamental equations of motion that govern fluid flow, are solved to simulate the flow field around a particular arrangement of surface obstructions within a bounded domain in these methods (Davidson, 2004). After creating a mesh to divide the domain into discrete grid cells, it is necessary to use numerical techniques to resolve the flow field because there is no exact solution to the equations. The turbulence model used has a significant impact on both the required computational resources and the accuracy of CFD simulations. Large-eddy simulations (LES) or Reynolds Averaged models (RANS) are typically utilized for urban meteorology and wind resource prediction. LES is a method for transient modelling that uses a sub-grid turbulence model to calculate sub-grid scale turbulence and fully resolves all scales of turbulence larger than the mesh resolution. Conversely, RANS methods ascertain all the different sizes of choppiness with parameterized, time-arrived at the midpoint of models. LES simulations are typically more accurate than RANS simulations as a result. However, more computational resources, processing time, and modelling expertise are required to achieve this potentially higher accuracy. Small-scale wind site assessments, especially for domestic purposes, typically require prohibitive computational resources and expertise, even for simpler RANS approaches. Additionally, it is impractical to apply these techniques to full cities due to the substantial computational resources required for CFD. The surface geometry has either been drastically simplified in previous city-scale simulations or parameterized rather than fully resolving building-scale flow, studies of relatively small local areas less than 10 km^2 are the most common application of CFD (Hassid and Galperin, 2004). Therefore, a simpler model, such as a wind atlas methodology, is typically required to estimate the boundary conditions for a smaller-scale CFD model when predicting urban wind resources using CFD (Landberg *et al.*, 2003). However, CFD has proven to be useful in comprehending the city's wind resources. CFD has been used by several researchers to investigate above-ground wind resources in simplified urban geometries. These studies will be discussed in greater detail in Section 1.4.5. Additionally, the evaluation of simpler, spatially averaged flow models for use in urban areas continues to benefit greatly from CFD.

(Yang *et al.*, 2016) study established that utilizing urban wind energy to form electricity generation modules over a distribution network has enormous potential to maximize wind power production in densely populated regions. They developed CFD based evaluation procedures to determine potential wind turbine mounting sites and obtain wind power estimates while considering the details of the local urban topography and boundary conditions of micro-environments. The predictions, which include wind velocity and direction as well as turbulence intensity, are compared with field measurements obtained using ultrasonic anemometers and thermal flow velocity probes at 10 monitored sites located on five different floors of an objective building to validate the computational model and achieve a better result. Similarly, Wind flow study around structures is of tremendous relevance in terms of wind energy assessment, pollution dispersion management, natural ventilation, and pedestrian wind comfort and safety. In accordance to the work of (Toja-Silva, Colmenar-Santos and Castro-Gil, 2013), RANS models are still commonly employed since LES turbulence models are computationally time intensive when applied to real-world geometries. However, RANS models are quite sensitive to the turbulence parameterisation used, and the results can vary depending on the application. The wind flow around an isolated building is simulated in this study utilising various forms of RANS turbulence models in the open-source code OpenFoam, and the results are compared to benchmark experimental data. A grid dependency analysis was performed to confirm the numerical accuracy of the simulations. The wind flow characteristics at each location are also examined from the standpoint of wind energy generation, and the most appropriate wind turbine model for wind energy exploitation at each part of the building roof is selected. Even though, the paper established why the

RAN turbulence model was preferred to LES; It was silent on the impact of the choices made with respect to the turbulence model parameters.

2.7 Summary

This chapter reviewed the literature relating to renewable energy, focusing on an increasing international energy portfolio divergence towards non-fossil electricity generation, the opportunities for small/micro wind energy systems implementation in urban areas, and using the computational fluid dynamics capabilities to make predictions of the impact of wind patterns in urban areas for bladeless wind turbine implementation. Wind energy, as the most widely applied renewable energy, is globally considered the best option to serve this transition While there is global appreciation of the merits of such a green economy, Alternative fuels like shale gas/oil and possibly Methane Hydrate may take an antagonistic stance in the future, despite widespread recognition of the advantages of a green economy. Even though these fossil fuels have immediate advantages, they are still fossil fuels, are not a long-term energy source, and best serve as a delaying mechanism for the inevitable day when all fossil fuels will run out. The European context for renewable energy is supported by regulatory statutes that impose stringent obligations on European states. NREAP, the national energy strategy, must be developed by each state. These arrangements are having a tremendous effect with 25 of the 27 EU individuals hoping to surpass their 2020 targets. Indeed, Ireland is currently more than 1.5% ahead of the EU RES-E Directive for 2020 with its own ambitious (and self-imposed) goal of producing 40% of its electricity from renewable sources. This wind energy shortfall can be made up for by small wind energy systems. Small-scale wind turbines (SWTs) with less than 100 kW are becoming more common worldwide, with an estimated 650,000 units producing 382 GWh of energy annually. This contribution is compared to the total wind power capacity that is currently in use, which accounts for between 2 and 3% of global electricity consumption (at the end of 2011) difficulties as media to capture the wind energy. That said, there are studies that suggest that with emphasis on understanding the wind resource, they could be a viable green option – even in urban environments

Generally, the weibull investigation can give helpful data to the large-scale siting of wind turbines however miss the mark on accuracy for micro-environment siting. Therefore, in order to enhance the power output of wind turbines in urbanized areas, micro-siting necessitates more precise wind field statistics and high-resolution measurements (Park and Law, 2015). For the assurance of wind stream field, the usually approach used to procure neighbourhood wind information is nearby estimations; notwithstanding, they are additionally exorbitant and tedious (Blocken, 2014). Since modern computer systems have a growing computational power-to-cost ratio, CFD techniques have been confirmed as an affordable alternative for evaluating the application and installation of micro-wind turbines on various potential sites in congested urban environments with less time and investment (van Hooff and Blocken, 2012). CFD simulations and field measurements were used in several study to analyse the wind resources available in an urban environment. The predicted wind speed, direction, and turbulence level were compared with the experimental data to validate the computational model in order to improve the accuracy of the estimates of wind power by using CFD-based evaluation procedures to determine potential mounting sites and urban wind power production by taking into account the details of the local urban topography and boundary conditions of the micro-environment.

Table 2-1 Examples of some recent studies considered in the Literature review capabilities of the different types of patterns/designs.

Study	Data collection approach	Site Model (Concerned building)	Simulated Flow	Prediction/Errors	Key Findings
(Razak et al., 2012)	CFD	Interdisciplinary Graduate School of Engineering Sciences, Kyushu University, Japan dimensions of 720 mm × 720 mm	Large-eddy simulation (LES)	The spatially averaged velocity of arrays with λp over 33% show strong reverse flow below 0.16h due to the skimming flow regime.	The spatially-averaged mean wind speed monotonically decreases with the packing density and aspect ratio increases. The pedestrian means wind shows the power law relationship to the frontal area ratio of the building.
(Hemida *et al.*, 2020)	Wind tunnel experiments	The atmospheric boundary layer wind tunnel of the Ruhr-University Bochum, Germany. The wind tunnel has a cross-section of 1.6 x 1.8 m^2 and a test section length of 9.4 m.	CEDVAL	No Validation	Studies show that the surface pressure contours consistently for a given wind direction. At 0 wind direction, a separation bubble is detected, while cone vortices dominate at 30 and 45.
(Yang *et al.*, 2016)	WindMaster 3D sonic anemometers	The Integrated Technology Complex Building (ITCB) is used as the objective building in this study to assess the capacity of urban wind power generation. The ITCB is located on the National Taipei University of Technology (NTUT) campus Taiwan.	CFD simulations and field measurements.	The predicted wind speed, direction and turbulence level are compared with the experimental data to validate the computational model.	The predicted wind direction matches well with the measured results in general. Besides, the realizable k—e model provides more reasonable predictions of turbulence intensity for simulations of the swirling and separating flows around buildings than those with the use of the standard and RNG k–e Model.
(L. Ledo, P.B. Kosasih, 2011)	Wind tunnel tests	wind flow characteristics in three suburban landscapes characterized by houses with different roof profiles, namely: pitched roofs, pyramidal roofs and flat roofs.	CFD	Wind flow above the roofs is complex and cannot be predicted from the wind data or the wind atlas alone.	Results show how the wind flow characteristics are strongly dependent on the profile of the roofs

The reviewed papers did extensive work with the use of CFD and turbulence models utilization; However, there's a study gap between how the choices of turbulence model impact the flow pattern and also the sustainable wind energy parameters such as the turbulence kinetic energy, Turbulence Intensity, Velocity magnitude etc. Furthermore, there's also need to address the different urban canyon and staggered configurations which had been left unattended by reviewed research papers. My present research is to address these study gaps.

Chapter 3 Methodology

In this chapter, a methodology is developed for the research in the following approach: studied site – which is basically the first to consider as it's required to have an area or site of interest, which was selected based on the availability of experimental data around the building and the field measurement can be termed as the meteorological and experimental data collection process; this is an essential method that follows after confirming the site of study/objective buildings. The third approach is the wind data analysis; the collected data was analysed to match a reliable standard; the collected data included wind direction which is the fourth approach and an integral parameter for wind resource and for wind turbine implementation.

The first four approaches can be categorized as experimental; thus, the numerical framework comprises the computational fluid dynamics, which is the numerical modelling of the fluid (In this case, wind). This also include the turbulence modelling approaches, which has different governing equations and it's a major factor in how the wind pattern impact the studied site/buildings. The numerical framework through the CFD approach, involves other factors such as the boundary conditions; which gives us the detailed information about buildings domain and the solver settings; which is the detailed systematic CFD procedures including – 4.1 Grid independence test (meshing).

In Chapter 5, analytical method is used to study output such as the wind velocity, turbulent kinetic energy etc. just as the CFD method in other to have comparison study between these methods. Furthermore, the urban aerodynamics was performed which was to study the impact of urban configurations and height on the wind patterns

3.1 Studied site

The Bowland Tower is used as the objective building in this study to assess the capacity of urban wind patterns because the building is the tallest on campus and has other wing buildings which fits into the variation of height, shapes, and arrangement; the bowland tower is located on the Lancaster University campus (54°00'36.43''N and 2°47'06.56''E) in Lancaster, Lancashire in NorthWest England, UK. The Bowland tower, which is 18.6m in length, 40.5m in width and 38.77m in height, is a fifteen-story structure with raised floors with other buildings which were also considered as monitored points for the study. These buildings are Bowland South, slaidburn house, and the energy centre and used as a research facility and has teaching classrooms, storage of equipment for various disciplines and departments, offices for faculty/staff as well as project and administrative support, and finally, a venue for campus gatherings after classes. Fig. 3-1 shows (a) the location of the studied site (including the Bowland tower, Lancaster University Campus) obtained from Google Maps, (b) a picture of the Bowland Tower and the other monitored buildings(c) the computational model ready for simulations and (d) the computational model of the buildings undergoing CFD studies.

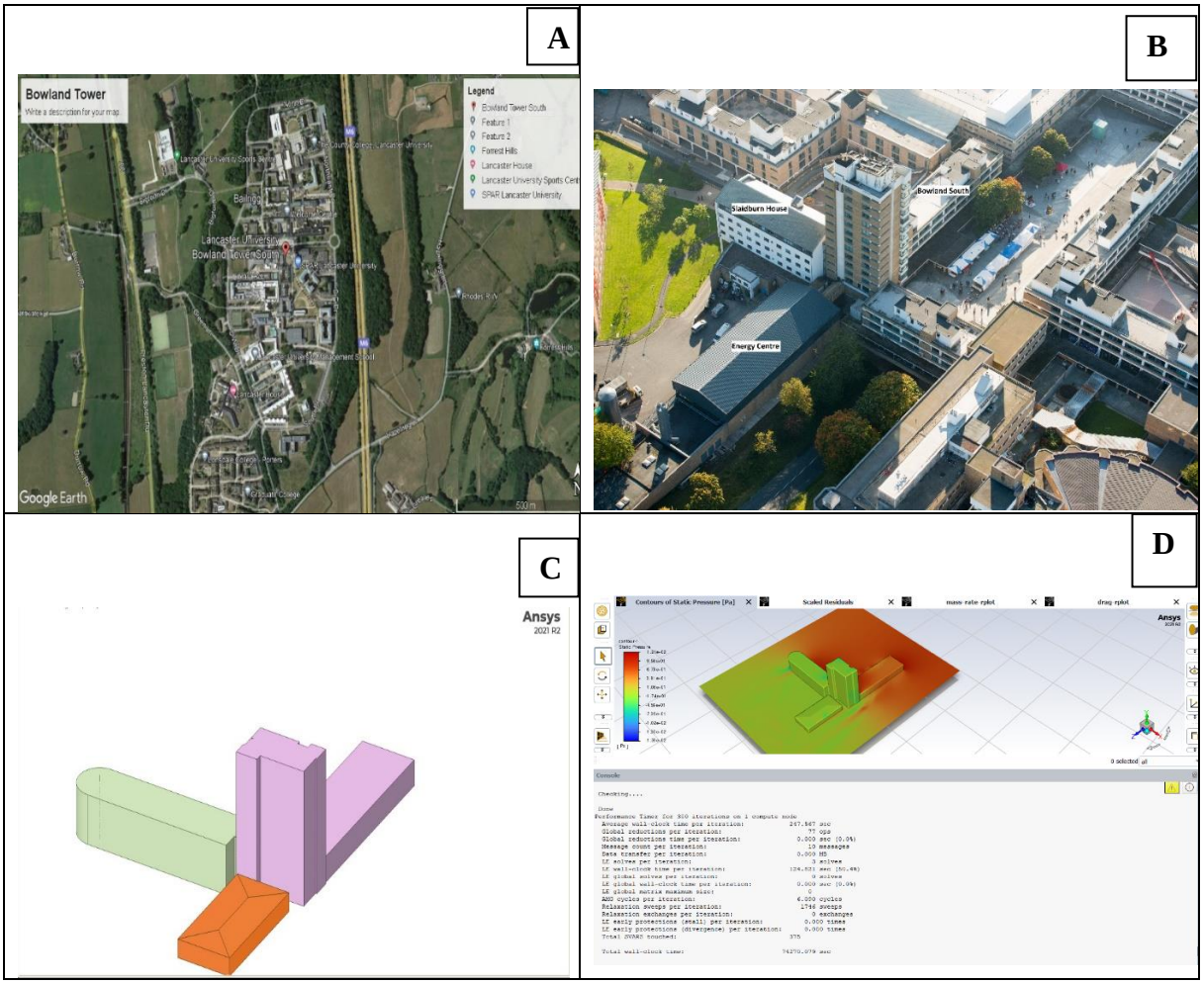

Figure 3-1 (a) the location of the studied site (Lancaster University) (b) a picture of the Bowland Tower and the other monitored buildings(c) the computational model ready for simulations and (d) the computational model solution

3.2 Field-measurements

The measurements used to assess three-dimensional (3D) wind velocities around the Bowland tower were collected from 01 January 2010 to 31 December 2021 during the hours of 00:00—23:59. The experimental results were utilized to validate those generated by the CFD software to accurately assess the potential wind power and turbulence levels for suitable mounting sites of micro-turbines. Fig. 3-2 are the photos and main specifications of the measurement instruments, which include an IEC 61400-12 Class 1 Anemometer (Campbell Ltd) in Fig. 3-2(a) and a RS PRO AVM-01 in Fig. 3-2(b). The wind flow was measured by using the IEC 61400-12 Class 1 Anemometer and RS PRO AVM-01 which provided data on the wind speed and direction with resolutions and accuracies of 0 to 77 m/s/0.1° and <1.5% RMS/2°, respectively, in the range of 0— 45 m/s.

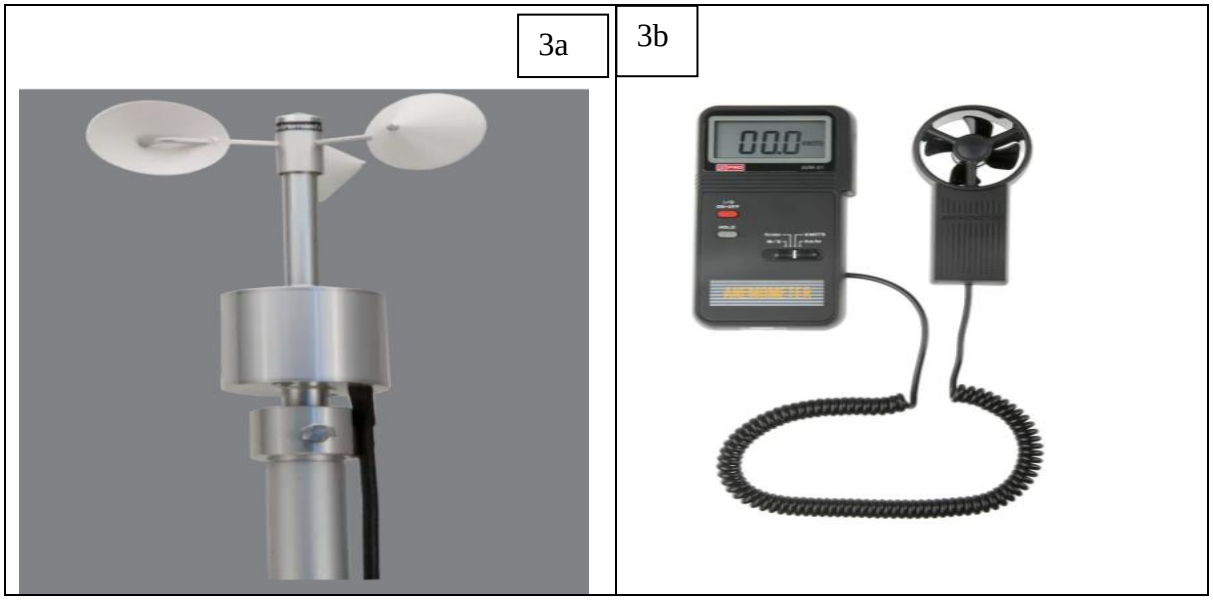

Figure 3-2 (a) IEC 61400-12 Class 1 Anemometer (Campbell Ltd) and (b) a RS PRO AVM-01.

3.3 Wind Data Analysis

In order to obtain reasonable and practical inlet reference for the wind predictions evaluation and flow simulation of the reference buildings, hourly wind data of two weather stations are used to analyse the wind power potentials (Bhandari, Shrestha and New, 2012) . The wind data from 2010 to 2021, for the Centre for Environmental Data Analysis (CEDA) data (see Eq.47-58) without surrounding obstacles, represent the wind conditions in United Kingdom; while the weather data from Jan. 2021 to Dec. 2021, for the Hazlerigg weather data, Lancaster University campus (see Eq.59-62) can only represent the wind conditions of the specific buildings. These long-time data up for the whole year can be solid practical wind evidence for the analysis and prediction in this work; the data was scrapped, cleaned and analysed using some statistical methods with Python programming language. The reference building, bowland tower building in the university campus, is located very near to Hazlerigg weather data centre.

3.4 Wind Direction

Wind is changing all the time, and sixteen directions are equally divided into in a circle, in which each direction contains 45◦ with 22.5◦ to the left and right of the direction point. In detail, the sixteen directions are North (N), Northeast (NE), East (E), Southeast (SE), South (S), Southwest (SW), West (W), Northwest (NW), West-northwest (WNW), North-northwest (NNW), North-northeast (NNE), East-northeast (ENE), East-southeast (ESE), South-southeast (SSE), South-southwest (SSW), West-southwest (WSW). Based on the provided weather data, wind direction distributions are calculated by self-programmed statistical methods and a windrose was developed. For Hazlerigg weather station, the prevailing wind direction is the South-Southeast, and other dominant directions are East-southeast (ESE) and Northeast (NE), as demonstrated on the windrose in fig. 3-3. The most common wind speed is between 4-8m/s as depicted with blue on the windrose, the second most common windspeed is between 0-4m/s and represented by the orange colour while the least windspeed is >12m/s category. For the CEDA data, the prevailing wind direction is the South- Southwest, and over 50% wind flows from the direction (see Table 31). Less wind blows from the North and West-

Southwest, and it could be as a result of the meteorological station having a rough terrain which could affect the local wind direction and wind speed distributions

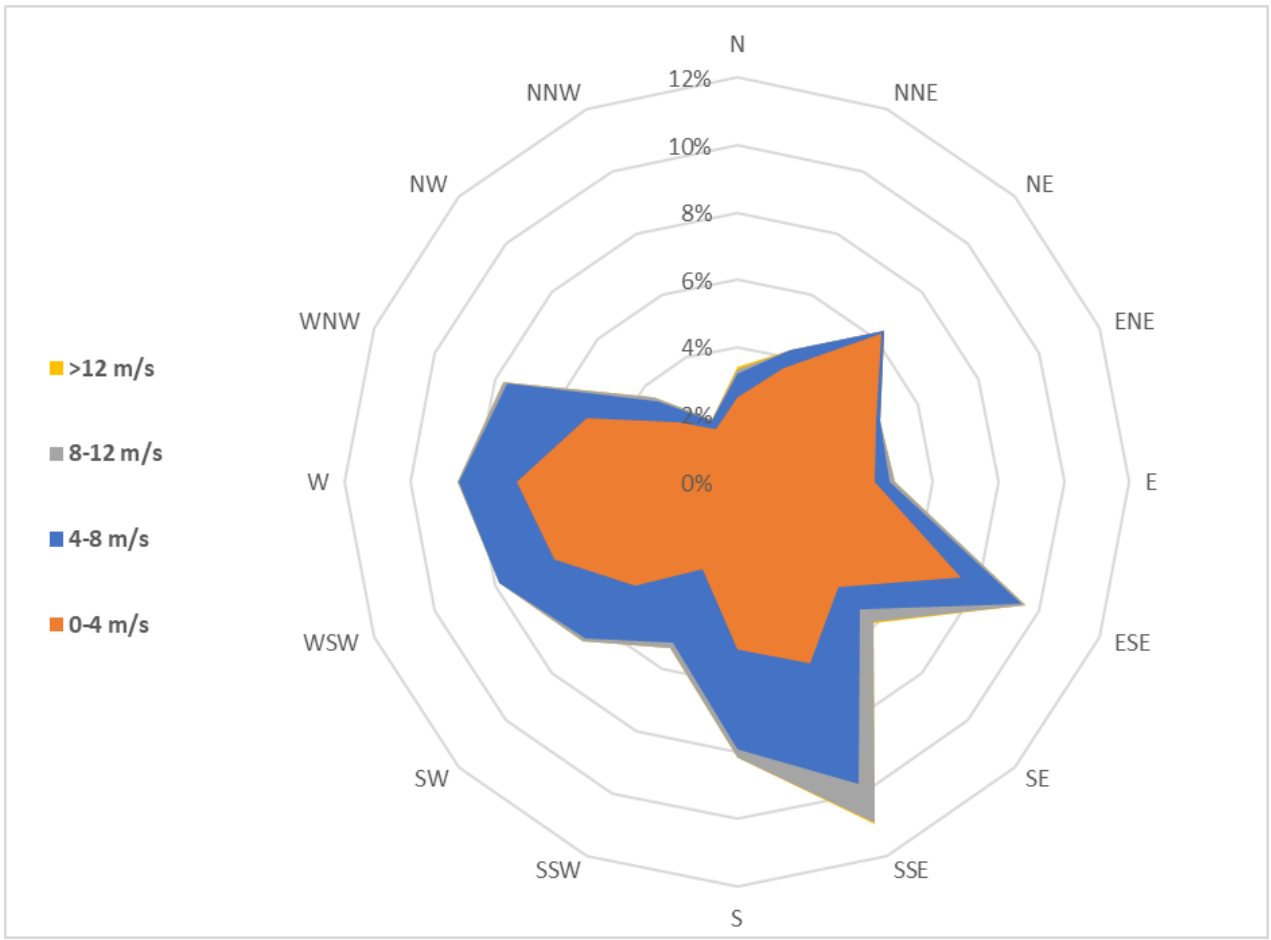

Figure 3-3 2021 Data Wind Rose of Hazlerigg weather station, Lancaster University.

Table 3-1 Analysed data of both CEDA and Hazelrigg.

	CEDA_2021			**Hazelrigg Weather Data Lancaster_2021**				Bowland Tower Floors with Height
OB_END_TIME	MEAN_WIND_DIR	MEAN_WIND_SPEED	Wind Direction	Ave. Windspeed (m/s)	Wind Direction (Deg.)	Air Pressure Mbar	Floor	Height
2021-01	199.7094	9.167546	SSW	3.190864	154.3224	999.5668	14	38.77
2021-02	158.0053	11.87151	SSE	4.593227	137.1428	1001.942	13	36.27
2021-03	209.3522	10.34094	SSW	3.635484	189.277	1009.041	12	33.27
2021-04	173.4435	7.88167	S	2.480715	160.5885	1013.314	11	31.27
2021-05	198.4866	8.709044	SSW	3.155234	186.3337	998.0081	10	28.77
2021-06	189.813	7.589378	S	2.390393	178.0231	1008.779	9	26.27
2021-07	196.0351	6.674687	SSW	2.042002	184.5304	1004.274	8	23.77
2021-08	193.0525	7.703649	SSW	2.628083	174.7697	1006.099	7	18.77
2021-09	188.3318	7.615281	S	2.45735	169.2182	1006.898	6	16.27
2021-10	213.9067	9.98462	SW	4.005903	187.9067	201.3838	5	13.77
2021-11	240.7617	9.64719	WSW	3.416198	195.6176	1005.867	4	11.27
2021-12	196.2455	9.848461	SSW	3.634599	181.609	999.4922	3	8.77
							2	6.12
							1	3.47
Total Average	**196.4286**	**8.919498**		**3.135838**	**174.9449**		0	0

3.5 Computational Fluid Dynamics

A theoretical model implemented through ANSYS Fluent software V2021 was used to simulate the urban wind flow over the Bowland tower building. A solid model of the building was developed with design modeller and the terrain of the studied site was generated by obtaining the details of the extent and geometric shape from the 3D contours provided by the faculty. At the design modeller, the boundary conditions were specified, and the solid model was then transferred to a pre-processor of ANSYS Fluent to construct a numerical model by using the grid generator module, also known as meshing. In order to determine interaction of the wind with the buildings, calculations were done to determine the wind flow field.

The computational analysis was based on steady-state conservation equations of mass and momentum for the incompressible turbulent flow with the governing equations given as follows.

$$\frac{\partial U_i}{\partial X_i} = 0, \qquad 5$$

$$\frac{\partial \rho U_i U_j}{\partial X_j} = -\frac{\partial p}{\partial X_i} + \rho g_i + \frac{\delta}{\delta x_j}\left[\mu + \mu_i\left(\frac{\delta U_i}{\delta x_j} + \frac{\delta U_j}{\delta x_i}\right)\right], \quad 6$$

The symbols are represented as follows; *Ui* is the velocity component in the *i* direction, whereas $\rho, P, \mu, \mu_i and\ \rho g_i$, denote the pressure, density, laminar viscosity, turbulent viscosity, and gravitational force, respectively. In the calculations, the governing equations were discretized by using a finite control volume approach. The least square cell-based method for gradient evaluation, the second order setting for pressure treatment, and the second order upwind scheme for solving the moment, turbulent kinetic energy and turbulent dissipation rate equations are all used for the discretization schemes in CFD calculations. An iterative numerical method, the coupled scheme which obtains a robust and efficient single phase implementation for steady-state flows, with superior performance compared to the segregated solution schemes was utilized for velocity—pressure coupling (ANSYS, 2009). A steady solution was obtained with the convergence of the normalized residual errors of the flow variables (*u, v, w, p, k and* ε) to 10^{-4} and a mass balance check lower than 1% for achieving the wind field environments.

To install bladeless wind turbines over urban areas, accurate simulation data of the airflow across real building encompasses, can yield good estimates of the wind power potential. Therefore, numerical simulations were conducted by using ANSYS fluent software to validate the computational model to compare the predictions with the measured results. In addition, most previous research studies were carried out by using steady-state Reynolds-averaged Navier—Stokes (RANS) equations with the use of wind tunnel measurements to validate the simulation results. However, to the best of my knowledge and with respect to the papers considered in the literature review, only few studies in the literature review considered the complexity of urban building shapes by verifying the calculated wind flow properties against data that are obtained on-site.

3.6 Turbulence model

In view of the complex flow phenomenon associated with the wind flow across the Bowland tower, the SST k—ω model and Renormalization Group (RNG) k −ε turbulence model were adopted in this study for turbulence closure.

3.6.1 SST k---ω model

One of the most widely used models for capturing the influence of turbulent flow conditions is the k-omega (k—ω) turbulence model. It belongs to the Reynolds-averaged Navier-Stokes (RANS) family of turbulence models, which models all turbulence effects.

SST is an abbreviation for shear stress transmission. In the free-stream, the SST formulation flips to a k−ϵ behaviour, which avoids the k—ω problem of being sensitive to the inlet free-stream turbulence qualities. The k—ω SST model predicts flow separation better than most RANS models and explains for its good behaviour in adverse pressure gradients. It can account for the primary shear stress transfer in adverse pressure gradient boundary layers. Because of its high accuracy to expense ratio, it is the most often used model in the business. A blending function is used to transition between the two sets of equations in the second set of k- equations. Even with significantly separated locations, the SST model has been found to yield very acceptable estimations of wall constrained flows. In work of (Georgiadis *et al.*, 2006), the SST model (see eq.7-23) was discovered to produce the best forecasts

of several one- and two-equation models in the Wind code for separated nozzle flows. For a detailed description of the model and the equations involved see (Menter, 1994)

3.6.1.1 Mathematical Representation of SST k---ω model

Kinematic Eddy Viscosity, $V_T = \frac{a_1 K}{\max(a_1 w, sF_2)}$ (7)

Turbulence Kinetic Energy, $\frac{\delta k}{\delta t} + U_J \frac{\delta k}{\delta x_j} = \rho_k - \beta^* k_w + \frac{\delta}{\delta x_j}\left[(V + \delta_k V_T)\frac{\delta k}{\delta x_j}\right]$ (8)

Specific Dissipation Energy, $\frac{\delta w}{\delta t} + U_J \frac{\delta w}{\delta x_j} = \alpha_k - \beta k_w + \frac{\delta}{\delta x_j}\left[(V + \delta_w V_T)\frac{\delta w}{\delta x_j}\right] + 2(1 - F_1)\delta w_2 \frac{1}{w}\frac{\delta k}{\delta x_i}\frac{\delta w}{\delta x_i}$ (9)

Closure Coefficient and Auxiliary Relations,

$$F_2 = tanh\left[[\max\left(\frac{2\sqrt{k}}{\beta^* wy}, \frac{500v}{y^2 w}\right)]\right] \quad (10)$$

$$P_k = \min(\tau_{ij}\frac{\delta u_i}{\delta x_j}, 10\beta^* kw) \quad (11)$$

$$F_1 = tanh\left\{\{\min\left[\max\left(\frac{\sqrt{k}}{\beta^* wy}, \frac{500v}{y^2 w}\right), \frac{4\sigma w^2 k}{CDkwy^2}\right]\}^4\right\} \quad (12)$$

$$CDkw = \max(2\rho\sigma w^2 \frac{1}{w}\frac{\delta y}{\delta x_i}\frac{\delta w}{\delta x_i}, 10^{-10}) \quad (13)$$

$$\emptyset = \emptyset_1 F_1 + \emptyset_2(1 - F_1) \quad (14)$$

$$\alpha_1 = 0.55 \quad (15)$$

$$\alpha_2 = 0.44 \quad (16)$$

$$\beta_1 = 0.075 \quad (17)$$

$$\beta_2 = 0.0828 \quad (18)$$

$$\beta^* = 0.09 \quad (19)$$

$$\sigma_{k1} = 0.85 \quad (20)$$

$$\sigma_{k2} = 1 \quad (21)$$

$$\sigma_{w1} = 0.5 \quad (22)$$

$$\sigma_{w2} = 0.856 \quad (23)$$

The density and viscosity of air were 1.188 kg/m^3 and 1.841 x 10^{-5} N s/m^2 with an annual mean temperature of 24.2 °C. In this investigation, we would also explore the prediction capability (in terms of the magnitude and direction of the wind velocity, and turbulence intensity) of one more conventional high-Reynolds number RNG k—e, for comparison purposes.

3.6.2 RNG k– ε model

The k-epsilon (k–ϵ) turbulence model is the most used to simulate mean flow characteristics in turbulent flow situations. It belongs to the Reynolds-averaged Navier Stokes (RANS) family of turbulence models, which models all turbulence effects.

It is a model with two equations. That is, in addition to the conservation equations, it solves two transport equations (PDEs) that account for history effects such as convection and turbulent energy

diffusion. Turbulent kinetic energy (k), which defines the energy in turbulence, and turbulent dissipation rate (ϵ), which determines the rate of turbulent kinetic energy dissipation, are the two conveyed variables (Ricardo Gasparini, 2020). RANS models all turbulence effects using time-based, ensemble-averaged Navier-Stokes equations. Eventhough, RANS produces lower resolution analysis than DNS or LES, it is extensively employed in engineering applications due to the practical feature of not requiring high-resolution computation grids. Unlike the complicated flow fields within and outside a wind turbine, it is difficult to develop quick adverse pressure gradients in the flow direction in most circumstances of wind condition analysis. As a result, the k- ε turbulence model, which accurately analyses turbulence behaviour in free-stream regions with small pressure gradients, is preferred for RANS numerical analysis over the Wilcox k- ω turbulence model (Georgiadis, Yoder and Engblom, 2006), which provides accurate forecasts of boundary layer separation in viscous sub-layer regions with adverse pressure gradients. Researchers frequently employ the k- ε turbulence model for topography analysis.

The renormalization group (RNG)-based (see Eq.24-25) k-turbulence model, in particular, produces forecasts with excellent reliability when analysing complicated terrains (Jae-ho Jeong and Kwangtae Ha, 2020). As a result, the RNG-based k-turbulence model was utilised in this research. Even though the wall grid-scale is not enough near at the surface, the current numerical analysis was also conducted using the shear stress transport (SST) turbulence model, which is based on the k- ω turbulence model, in order to evaluate the turbulence model's sensitivity. The Eulerian conservation equations govern the wind flow, hence, the Renormalization Group (RNG) k −ε turbulence model is employed as the second turbulence model since it is demonstrated to be properly enough for wind flow simulation (Gao and Lee, 2011).

3.6.2.1 Mathematical Representation of RNG k− ε model

Based on the assumption that the wind flow is incompressible, the Reynolds averaged continuity and momentum formula can be expressed as equations 5 and 6. Furthermore, RNG k − ε turbulent model is employed as below to close the fluid equation system in Equations 5 and 6:

$$\frac{\delta k}{\delta t} + \cup_k \frac{\delta k}{\delta x_k} = \frac{\delta}{\delta x_k}\left(\frac{\alpha_k \mu_t}{\rho}\frac{\delta k}{\delta x_k}\right) + 2\frac{\mu_t}{\rho} s_{ij} s_{ij} - \varepsilon \quad (24)$$

$$\frac{\delta \varepsilon}{\delta t} + \cup_k \frac{\delta \varepsilon}{\delta x_k} = \frac{\delta}{\delta x_k}\left(\frac{\alpha_\varepsilon \mu_t}{\rho}\frac{\delta \varepsilon}{\delta x_k}\right) + C_{1\varepsilon}\frac{\varepsilon}{k}\left(2\frac{\mu_t}{\rho} s_{ij} s_{ij}\right) - C_{1\varepsilon}\frac{\varepsilon^2}{k} - R_\varepsilon \quad (25)$$

where k is turbulent kinetic energy, ε stands for turbulent dissipation rate, t means eddy viscosity, sij is average strain rate tensor, the constants are C1ε = 1.42, C2ε = 1.68, C = 0.085; ˛k = ˛ε ≈ 1.393.

3.7 Boundary Conditions

The schematic of the boundary conditions is shown in Fig.3-4. An ambient pressure of 1 atm was employed at the outlet of the calculation domain. Zero normal gradients of $\rho, k, and\ \varepsilon$ were imposed onto the solid surface, with log-law wall functions applied to the near surface grids of the buildings. Boundary conditions were used for all flow variables at the top and lateral boundaries placed 38.77 H and 50 W from the boundaries of the building models, where H and W denote the height of the Bowland tower and the width of the built models respectively. Furthermore, the upstream and downstream domain lengths were approximately 3D and 6.5D respectively from the buildings, where D denotes the length of the built area to avoid the occurrence of unintended stream wise gradients as well as allow the development of a wake region behind the buildings, which can facilitate the convergence of simulations.

Table 3-2 Parameters for Subjected Building

Building (m)	**Width (W)**	**Length (L)**	**Height (H)**
Bowland Tower (A)	50	18.6	38.77
Slaidburn House (B)	194.25	133.60	24
Bowland South (C)	70	150	20
Energy Centre (D)	50	100	16.30

Table 3-3 Parameter studies variations in CFD simulation.

	Parameters	**Value**
Geometry	Domain size(H)	H= 38.77/24/20/16.30(m)
Mesh	Relevance centre (RC)	Coarse/medium/fine
	Smoothing	Low/medium/high
	First layer thickness from the ground inflation	T_g = 0.2/0.3/0.4/0.5(m)
	Number of inflation layers for both ground	N= 5/8/10/14
	Ground inflation transition ratio	R_g= 1.1/1.13/1.16
Number of iterations	N >=200	200/300/400/500
Boundary Condition	Roughness height (m) for wall function	Ks = 0/0.1/0.5/0.8/1/1.2/1.5 (m)
	Roughness constant for wall function	Cs = 0.5/0.99
Turbulence models and solution method	Launcher option Turbulence model Spatial discretization	Single/double precision $k-\varepsilon$ Standard/ $k-\varepsilon$ RNG/ $k-\varepsilon$ Realizable/$SST-\omega$ Launcher option: double precision; algorithm scheme: SIMPLE/Coupled Pressure: ½ order, momentum, k, ε: 2 order upwind/QUICK

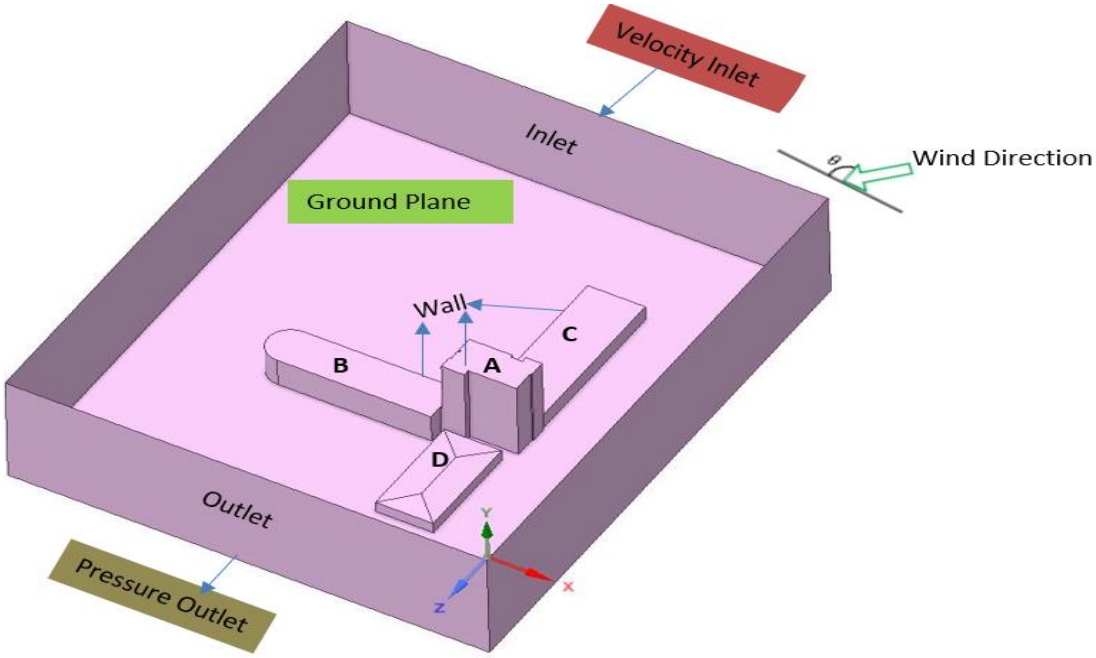

Figure 3-4 Boundary Conditions Schematic

3.8 Solver settings

The simulations performance was done with a commercial CFD code Ansys Fluent 2021R2. The SST model equations were solved in combination with the Renormalization Group (RNG) k −ε turbulence model. The COUPLED algorithm was used for pressure velocity coupling, pressure interpolation was second order and second-order discretization schemes were used for both the convection terms and the viscous terms of the governing equations. Convergence was assumed to obtain when all the scaled residuals levelled off and reached a minimum of 10^{-6} for x,10^{-4} for y-momentum and for k, ε, and continuity.

3.9 CFD-based evaluation procedures.

CFD-based evaluation procedures for evaluating the impact of wind pattern and turbulence intensity at potential mounting sites are given in Figure 3-5 and steps for the procedure are outlined below:

1. As the prevailing wind flow condition, climate data are obtained from a local meteorological station to build a wind rose chart that computes the ABL velocity, turbulence kinetic energy, and dissipation rate profiles.
2. Wind velocity and direction, as well as turbulence intensity, are evaluated to validate CFD estimates of local air-flow characteristics for accurate wind energy evaluation and wind turbine implementation.
3. The computational model is created by replicating the complicated urban topography of the examined site (with the objective building in the centre).
4. CFD simulations are used to forecast local wind characteristics such as wind velocity, power factor, and turbulence intensity.
5. As established by Step (4), regions with high wind power factor and low wind turbulence levels are selected for macro-siting the objective building.

6. The estimated wind power density and wind turbulence intensity profiles from Step (5) are utilised to select potential implementation sites for micro-siting the objective building.
7. IEC Standard 61400-2 is used to rule out potential mounting sites with wind turbulence intensity more than 18%, indicating that the site is unsuitable for installing micro-turbines.
8. To identify the final sites for placing the micro-turbines, the lowest mounting height and power factor are optimised.

Before installing micro-turbines, a comprehensive assessment of wind resources for suitable mounting sites can be realised utilising the aforementioned evaluation processes.

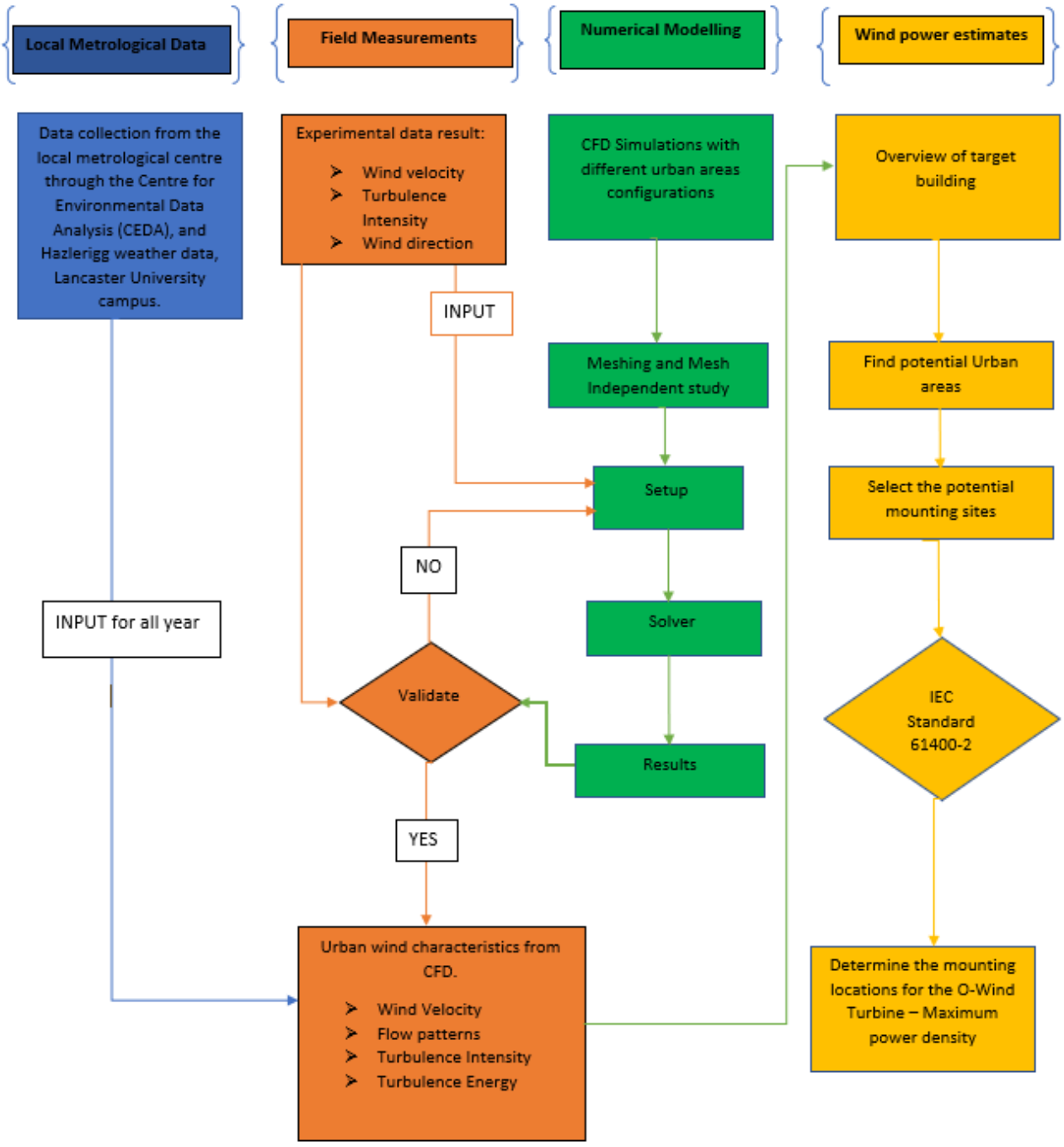

Figure 3-5. Schematic representation of the procedures for evaluating the impact of wind pattern and turbulence intensity at potential mounting sites (Faro A.A)

Chapter 4 CFD simulations: Mesh details

Using the Ansys Fluent-CFD software, a high-quality unstructured mesh comprising tetrahedral and prism elements was produced. Fig. 4-2a and 4-2b depict the building mesh with a zoomed view of the mesh at the top and side region. To overcome the boundary layer effects, a sufficiently fine mesh was formed on the inlet with 5 inflating layers and an initial height of 1×10-5 m, which produces y+ 1. The inflation layer is extruded at the inlet surface with a growth rate of 1.2 and transition ratio of 0.272. Figure 4-1b depicts a zoomed-in image of the inflating layer mesh at the wall region. In Ansys FLUENT, the buildings domains were enclosed and meshed as group mesh interfaces. Systematic changes are made to the reference case that was outlined in the previous section; this is essential for the sensitivity of the results to various geometrical and computational parameters to be analysed. In every section, one of the geometrical or computational parameters is varied, while all others are kept identical to those in the reference case.

4.1 Grid independence analysis

When it comes to numerical simulations, the results are as good as the mesh – By this, I mean that a "poor" mesh will give a "poor" or inaccurate result. Therefore, ensuring that the mesh is "good enough" is essential to producing reliable results. There are multiple ways of verifying that a model mesh is acceptable (FEA, 2022). One of these is conducting a mesh independence study. A mesh independence (or grid independence) study could be said to be an act which an analyst can perform to determine the dependence of the results on different mesh qualities such as mesh sizes, mesh density, skewness etc. Performing a grid-sensitivity analysis is important to reduce the discretization errors and the computational time. In this study, a grid-sensitivity analysis was performed based on two additional grids, a coarser grid and a finer grid.

4.1.1 Impact of Mesh Quality

Different metrics can be used to judge the quality of a mesh, which are often based on the geometrical qualities of the mesh cells (e.g., Aspect ratio) or the relationship between neighbouring cells (e.g., non-orthogonality). Because the suitability of a mesh for a simulation is also heavily influenced by the simulated physics, the simulation solver, and the geometrical domain, quality metrics can only provide an indication of whether a mesh is a suitable fit for a simulation setup. All the simulations were very good on mesh quality as indicated on the mesh quality metrics. Fig. 4-1a offers useful ranges for certain mesh quality measures based on our best practises. The term "maximum" refers to the highest quality metric that allows the simulation to execute, most likely without mesh quality-related solver divergence. The term "recommended" refers to the maximum suggested range for guaranteeing acceptable mesh quality.

It is vital to note that the following figures are merely suggestions, not requirements. For example, if the skewness is more than 85, the CFD simulations will fail 80% of the time. This does not imply that a simulation with a mesh non-orthogonality greater than 86 will always fail or that a simulation with a mesh skewness greater than 84 will always succeed. Low-quality meshes, on the other hand, will almost certainly create numerical mistakes, causing the simulations to fail or produce incorrect results.

Table 4-1 Mesh Quality check (ANSYS, 2015)

Good quality mesh means that…	*Bad quality mesh can cause;*	*Mesh quality recommendations*
• *Mesh quality criteria are within correct range e.g., Orthogonal quality* • *Mesh is valid for studied physics e.g., Boundary layer* • *Solution is grid independent* • *Important geometric details are well captured*	• *Convergence difficulties* • *Bad physics description* • *Diffuse solution*	• Low Orthogonal Quality or high skewness values are not recommended. • Generally, try to keep minimum orthogonal quality > 0.1, or maximum skewness < 0.95. • However, these values may be different depending on the physics and the location of the cell.

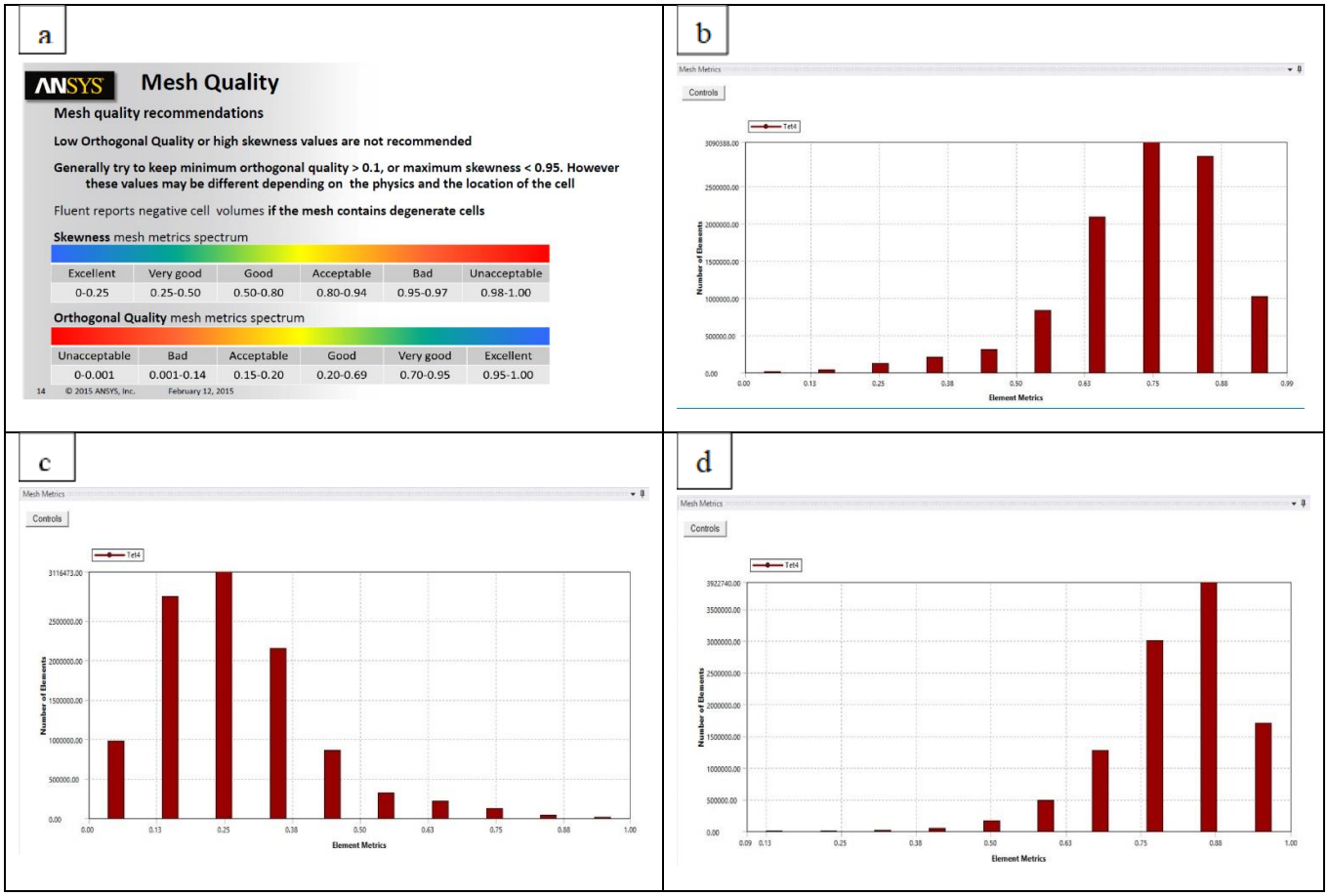

Figure 4-1 (a) ANSYS Mesh Metrics Recommendations (b) Mesh Orthogonal quality metrics (c) Mesh Skewness metrics (d) Mesh Element quality metrics (Ansys 2022).

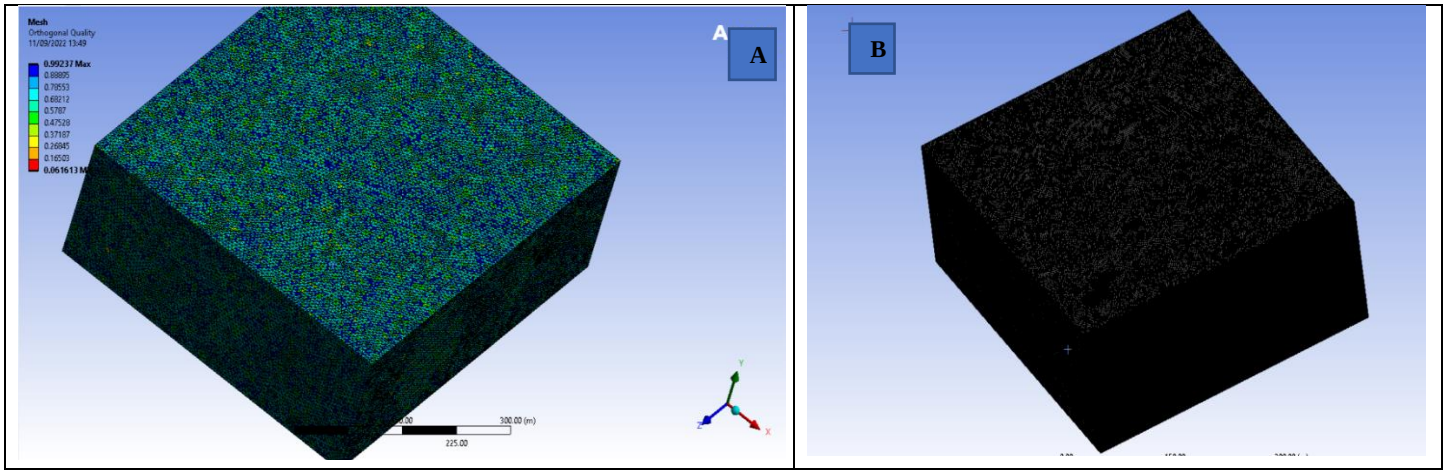

Figure 4-2 (a) Mesh Orthogonal quality passed both min. and max. requirement. (b) Finest mesh size

4.1.2 Impact of Mesh sizes

To establish the accuracy of the CFD solution, and to keep the computational costs low, the buildings were analysed using: the SST k- ω model, and RNG model, at uniform Vin = 8.92m/s, and $\lambda = 1$. The grid convergence study was performed by developing three different meshes: with a coarse, medium, and fine grid for the subjected building to predict the pressure coefficients (Cp) on normalized mesh cells to determine how the mesh quality affects CFD simulation results. The number of nodes, Cp, and the simulation time for the four mesh sizes cases simulated using the SST model are highlighted in table below:

Table 4-2 Mesh sizes and respective nodes, elements, and Simulation time

Mesh Size(m)	Node	Element	Cp	CFD Simulation time	H1(m)	H2(m)	H3(m)
5 (M1)	145680	777946	104.9	10hrs,21 mins	38.77	28.77	16.27
2.5 (M2)	1038908	5656399	134.6	20hrs,47 mins	36.27	26.27	13.77
1.5(M3)	1282342	6949465	57.76	28hrs, 33mins	33.27	23.77	11.27
1 (M4)	1968890	10575699	28.35	36hrs, 15mins	31.27	18.77	8.77

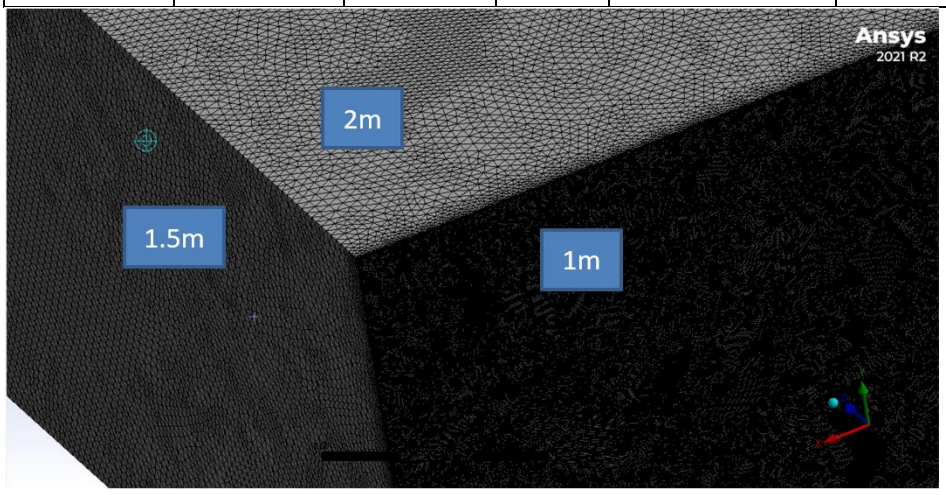

Figure 4-3 Three Mesh sizes on the same building enclosure; coarse, medium, and fine mesh.

It is very clear that CFD simulation time is highly dependent on the number of mesh nodes considered. The four meshes generated have near wall resolution i.e., y+ < 10 by using the standard wall function approach to avoid unsatisfactory results when using the SST k – ε model. The overall mesh setup of the building models with an enlarged view of the numerical grids near the building is shown in Fig. 4-3 and the predicted pressure coefficients at monitored points for four different grids are shown in Table 5. The mesh system (Table 5) has two main sections: the building enclosure formed by four connected parts of the construction and the surrounding area with a computational domain of 100m (in length) x 200m (in width) x 75m (in height), respectively. Finer grids were placed in the areas that adjoined the solid surface boundaries of the structures. For the locality around the Bowland tower, the average cell length was around 1.5 m with the smallest spacing of 0.16 m to resolve the steep variations of the flow properties associated with the interaction of the wind with the buildings.

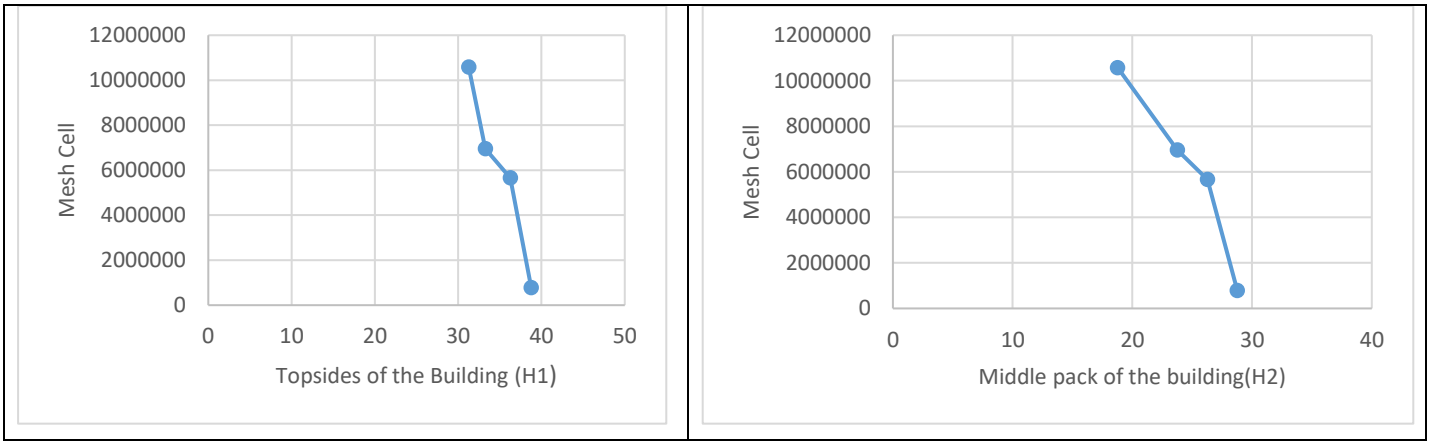

Figure 4-4 Results for grid-sensitivity analysis: mesh cells value along (a) Topsides of the building(H1) and (b) Middle pack of the building(H2).

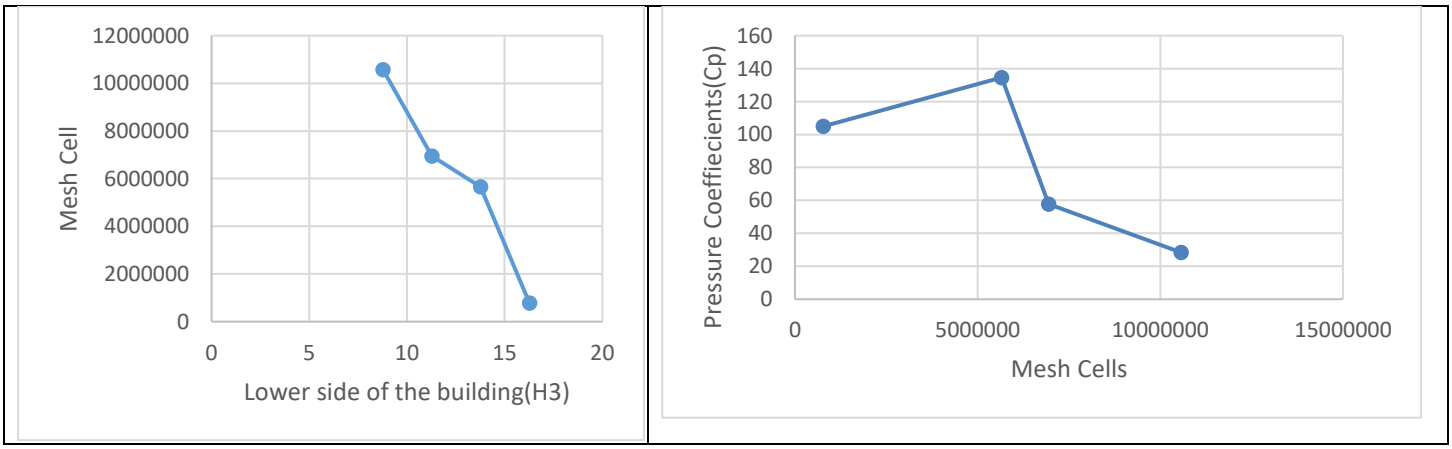

Figure 4-5 Results for grid-sensitivity analysis: (a)mesh cells value along (H3); (b) Cp vs Mesh Cells

The CFD simulations required the y+ values between 30 and 300 to maintain the proper near-wall mesh quality for using the standard wall functions. Hence, the cells at the walls were carefully arranged to fulfil this constraint. As mentioned before, the coarse mesh had 777,946 cells, the medium grid had 5,656,399 cells, while the fine grid had 10,575,699 cells. The four mesh sizes are shown in Tab.4-2 and the results for height variation on the three grids are compared in Fig. 4-4 and 4-5, indicating only a very limited dependence of the results on the grid resolution. The dependence of CP

on mesh refinement, indicated in Fig. 4.5 seems large, this could be as a result of several potential issues such as:

1. **Non-uniformity:** The mesh resolution might vary significantly in the vertical direction. This non-uniformity could lead to inaccuracies in capturing variations or phenomena occurring specifically at different heights within the simulated domain.

2. **Under-resolved or Over-resolved Regions:** Some areas of the simulation domain might have insufficient mesh elements (under-resolved), while others might have excessive elements (over-resolved) concerning the height dimension. This imbalance can affect the accuracy of the simulation results, especially if important phenomena occur at specific heights.

3. **Boundary Layer Resolution:** In fluid dynamics simulations, accurately capturing the boundary layer near surfaces is crucial. Inconsistency in mesh resolution concerning height can impact the fidelity of the boundary layer representation, affecting the simulation's accuracy, particularly in flow-related studies.

Addressing the inconsistency of the mesh to height often involves refining or adjusting the mesh to ensure a more uniform and appropriate resolution throughout the entire domain, especially concerning variations in the vertical direction. Techniques like mesh refinement, adaptive meshing, or adjusting mesh density in specific regions might be employed to improve the mesh's consistency concerning height and enhance the accuracy of the simulation results. In order to address this problem, we subjected the study to grid dependency study. It is also important to note that the mesh resolution plays a pivotal role in the final CFD results. The mesh nodes need to be small to resolve the boundary layer on the subjected surfaces. The highest CP obtained from the mesh independent study is 134.6 for M2 from the SST model. M3 and M4 account for nearly 10% difference in the estimated pressure coefficients, but the final CFD simulation time required for convergence of the two meshes has a significant difference when the conventional mesh independency method is employed. It is clear from the final CFD simulation results that the simulation time is highly dependent on the number of mesh nodes, and the turbulence model selected.

4.2 Grid dependency study

This study was conducted on the designed wind prediction model on the Bowland tower through analysis of Mesh Independent Study (MIS) and Calculation Verification, respectively. Mesh Independent study was determined for both the SST k—ω model and RNG k −ε turbulence model around Maximum Turbulence kinetic energy (TKE), Wind Velocities, and Turbulence Intensities (TI) calculated using fluent model and the method adopted are Calculation Verification (CV), and the grid selected was validated using GCI (Roache, 1998). For CV method, mesh element sizes were progressively increased while corresponding numerical variables such as Maximum TKE, Wind Velocities, and Turbulence Intensities were recorded for each simulation. The mesh element sizes of a tetrahedral mesh considered are 5 m, 2.5 m, 1.5 m and 1 m, respectively.

Table 4-3 Numerical variables were obtained from the CFD simulations for the grid dependency study.

Turbulence Model	Mesh sizes(m)	Maximum TKE (m^2 s^-2)	Maximum Velocity (m s^-1)	Maximum TI (%)
SST k—$\boldsymbol{\omega}$	1	10.3	20.3	261
SST k—$\boldsymbol{\omega}$	2.5	9.82	19.4	253
SST k—$\boldsymbol{\omega}$	5	1.38	6.25	95.5
RNG k −ε	1	16.7	19.3	431
RNG k −ε	2.5	5.95	19.2	269
RNG k −ε	5	1.42	17.8	96.8

The order of accuracy in computational methods refers to how quickly the error of an approximation decreases as the mesh or grid size decreases. It's a measure of how well a numerical method approximates the true solution as the resolution of the mesh increases.

In numerical simulations, a common way to estimate the order of accuracy is by conducting a convergence study. The order of accuracy for the exact mesh size was determined using equation 26 for three (3) best consecutive numerical variables at different mesh element sizes.

$$W_{eaxct} = W_h + Ah^p + H.O.T\ as\ \underset{h}{\rightarrow} 0 \tag{26}$$

Where A= constant, H = Higher order terms, which tend to zero faster than the lowest order error term (the second term on the right) as h tends to zero, h_i = grid size (finest, intermediate and coarse sizes), W_i= numerical variables, p = order of accuracy and W_{hi}= numerical variable at any grid size, h_i.

The grid size was assumed to be small enough that the H are negligible compared to the lowest order error term. When this is so, the numerical solution is said to be in the Asymptotic Convergence regime. The derived equations when equation 26 was used for the three element sizes (1 m denotes as 1, 2.5 m denotes as 2 and 5 m denotes as 3) were used where subscript 1,2,3 referred respectively to the finest, intermediate, and coarsest numerical solutions for the System Response Quantities (SRQ) of interest(Faro et al., 2021).

$$\mathrm{W_1} = 10.3 + \mathrm{A}(1^{\mathrm{P}}) \tag{27}$$

$$\mathrm{W_2} = 9.82 + \mathrm{A}(2.5^{\mathrm{P}}) \tag{28}$$

$$\mathrm{W_3} = 1.38 + \mathrm{A}(5^{\mathrm{P}}) \tag{29}$$

Re-arranging,

$$\mathrm{W_1} = 10.3 + \mathrm{A^p} \tag{30}$$

$$\mathrm{W_2} = 9.82 + 2.5\mathrm{A^p} \tag{31}$$

$$\mathrm{W_3} = 1.38 + 5\mathrm{A^p} \tag{32}$$

Eliminating A and rearrangement leads to

$$\frac{\mathrm{W_2} - \mathrm{W_1}}{\mathrm{W_3} - \mathrm{W_2}} = \frac{\mathrm{h_1^p} - \mathrm{h_2^p}}{\mathrm{h_2^p} - \mathrm{h_3^p}} \tag{33}$$

Subscript 1,2,3 refer respectively to the finest, intermediate, and coarsest numerical solutions for the SRQ (System Response Quantities) of interest.

$$p = \frac{\ln\frac{W_3 - W_2}{W_2 - W_1}}{\ln\left(h_2/h_1\right)} \quad (34)$$

$$W_N - W_1 = \frac{\epsilon}{\left(h_2/h_1\right)^p - 1} W_1 \quad (35)$$

$$\epsilon = (W_1 - W_2)/W_1 \quad (36)$$

From equation (34),

$$p = \frac{\ln\frac{1.38 - 9.82}{9.82 - 10.3}}{\ln\left(2.5/1\right)} \quad (37)$$

$$p = 3.13 \quad (38)$$

Where W_N is Richardson extrapolation based on three grids and ϵ is the estimated fractional error in the fine grid solution. This value of W_N is a Richardson extrapolation based on three grids Equations 36 and 35 were used for computation of fractional error and exact maximum stress (W_N)

$$\epsilon = \frac{(10.3 - 9.82)}{10.3} = \frac{0.48}{10.3}, \epsilon = 0.0466 \quad (39)$$

$$W_N - 10.3 = \frac{0.0466}{\left(2.5/1\right)^{3.13} - 1} (10.3)$$

$$W_N = \left[\frac{0.0466}{16.60}(10.3)\right] + 10.3$$

$$W_N = 10.3 \quad (40)$$

However, to standardize reporting a numerical error estimate, GCI was defined a grid based on the right side of equation (36) in, and it has been fairly widely adopted in the CFD Community. Dividing equation (36) by w_1 and multiplying by a wind load calculation safety factor (F_S) of 1.35 (SPRA, 2019) for convergence studies with a minimum of 3 grids to demonstrate the observed order of convergence(Roache, 1998)

$$GCI = F_S \frac{|\epsilon|}{\left(h_2/h_1\right)^p - 1} \quad (41)$$

$$GCI = (1.35)\frac{|0.0466|}{16.60}$$

$$GCI = 0.0038 \quad (42)$$

The steps adopted for the computation of W exact and GCI of one of the numerical variables, Maximum TKE are presented in equation (26) – (42), these steps are repeated for other variables. The W exact and GCI of other variables are computed in Table 4-4.

Table 4-4 Grid dependency study results

Turbulence Model	Numerical Variables	ϵ	W_N	p	GCI
SST k—ω	TKE (m^2 s^-2)	0.0466	10.33	3.13	0.0038
SST k—ω	Velocity (m s^-1)	0.044	20.36	2.93	0.0044
SST k—ω	TI (%)	0.0306	261.43	3.25	0.0022
RNG k −ε	TKE (m^2 s^-2)	0.644	24.57	0.94	0.636
RNG k −ε	Velocity (m s^-1)	0.0155	19.4	1.51	0.007
RNG k −ε	TI (%)	0.376	635.9	0.0636	0.64

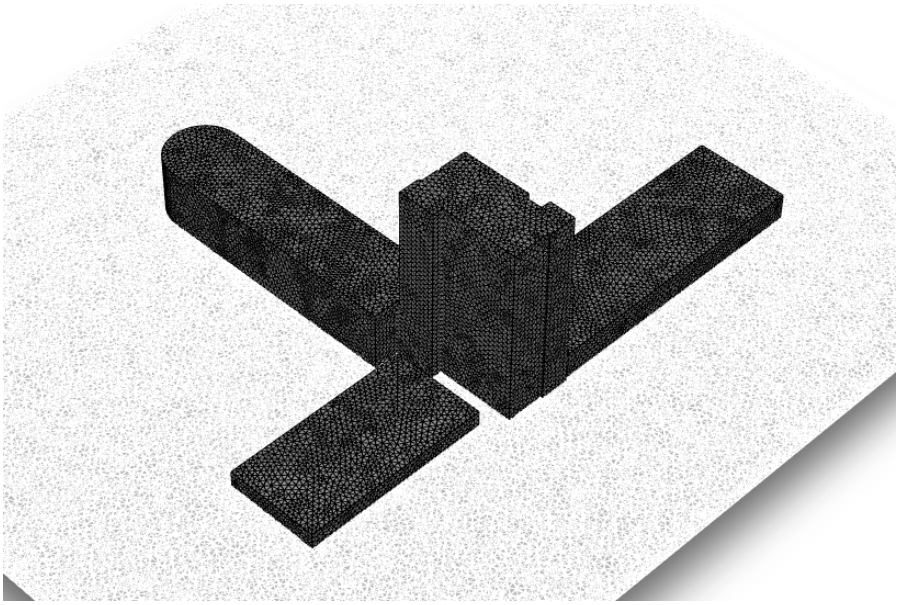

Figure 4-6 The refined meshes obtained for the convergency analysis, using the fluent meshing.

Numerical variables such as the TKE, velocity, and TI metrics are used to assess the validity of the model. The value of unknown model parameters is first estimated from a variation of element size with the respective response presented in Fig. 4-3. The obtained numerical variables were used for the computation of GCI, and errors are all used in the validation assessment as computed in equation (26) – (42), and tabulated in Table 4-4.

GCI provided information on the grid, and the error bound that indicated the convergence of the solution obtained. The estimated fractional error obtained as presented in Table 4-4, indicate that all the values obtained are good approximation with good accuracy ($\epsilon < 1$) for a fine grid between $W1$ and $W2$. The calculated GCI values have four out of the six reported values less than 0.08, which implies that the grid selected is solution independent (Roache, 1998) . These four GCI's are largely influenced by the SST turbulence model.

Chapter 5 Analytical Method

Fluid dynamics can be addressed with computational methods, and, to much smaller extent, with analytical methods. Analytical methods refer to mathematical or theoretical approaches that aim to solve fluid flow problems using analytical equations rather than numerical approximation or discretization techniques. While CFD often relies heavily on numerical methods due to the complexity of fluid dynamics equations, some analytical methods do exist within the field:

1. Exact Solutions: For highly simplified or idealized cases, it's possible to derive exact analytical solutions to certain fluid flow problems. These solutions usually come from simplified forms of the Navier-Stokes equations for specific cases, such as laminar, steady, incompressible flow in simple geometries like pipes or channels.
2. Closed-Form Solutions: In some cases, solutions to certain simplified forms of fluid flow problems can be obtained in closed-form, meaning they are represented by explicit mathematical equations. These solutions might not account for all real-world complexities but can provide valuable insights into fluid behaviour.
3. Linearized Solutions: Linearized versions of the Navier-Stokes equations might have analytical solutions for some specific cases, such as small perturbations or linearized boundary conditions around a known flow solution.
4. Perturbation Methods: Perturbation methods involve approximating complex solutions by breaking them down into a series expansion based on a known or simplified solution and solving for corrections using iterative techniques.
5. Asymptotic Methods: Asymptotic methods involve analysing the behaviour of fluid flow problems under certain limits (e.g., small or large Reynolds numbers) to derive approximate analytical solutions.

However, it's important to note that while analytical methods can provide insights and solutions for simplified or idealized cases, real-world fluid flow problems are often complex and nonlinear. Therefore, many practical applications in CFD require numerical methods (such as finite difference, finite volume, finite element methods, etc.) to solve the Navier-Stokes equations numerically on discrete meshes or grids. Analytical methods in CFD are useful for validating numerical simulations, providing benchmark solutions for specific cases, and gaining fundamental understanding, but they are often limited in their applicability to highly idealized or simplified scenarios.

5.1 Atmospheric Boundary Layer

An atmospheric boundary layer (ABL) consists of the lower regions of the atmosphere, which are still influenced by the earth's features and processes. For CFD applications, we are mostly interested in the developed velocity and turbulence profiles (Ricardo Gasparini, 2020). In some fields, such as the architectural industry, setting a velocity profile at the inlet may be required. Prescribing an ABL can also be important in some applications, such as:

- Wind comfort analysis.
- External aerodynamics in general (cars, cities).
- Any other application where a developed velocity profile at the inlet is relevant.

5.1.1 Model for an ABL Profile

The velocity is a logarithmic profile, starting at 0 m/s on the ground. It's, therefore, a function of height (z):

$$U(z) = \frac{U^*}{K} . \ln\left(\frac{z+z_0}{z_0}\right), \quad (43)$$

Where:

- *K* is the von Karman constant, usually taken in the range of 0.40 ± 0.02.
- *z* is the height in which the velocity is calculated.
- z_0 is the aerodynamic roughness length. Still according to [2], the values for z_0 vary based on landscape:
    - 0.0002 for sea or lakes.
    - 0.005 for smooth landscape, without obstacles/vegetation.
    - 0.03 in case of an open land with grass.
    - 0.1 for a cultivated area (farms, small obstacles).
    - 0.25 if high crops and scattered obstacles are present.
    - 0.5 for large vegetation, farms, clumps of forest.
    - 1 for a closed landscape, like mature forests and homogeneous cities and villages.
    - 2 or higher for centres of large towns, areas with buildings or forests with irregular height.

U^*=Friction velocity; $U^* = K.\frac{U_{ref}}{\ln\left(\frac{H_{ref}+z_0}{z_0}\right)}$ (44)

$$U(z) = \frac{U^*}{K} . \ln\left(\frac{z+z_0}{z_0}\right) \quad (45)$$

From Table 1, the Bowland tower floors with height(z) are considered for both the CEDA and Lancaster Hazlerigg Weather Data

CEDA

$$U^* = K.\frac{U_{ref}}{\ln\left(\frac{H_{ref}+z_0}{z_0}\right)} \quad (46)$$

$$U^* = (0.4).\left(\frac{8.92}{3.015}\right) \quad (47)$$

$$= (0.4)(2.96) \quad (48)$$

$$U^* = 1.18 \quad (49)$$

$$U(floor\ 0) = \frac{1.18}{0.4} . \ln\left(\frac{0+2}{2}\right) \quad (50)$$

$$=(2.95)(0) \quad (51)$$

$$U(floor\ 0) = 0 \quad (52)$$

$$U(floor\ 1) = \frac{1.18}{0.4} . \ln\left(\frac{3.47+2}{2}\right) \quad (53)$$

$$=(2.95)(1.006) \quad (54)$$

$$U(floor\ 1) = 2.97 \quad (55)$$

Lancaster Hazlerigg Weather Data

$$U^* = K.\frac{U_{ref}}{\ln\left(\frac{H_{ref}+z_0}{z_0}\right)} \quad (56)$$

$$U^* = (0.4).\left(\frac{3.13}{3.015}\right) \quad (57)$$

$$= (0.4)(1.038) \quad (58)$$

$$U^* = 3.25 \quad (59)$$

$$U(floor\ 0) = \frac{3.25}{0.4} . \ln\left(\frac{0+2}{2}\right) \quad (60)$$

$$=(8.125)(0) \quad (61)$$

$$U(floor\ 0) = 0 \quad (62)$$

$$U(floor\ 1) = \frac{3.25}{0.4} . \ln\left(\frac{3.47+2}{2}\right) \quad (63)$$

$$=(8.125)(1.006) \quad (64)$$

$$U(floor\ 1) = 8.17 \quad (65)$$

Other floors with corresponding velocity calculations are tabulated below

5.2 Turbulent Intensity, Iv(z) at height, z is defined as the standard deviation of the turbulence divided by the mean wind velocity.

Turbulent Intensity, I $=\sqrt{\sum_{i=1}^{N}(Ui-U)^2/(N-1)/U}$

For turbulent intensity across the building height, U=8.92, Ui=instantaneous velocity, N=15.

$$\sqrt{((0-8.92)^2/(15-1)/8.92 + (2.97-8.92)^2/(15-1)/8.92 + (4.13-8.92)^2/(15-1)/8.92}$$
$$+ (4.97-8.92)^2/(15-1)/8.92 + (5.58-8.92)^2/(15-1)/8.92 + (6.09-8.92)^2/(15-1)/8.92$$
$$+ (6.53-8.92)^2/(15-1)/8.92 + (6.90-8.92)^2/(15-1)/8.92 + (7.54-8.92)^2/(15-1)/8.92$$
$$+ (7.81-8.92)^2/(15-1)/8.92 + (8.06-8.92)^2/(15-1)/8.92 + (8.29-8.92)^2/(15-1)/8.92$$
$$+ (8.51-8.92^2/(15-1)/8.92 + (8.71-8.92)^2/(15-1)/8.92 + (8.89-8.92)^2/(15-1)/8.92)$$

$$= \sqrt{50.68 + 22.55 + 14.61 + 9.94 + 7.10 + 5.10 + 3.64 + 2.60 + 1.21 + 0.78 + 0.47 + 0.25 + 0.11 + 0.03 + 0.00057}$$

I =$\sqrt{119.07}$ =10.91% i.e. I = 0.1091. (66)

5.3 Turbulent kinetic energy, $\mathrm{k} = \frac{3}{2}(UI)^2$ (67)

$$\mathrm{k} = \frac{3}{2}(2.97 * 0.1091)^2 = 0.1575 \quad (68)$$

5.4 Turbulence dissipation, $\varepsilon = \mathrm{C}_{\mu}\ \frac{\mathrm{k}^{\frac{3}{2}}}{\mathrm{l}}$ (69)

$$0.09 = \frac{0.1575^{\frac{3}{2}}}{0.22} = 0.0255 \quad (70)$$

5.5 Specific turbulent dissipation rate, $\omega = \frac{\varepsilon}{C_{\mu}k}$ (71)

$$\omega = \frac{0.02557}{(0.09)(0.1575)} = 1.804 \quad (72)$$

5.6 Wind power density, $P_A\ = \frac{1}{2}\rho V^3$ (73)

$$\rho = \frac{1.225kg}{m^3}; V = Instantanous\ velocity \quad (74)$$

$$P_A\ = \frac{1}{2}(1.225)(2.97)^3 = 16.05\ W/m\text{^}2 \quad (75)$$

All other calculated values (see eq.66-75) for Atmospheric Boundary Layer, Turbulent Intensity, Turbulent Kinetic Energy, Turbulence Dissipation, Specific Turbulent Dissipation Rate, Wind Power Distributions are presented in the Table 5-1 below.

Table 5-1. Analytical Method results of some essential deliverables.

Velocity(m/s)	Density	Wind power density, PA	V^2	Cμ	Turbulence Intensity, I	Turbulent kinetic energy, k	Turbulence Dissipation	Cu*K	Specific Turbulence Dissipation
8.89	1.225	430.43	79.03	0.3	0.1091	1.41	0.68	0.127	5.39
8.71	1.225	404.70	75.86	0.3	0.1091	1.35	0.64	0.1219	5.29
8.51	1.225	377.48	72.42	0.3	0.1091	1.29	0.60	0.1164	5.16
8.29	1.225	348.95	68.72	0.3	0.1091	1.24	0.55	0.1104	5.04
8.06	1.225	320.70	64.96	0.3	0.1091	1.15	0.51	0.1044	4.89
7.81	1.225	291.78	60.99	0.3	0.1091	1.08	0.46	0.098	4.74
7.54	1.225	262.55	56.85	0.3	0.1091	1.01	0.43	0.0914	4.57
6.9	1.225	201.22	47.61	0.3	0.1091	0.85	0.32	0.0765	4.19
6.53	1.225	170.54	42.64	0.3	0.1091	0.76	0.27	0.0685	3.96
6.09	1.225	138.35	37.08	0.3	0.1091	0.66	0.22	0.0596	3.69
5.58	1.225	106.46	31.13	0.3	0.1091	0.56	0.17	0.05	3.38
4.97	1.225	75.20	24.70	0.3	0.1091	0.44	0.11	0.0397	3.01
4.13	1.225	43.14	17.05	0.3	0.1091	0.30	0.07	0.0274	2.50
2.97	1.225	16.04	8.82	0.3	0.1091	0.16	0.03	0.0142	1.80
0	1.225	0	0	0.3	0.1091	0	0	0	0

The amplification factor can be related to the stability and accuracy of the numerical scheme employed in the simulation. It quantifies how errors in one time step or iteration are magnified or damped in subsequent steps. For the evaluation of the wind energy potential over the roof compared with that of the same area at the same altitude in the free wind, an amplification factor F was defined as:

5.7 Amplification Factor, $f = \frac{M'}{(A)(U_H)^3} = \frac{(U^3)}{(U_H)^3}$ (76)

where A is the total area of the plan over the roof, U_H is the reference velocity at height H in the free wind (without buildings) with the same simulation condition, which can be calculated directly from table

Therefore, in our case, to evaluate wind energy, a simplified indicator M was defined as:

$$M' = \sum_{i=1}^{n}(A_i * V_i^3) \quad (77)$$

where Ai represents the area of the corresponding velocity vi

Chapter 6 Results

In what follows, the simulation results, together with field measurement data from CEDA and Lancaster are presented and discussed, identifying the most appropriate turbulence models for the different regions of the building. Afterward, the characteristics of the wind flow are analyzed, bringing an evaluation of the possibility of wind exploitation and the most appropriate kind of impact for each region. Since this investigation focuses on the impact of wind patterns, we concentrate some parts of our analysis on the building roof shapes and urban aerodynamics. Hence, Either the qualitative or the quantitative components of the results can be the focus of the analysis. The quantitative aspects focus on the data's correctness when compared to the numbers from the field measurements, while the qualitative aspects concentrate on how the wind flow behaves on the roof. It is crucial to note this since some models, despite producing excellent quantitative findings, struggle to accurately simulate recirculation on building roofs.

6.1 Impact of Velocity

We test the RANS turbulence models and the SST turbulence model. The analysis of the results can focus on either qualitative or quantitative aspects. The comparison of the mean wind velocity (U), turbulence intensity, and turbulent kinetic energy (TKE) with the analytical method results is carried out at the vertical axes located at the central plane of the domain according to the diagram shown in Fig. 6-1a – 6-1b.

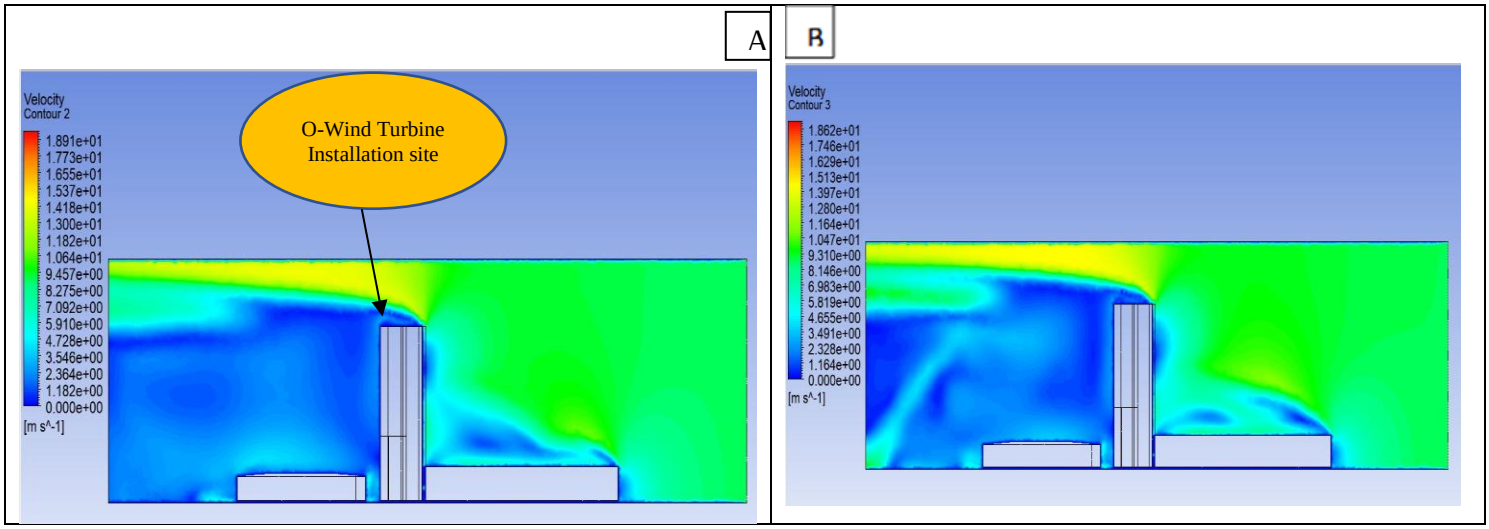

Figure 6-1. The velocity contours of the plane views around the Bowland tower depicted for (a) SST k—∈ turbulence model effect and (b) Renormalization Group (RNG) k −ε turbulence model effect.

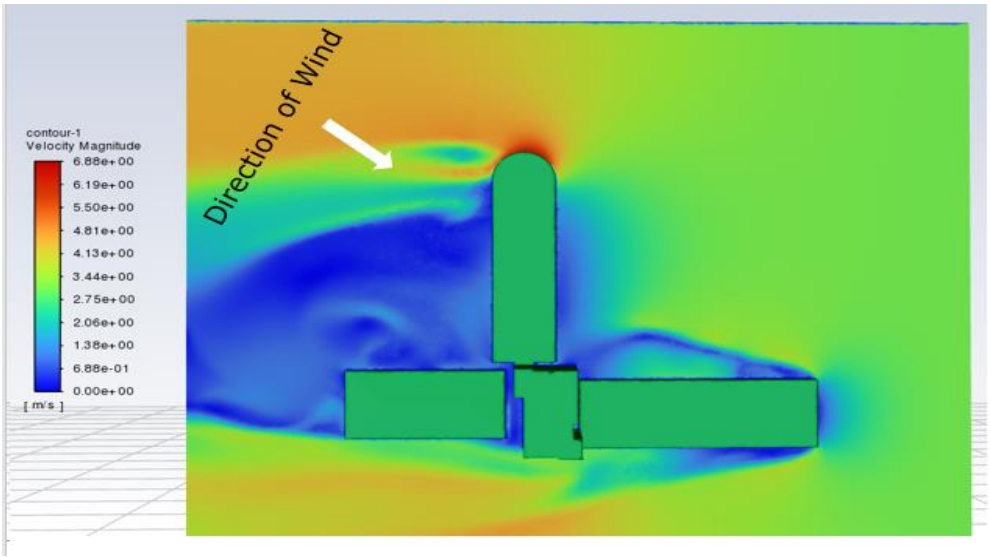

Fig. 6-1c. Velocity contour of the mid-plane (top view)

Velocity contours often correspond to pressure distributions around the building. High-velocity areas might correlate with lower pressures (areas of suction), while lower velocities may coincide with higher pressures (areas of compression). From the velocity contour on the building plane, we can see that the velocity increases in the region between the buildings (street) and around the buildings. A person walking on the street between the buildings will experience almost twice the upstream wind speed. The buildings block the wind and as a result, there is almost no wind behind the buildings (see Fig. 6.1c). Also, we can see that on the velocity contour plane there's higher velocity region, $1.891e+01\frac{m}{s}$ with Figure 6-1a compared to Figure 6-1b with a reduced top velocity, $1.862e+01\frac{m}{s}$; this can be as a result of the SST model adopted for 6-1a. SST-induced wind direction gradients also significantly modify the vorticity and divergence fields around the bowland building, weakening the vorticity response to crosswind SST gradients while enhancing the divergence response to downwind SST gradients.

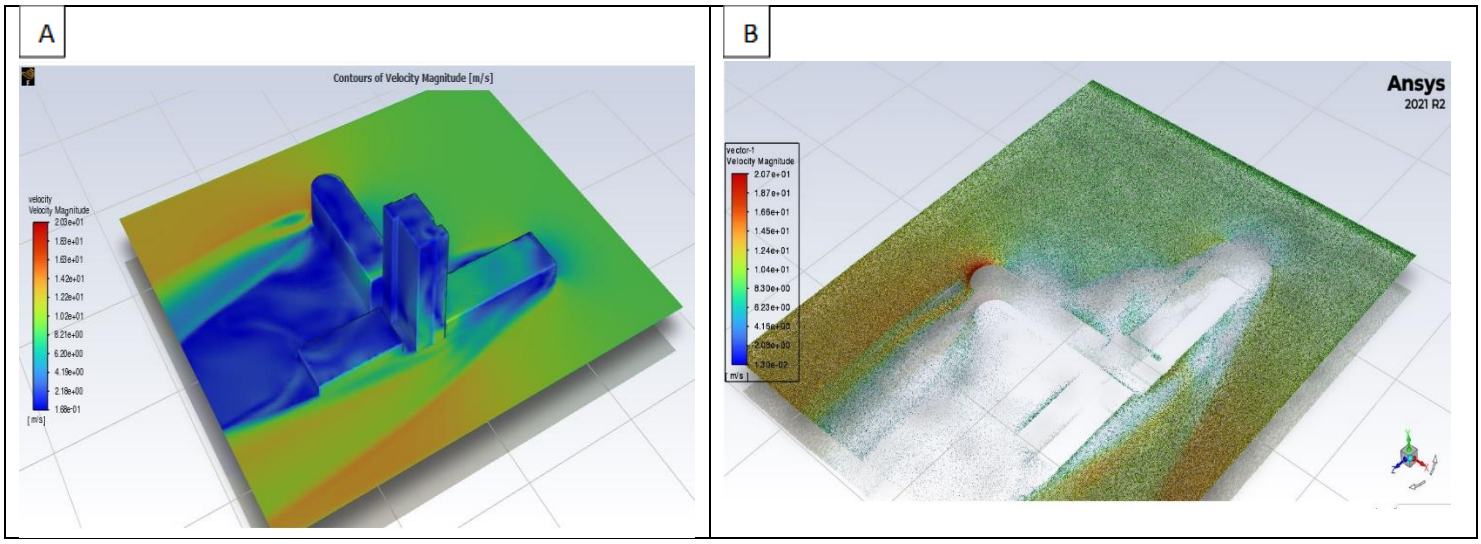

Figure 6-2. (a) The velocity magnitude of the building. (b) Velocity vectors around the buildings

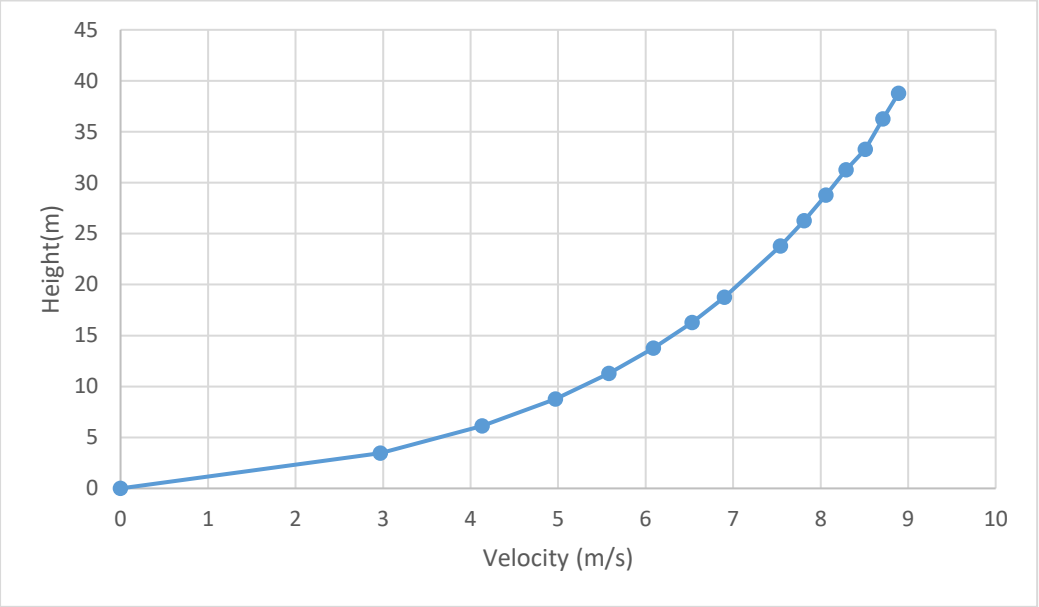

Figure 6-3. Wind velocity at different heights of the Bowland Tower.

From 6-2a & 6-2b, the recirculation zone typically forms on the leeward side of a building, where the flow separates from the surface and creates eddies or vortices. Recirculation zones can be observed along the sides of the building (building B, see table 2) facing the open area because of the flow separation at building corners; Hence, it's not advisable to install wind turbines in this region. Separation regions along street-faced sides are effectively suppressed by the flow accelerating along the street. The wind velocity is nearly 35% lower towards the middle of the building (Figure 6-1). It can also be seen that placing the wind turbine at a distance of 1 m – 3 m above the building top will lead to optimal power as the turbine is away from the maximum wind speeds. Since, the wind velocity increases with height as the wind velocity at different building height is shown in Fig. 6-3. The wind velocity of 8.89 m/s can be expected at the height of about 38.77 m.

6.2 Impact of Pressure

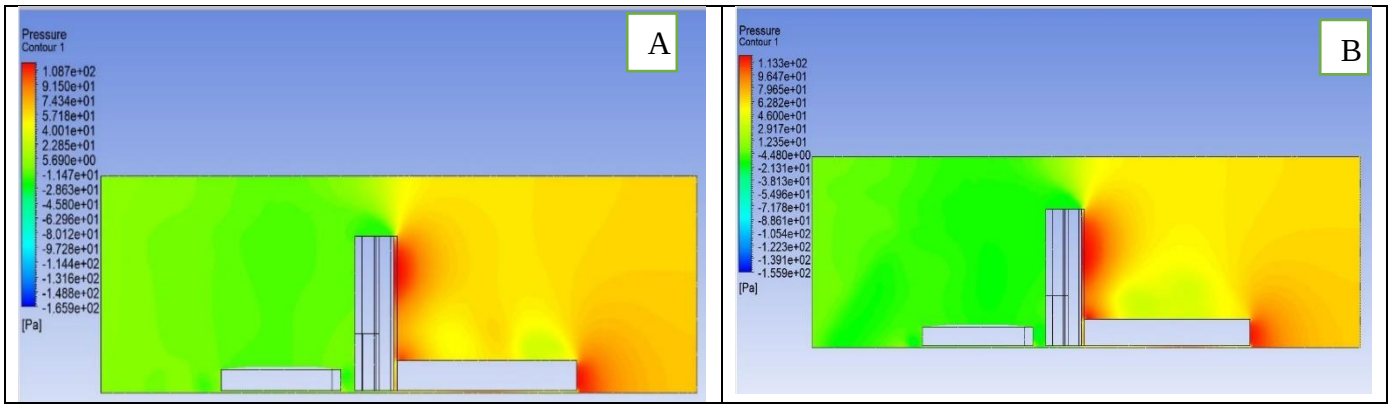

Figure 6-4.The Pressure magnitude (a) SST k—∈ turbulence model effect and (b) Renormalization Group (RNG) k –ε turbulence model effect.

From the pressure contour, it can be observed that the maximum pressure is experienced by the windward walls of the buildings facing. The maximum drag force on the building plane at SST k—∈

turbulence model effect is $1.087 * 10^2 N/m^2$ and while with Renormalization Group (RNG) k −ε turbulence model is $1.333 * 10^2 N/m^2$ and the total wall body drag force with SST model is $6.668 * 10^4 N$. Design considerations, like the geometric structure of the buildings and constructions materials, are then made by considering potential wind loads and ultimately on the wind turbine installation decisions.

6.3 Impact of Turbulence Kinetic Energy (TKE)

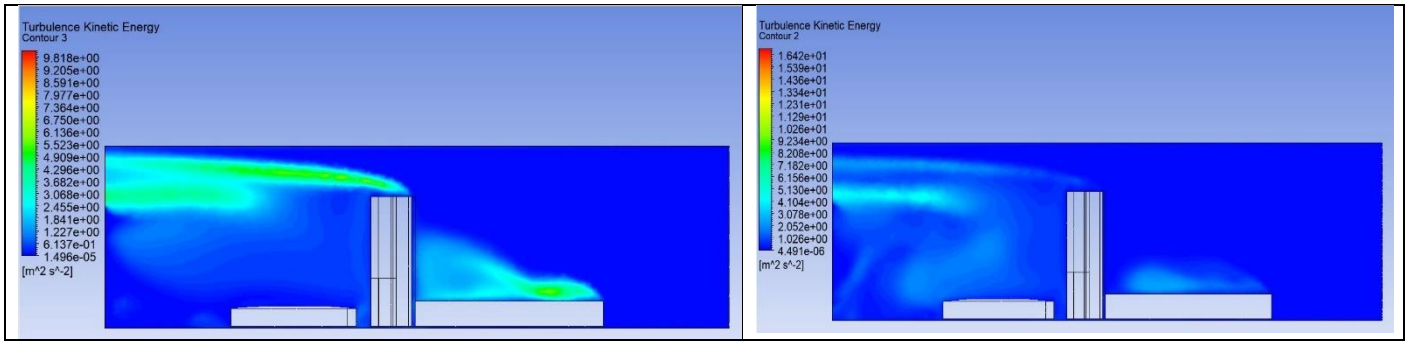

Figure 6-5.Turbulence Kinetic Energy (a) SST k—∈ turbulence model effect and (b) Renormalization Group (RNG) k −ε turbulence model effect.

The Impact of turbulence models have evidently influenced every output parameter in this research. One of the most essential capabilities of turbulent flows is TKE; Turbulent Kinetic Energy (TKE) can be used as a measure of generated flow turbulence. Figure 6-5a and 6-5b shows the TKE contours at various heights from the ground showing the separated flow is moderately turbulent with SST turbulence model and turbulent with the RNG turbulence model.

6.4 Impact of Turbulence Intensity (TI)

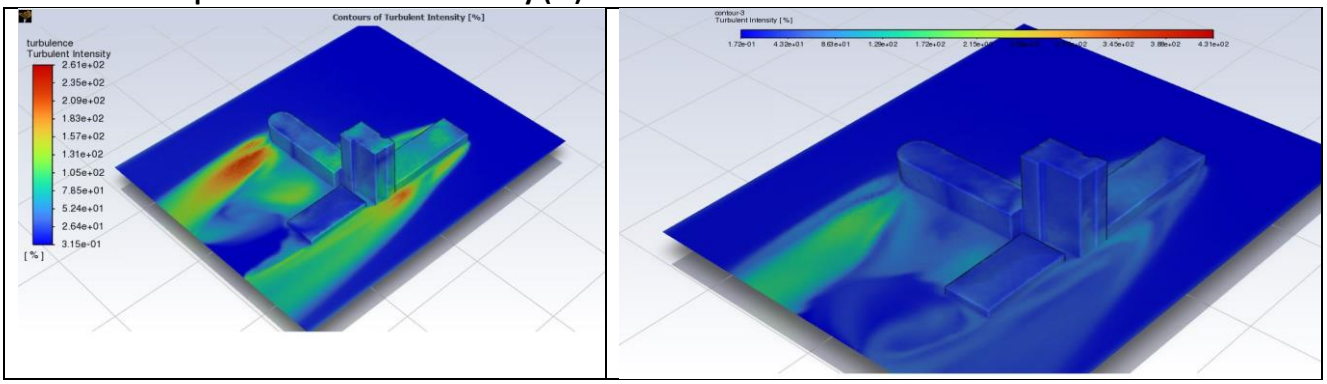

Figure 6-6. Turbulence Intensity (a) SST turbulence model effect and (b) Renormalization Group (RNG) k −ε turbulence model effect.

The shape of the building, especially the rooftop, impacts the velocity and turbulence intensity (this research further looks at different rooftops and urban configurations impact). The wind can be accelerated depending on the roof design. The turbulent intensity (TI) contours on the surface of the building including the surrounding area with the effect of two different turbulence models are shown in Fig. 6-6a and Fig. 6-6b shows the closeup view. The red area offers the maximum TI, while the blue area represents the low TI on the building. In Fig. 6-6a, maximum TI is observed close to the building floor specifically Building B. The TI then drops rapidly as the flow passes across the Building A. Hence, placing the wind turbine away from the Building B and 2.5 m above the rooftop is ideal. The average

turbulence intensity is around 52%, and it's along the surface of the building. Unlike SST model, the RNG model provided a more comfortable TI. The turbulence intensity decreases as it passes over the building, as shown in Fig. 6-6b. Complex flow phenomena, such as flow separation, vortices, or complex geometries, can lead to variations in turbulence intensity. Areas with strong flow turbulence, such as in the wake of bluff bodies or within recirculation zones, might exhibit higher turbulence intensity values.

6.5 Urban Aerodynamics: Impact of urban configuration and height on wind pattern.

The urban environment can be said to be an area with densely built-up settlements compared to other areas surrounding it. The aerodynamics of the urban environment is very complicated. Even though understanding the aerodynamics of urban environment has reportedly attracted considerable progress, urban wind flows are still being widely investigated experimentally and computationally. This is because urban flows are influenced by various components of urban environment that are not possible to be examined independently, such as complexity of building geometries and configurations which play significant role in impacting the flow pattern.

For this research, we did our urban aerodynamics investigation based on the following scenarios:

A. Configurations
   i. Urban Canyon
   ii. Staggered Urban
B. Roof Shapes
   i. Flat
   ii. Gabled
   iii. Pyramidal
   iv. Barrel Vaulted
C. Site and Height
   i. Campus: 10 m – 30 m
   ii. Residential: 4.5 m – 10 m
   iii. Business district area: 60 m – 120 m

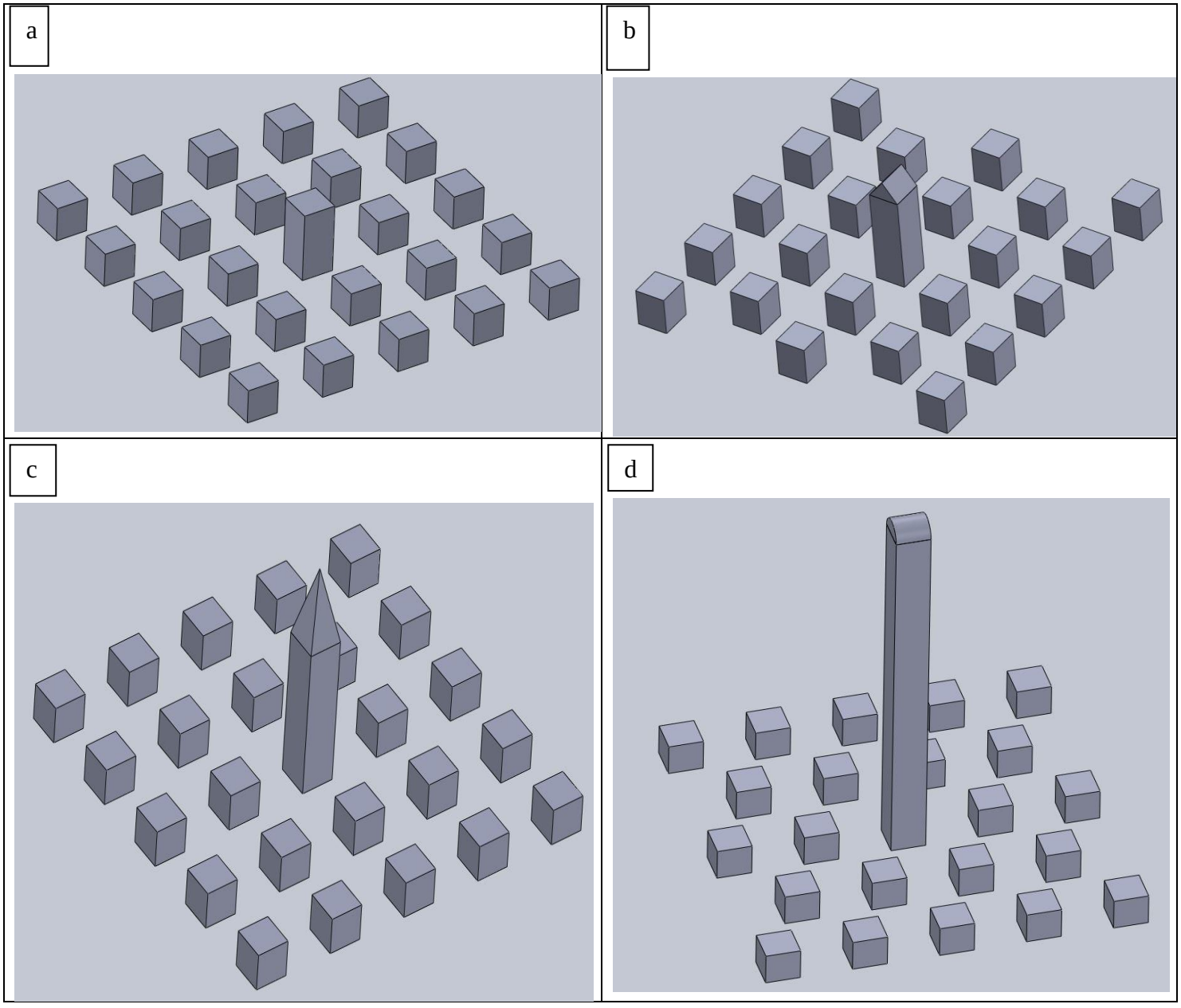

Figure 6-7: Building Geometries

The figures above show some of the urban configurations, roof shapes and height considered for the urban aerodynamics. Figure 6-7a and 6-7c are canyon urban configuration with flat and pyramidal roof shapes respectively. The Figure 6-7b and 6-7d are staggered urban configuration with gabled and barrel-vaulted roof shapes. These considerations were comprehensively studied and their impact on the wind flow pattern were accordingly obtained. Table 6.1 comprises of the simulated and results analysis of the urban aerodynamics study.

Table 6 1. Urban Aerodynamics CFD result

Configurations	Roof Shapes	Height (m)	Turbulence Model	Specific Dissipation Rate [s^-1]	Turbulence Eddy Dissipation [m^2 s^-3]	Turbulence Kinetic Energy [m^2 s^-2]	Velocity [m s^-1]	Density	Wind Power, PA
Urban Canyon	Flat	4.5	SST k-ω	20614.3158	0	1.39724	5.845465	1.225	122.33854
		4.5	RNG k-epsilon	0	3531.230555	1.554861	7.323176	1.225	240.54953
		10	SST k-ω	141377.456		1.489668	6.203042	1.225	146.19087
		10	RNG k-epsilon	0	2.16E+06	1.87E+02	8.47E+00	1.225	372.75352
		30	SST k-ω	51018.7582		1.060977	7.422323	1.225	250.45266
		30	RNG k-epsilon	0	3299.257486	1.701511	5.514901	1.225	102.7352
		60	SST k-ω	25632.4915		2.09641	2.45573	1.225	9.0708491
		60	RNG k-epsilon			7.57E+03	4.57E+00	1.225	5.85E+01
		120	SST k-ω	30632.4915		2.096409	5.171425	1.225	84.71041
		120	RNG k-epsilon	0	3.54E+09	2.27E+04	1.26E+00	1.225	1.2252303
	Gabled	4.5	SST k-ω	100644.27		1.450165	6.182099	1.225	144.71514
		4.5	RNG k-epsilon	0	3383.815377	1.499159	6.053203	1.225	135.85068
		30	SST k-ω	48162.5506		1.81199	5.24636	1.225	88.44644
		30	RNG k-epsilon	0	3783.815377	1.53556	5.86554	1.225	123.60331
		60	SST k-ω	48162.5506		2.071199	5.478936	1.225	100.73834
		60	RNG k-epsilon	0	3663.815377	1.64159	5.85303	1.225	122.81413
		120	SST k-ω	31251.6106	0.00E+00	2.45E+00	5.40E+00	1.225	96.329672
		120	RNG k-epsilon	0	2.77E+06	2.11E+00	5.40E+00	1.225	96.478852
	Barrel Vaulted	10	SST k-ω	124279.476	0	1.376366	6.619216	1.225	177.63386
		10	RNG k-epsilon	99711.1174	0	0.144877	2.235889	1.225	6.846314
		60	SST k-ω	208629.386	0	2.023183	4.909373	1.225	72.474326
		60	RNG k-epsilon	0	2.44E+08	4.37E+03	3.75E+01	1.225	32251.612
	Pyramidal	10	SST k-ω	113248.766		1.510638	6.21303	1.225	146.89819
		10	RNG k-epsilon	109818.834	0	0.15119	2.116249	1.225	5.8050557
Staggared Urban	Flat	4.5	SST k-ω	67132.6717	0	1.510369	7.598137	1.225	268.67512
		4.5	RNG k-epsilon	4005.4788	0	1.632911	7.739565	1.225	283.95907
		30	SST k-ω	36867.812		2.019413	6.688568	1.225	183.27597
		30	Realizable k-epsilon	0	1782.367143	1.514787	6.612561	1.225	177.09862
	Gabled	10	SST k-ω	41580.0428	0	1.272071	7.061329	1.225	215.65793
		10	RNG k-epsilon	0	1650.224185	1.153228	7.03369	1.225	213.13549
		60	SST k-ω	27191.7149		2.010068	6.053872	1.225	135.89573
		60	Realizable k-epsilon	0	133806.8859	126.860673	9.048222	1.225	453.72827

The Table 6.1 give a comprehensive study on the investigation of the effect of urban configurations with focus on parameters such as the height, turbulence model, specific dissipation rate, turbulence kinetic energy (TKE), wind velocity and wind power density.

The studies involved how the urban canyon configuration and staggered canyon configurations impact the wind flow pattern. The table also shows how these parameters change with different height and configuration. For an instance, we can see the effect of both the flat roof shape and height on the turbulence kinetic energy. Furthermore, graphs and simulations visualizations outputs are used below to explicitly explain some of the tabulated results.

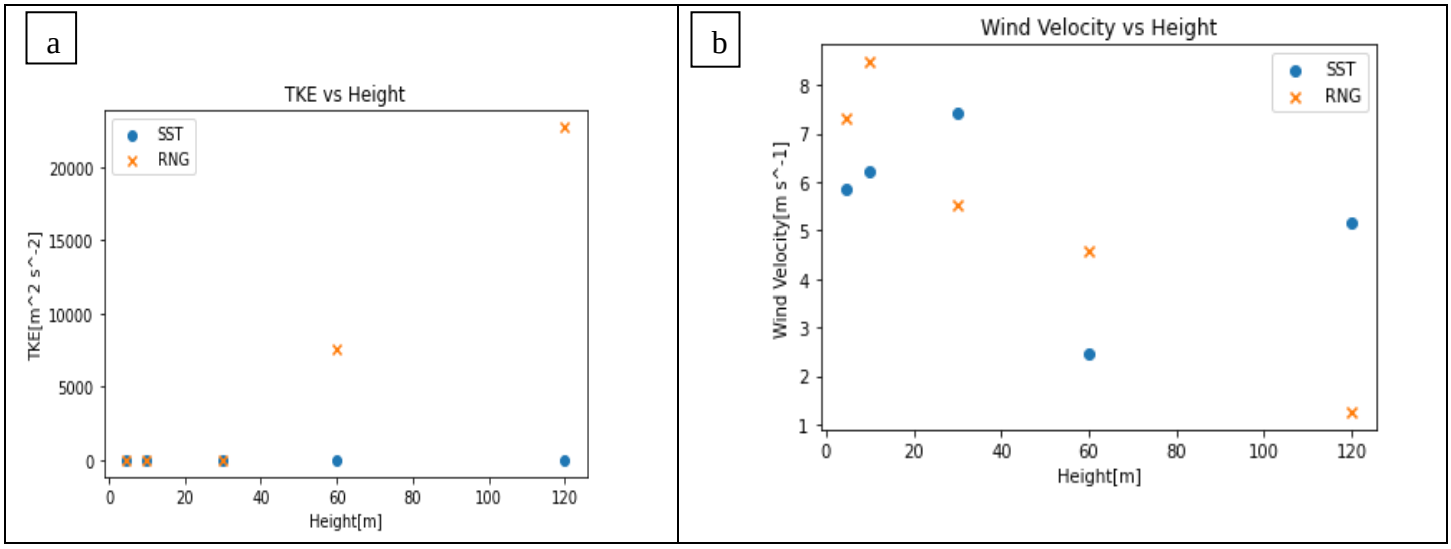

Figure 6-8. Urban Canyon, flat shape roof impact on TKE and Wind velocity for SST and RNG model.

The graphical output and figures above are the result from the simulation of urban canyon configuration with the consideration of the flat roof shape buildings with residential height of 4.5 m, campus with 10-30 m and business district area with 60 m-120 m. The figure considered two different turbulence models: the SST and RNG model. For the SST model, the TKE has a steady but slightly increment with the height while the RNG model initially showed a steady increment between 4.5 m till 30 m and then took a significant increment from height 60 m to 120 m. Unlike the TKE Vs Height relationship, the Wind velocity vs Height interaction gave a different output for both turbulence models. For the SST, the velocity at height, 30 m is the highest while height, 60 m has the lowest wind velocity. The RNG model displays a steady decrease in wind velocity with buildings height, which makes 10 m with the largest wind velocity and 120 m with the lowest wind velocity.

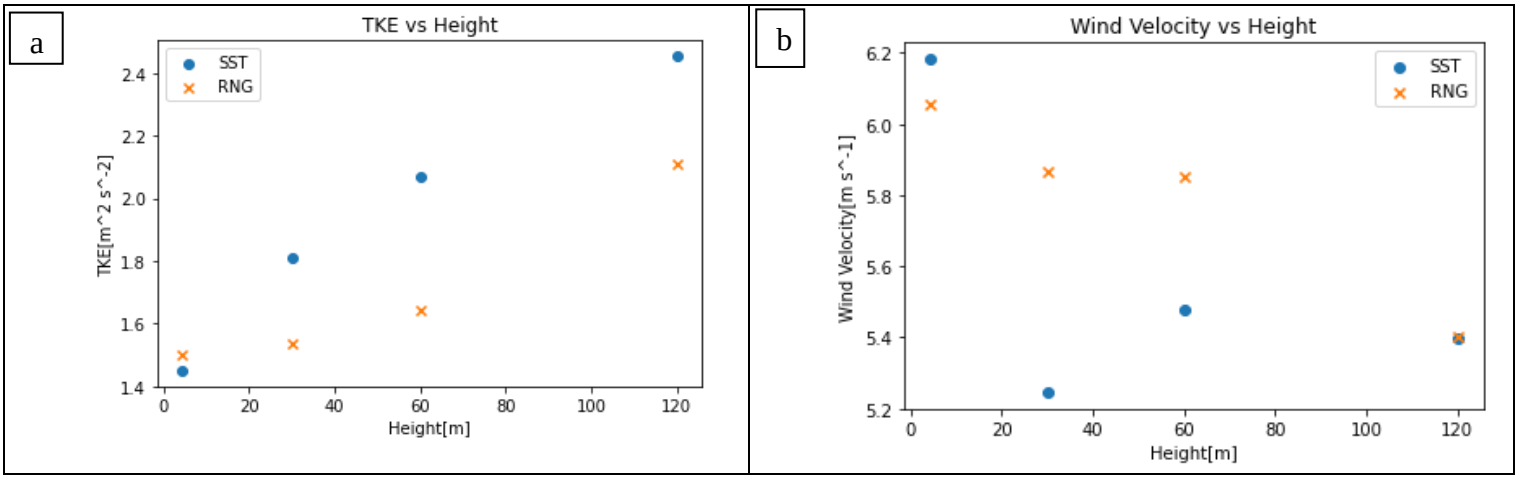

Figure 6-9.Urban Canyon, gabled shape roof impact on TKE and Wind velocity for SST k—∈ and RNG model.

From Figure 6-9a, the SST model shows that the turbulence kinetic energy increases with height and the RNG model display the same occurrence with the 120 m height having the highest TKE and the height 4.5m having the smallest TKE for both. It's a different understanding with the wind velocity vs height plot (see Figure 6-9b), as the SST model displayed some unsteady velocity values with the smallest building having the highest wind velocity while the building height 30 m has the lowest wind velocity. RNG model structures out an increment in wind velocity with respect to the lowest building i.e the smallest building has the highest wind velocity and vice versa. The impact of both the SST and RNG models are quite significance to the wind flow pattern and ultimately, for the wind turbine implementation.

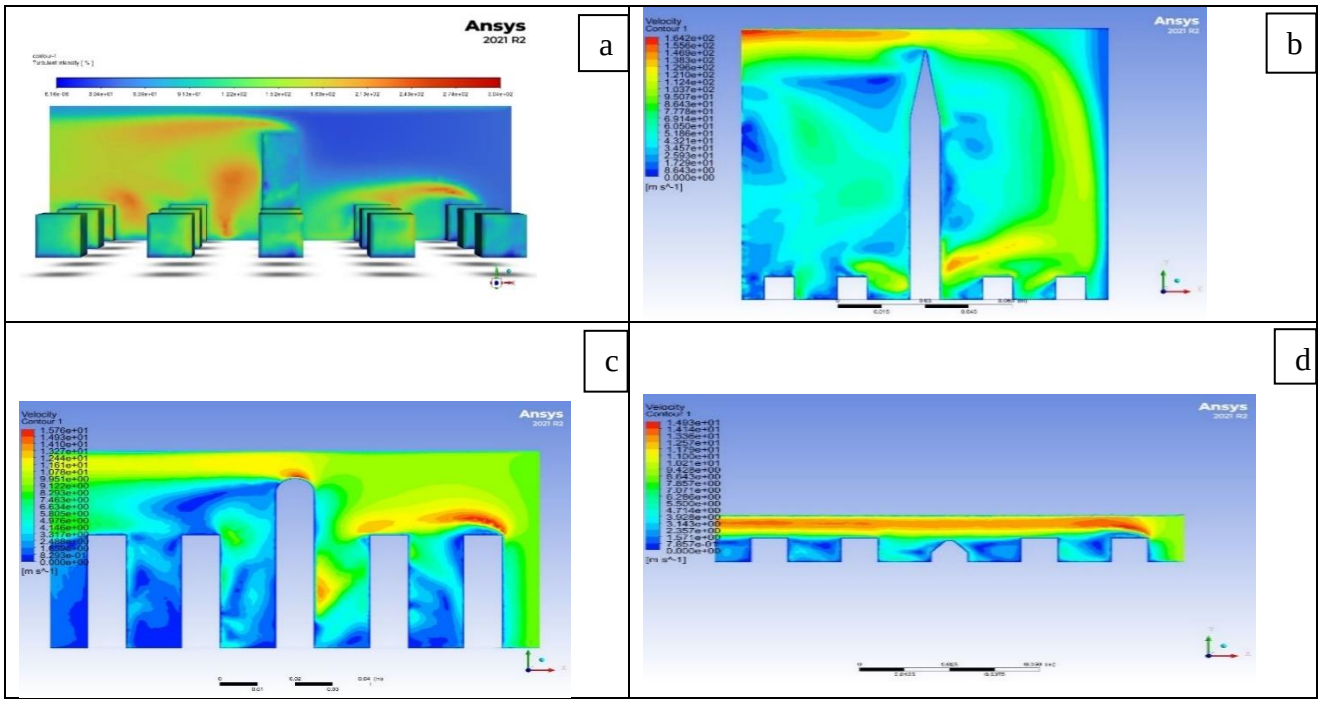

Figure 6-10.(a) Turbulence intensity contour of a 60 m building for a canyon urban configuration. (b) Wind velocity contour at 129 m for RNG turbulence model. (c) Gabled roof shape, 60m velocity contour. (d) The velocity contour of a barrel-vaulted building,10 m.

Furthermore, barrel vaulted and pyramidal roof shapes were also studied and the staggered urban configurations were equally studied for all roof shapes as indicated on the table 6-1. The barrel-vaulted roof was studied along height 10 m and 60 m, for both turbulence models. The TKE of the SST for height 10 m is lower than that of 60 m. For the same SST, the wind velocity is greater than that of 10 m, that means as the TKE increases with height and reduces with wind velocity across the barrel-vaulted roof shape. For the RNG, both the TKE and wind velocity increases with the height. The pyramidal roof shape indicates higher value for both the TKE and the wind velocity; though, only one height, 10 m was considered.

The second urban configuration considered was the staggered urban. Here we considered three (3) different turbulence modelling namely SST, RNG, and the realizable k-epsilon across four different heights. Some things changed with respect to the Bowland tower scenario; such as wind velocity decreasing with the height. These discrepancies observed and reported are as a result of different wind effect; these effects are explained as follows.

6.6 Wind Effects Generated by Buildings

Buildings produce three major wind effects: downwashing, channelling, and corner acceleration. Each of these will be illustrated using the above (Figure 6-7 – 6-10) urban aerodynamics as an example.

a. ***Downwashing***: When a tall building (see Figure 6-7a – 6-7d) is surrounded by shorter buildings, the downwash effect occurs. The tall skyscraper absorbs wind at upper levels and redirects it to the bottom, generating a three-dimensional downward flow. As a result, this impact frequently causes a substantial recirculation at ground level, resulting in increased wind activity. With our example, we can see the airflow moving downwards, increasing wind velocity at lower elevations from Fig. 6-8b and 6-9b.

b. ***Channelling:*** When buildings are close to one another, the channelling (also known as Venturi) effect occurs. The effect is sustained by a decrease in wind pressure, which causes wind acceleration in the narrow channel formed between the buildings. This impact can produce powerful gusts, which can be hazardous to pedestrians. This impact may be shown in our model, as narrow corridors enhance wind velocity see Fig. 6-10a – 6-10b.

c. ***Corner acceleration:*** When the wind hits the vertical edge of a tall building, which seems to be the reason we experienced the output in Fig. 6-8a and 6-8b, it causes corner acceleration. This effect is primarily caused by acute building forms, which cause acceleration at bends. Tall building corners are the areas that might cause the most discomfort in a built environment. Winds from the south-west cause considerable corner acceleration in our scenario, as shown above.

6.7 Assessment of wind energy amplification effect

To evaluate the wind energy concentration effect over the roof, we apply the amplification factor F (see Eq. (76)) to compare the wind potential of the roof shape configuration models with the free field wind potential. Models of reference buildings with H = 4.5 m, H = 30 m, H = 60 m, and H = 120 m were chosen for assessment here. To clarify the differences among different inlet angles, values of M from two symmetrical angles were averaged. Variations of the factor F between the turbulence model and roof shapes and among three assessment altitudes are shown.

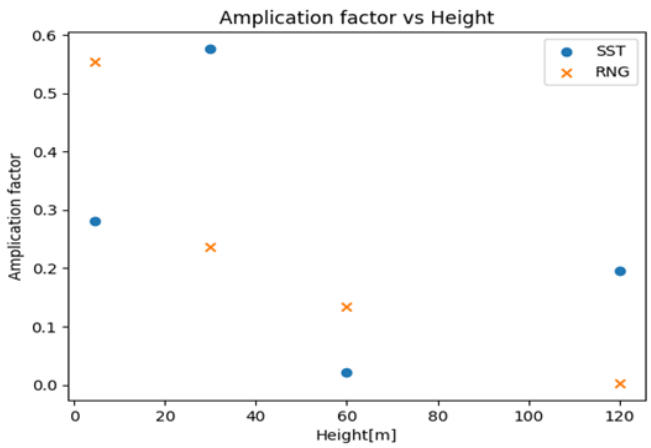

Figure 6-11 Wind energy amplification at the flat roof and different height

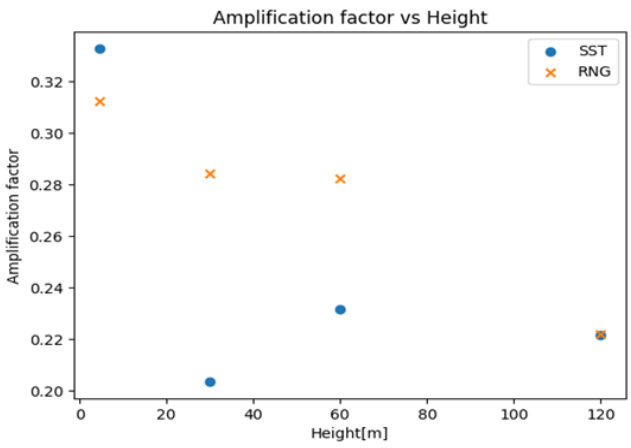

Figure 6-12 Wind energy amplification at the gabled roof and different height

From Fig. 7- 1 and 7-2 we can see that:

a. The amplification factor of SST k—ω model and flat roof shape; H= 4.5 m compared with that of H= 120 m shows obviously larger values when the test altitude is low enough to develop wind energy.
b. The amplification factor of model H= 30 m compared with that of H = 4.5 m and H = 120 m signify fluctuations in the wind energy development which is as a result of RNG model.
c. The gabled roof exhibit decreases in amplification factor with height for both the SST model and RNG model. It appears that the corner shape structures need to reach a specific height in order for wind energy generation over their roofs to be profitable and feasible.
d. The general amplification factor increases and then drops as the assessment altitude increases. This indicates that an optimal altitude for wind energy growth over the roof should exist. They can be evaluated if more altitudes are evaluated for any specific circumstances.

Chapter 7 Validation and Verification of results

Validation assessments are model accuracy assessments by comparing results obtained from either experiment with prediction or analyses obtained from simulation and determination of accuracy based on set rules. In addition, it is commonly necessary to assess the accuracy of a model's predictions for conditions where experimental data are not available (i.e., where extrapolation of the model is required).
The verification of the results is an integral part of any kind of simulation or modelling. Without verification it is not possible to be proved that the results are in correct direction and reliable. In this process, we have to compare the model's implementation and its associated data with the conceptual description/analytical method and specifications. Since there are no tunnel experiment data available for direct validation with our models, we made an extensive CFD parameter study validated by published tunnel experiment data and analytical method. In addition, the evaluation of the accuracy of the simulations results is very important as it gives a good ground for improvement in the simulations.

7.1 Verification using the relative error study

For relative error, the velocity, turbulence kinetic energy (TKE), and turbulence dissipation rate (TDR) of the Bowland tower were used by comparing the analytical method with the simulations results in all considered mesh sizes namely M1, M2, M3 and M4 respectively represented in the colour pane Blue (M1), Orange (M2), Green (M3), and Yellow (M4).

Relative error = (expected value - actual value) / actual value) x 100

The evaluation of the accuracy of the simulation results are very important as it gives a good ground for improvement in the simulations. For the TDR, results show that about 90% of the coarse mesh (M1) have values less than 1% while the Fine mesh (M2), Finer mesh (M3), and Finest mesh (M4) have about 94%, 95%, and 96% values less than 1%; which indicates that the smaller the mesh sizes, the most likely the accuracy of the results as compared to the analytical method. Although, there's an appearance of some large relative error points on the Finest mesh (M4), this could be as result of some deflected mesh algorithm due to computing. As indicated on the Table 7-1; TKE relative error % shows similar trend for all comparison of simulations with the MCM but the finer mesh (m3) shows the most consistent values. General relative error % of velocity across the four mesh sensitivities can be seen to have values less than 3%; this is quite interesting as it means that the value of the wind indicator (wind turbines) increases.

Table 7-1. Verification table showing the analytical method comparison with the mesh sensitivity study output.

Manual Computation Method (MCM)			M1 (Coarse Mesh)			M2(Fine Mesh)			M3(Finer Mesh)			M4(Finest Mesh)		
Velocity(m/s)	Turbulent kinetic energy, k	Specific Turbulence Dissipation	Specific Dissipation Rate [s^-1]	Turbulence Kinetic Energy [m^2 s^-2]	Velocity [m s^-1]	Specific Dissipation Rate [s^-1]	Turbulence Kinetic Energy [m^2 s^-2]	Velocity [m s^-1]	Specific Dissipation Rate [s^-1]	Turbulence Kinetic Energy [m^2 s^-2]	Velocity [m s^-1]	Specific Dissipation Rate [s^-1]	Turbulence Kinetic Energy [m^2 s^-2]	Velocity [m s^-1]
8.89	1.4110561	5.3994492	0.816	0.443	13.1	1.78	0.000141	8.83	63.1	0.0068	8.92	108	0.0123	8.92
8.71	1.354494	5.290124	2.33	0.000192	8.91	1.21	0.525	4.66	66.7	0.00728	8.92	132	0.0214	8.93
8.51	1.293004	5.1686516	2.7	0.000226	8.79	4.92	0.000426	8.93	265	0.0334	8.92	354	0.0455	8.92
8.29	1.2270149	5.0350319	7.89	0.000709	8.91	40.2	0.00419	8.92	47.8	0.00512	8.92	356	0.0458	8.92
8.06	1.1598741	4.8953387	6.76	1.93	6.9	165	0.0196	8.92	3.3	0.00362	8.94	148	0.0173	8.92
7.81	1.0890375	4.7434981	0.51	0.000235	10.4	0.914	0.0000684	9.3	0.516	0.000037	9.44	186	0.0223	8.92
7.54	1.0150407	4.5795104	0.498	0.0235	12	0.565	0.0000411	9.06	0.511	0.000585	11.5	94.2	0.0105	8.92
6.9	0.8500392	4.1907986	1.61	0.0361	8.93	0.852	0.0000962	9.31	49.5	0.00521	8.92	115	0.0131	8.92
6.53	0.7613198	3.9660746	0.57	0.0599	11	0.333	0.241	4.07	0.401	0.0000293	12.4	96.4	0.0108	8.92
6.09	0.6621789	3.6988353	0.424	0.0535	12.5	0.368	0.663	3.24	0.355	0.0182	14.1	113	0.0128	8.92
5.58	0.555916	3.3890806	40	0.00584	1.21	1.29	2.59	4.19	2.63	0.000249	1.87	117	0.0135	8.92
4.97	0.4410152	3.0185897	0.853	1.87	8.71	0.696	0.0537	14.1	76.5	0.00839	8.92	170	0.0201	8.92
4.13	0.3045376	2.5084055	10.4	0.957	0	0.612	1.43	2.03	51	0.00541	8.92	393	0.0512	8.92
2.97	0.1574902	1.8038655	3.03	0.0966	0	0.62	1.46	2.01	48.3	0.00508	8.92	4.17	3.32	8.14
0	0	0	5.67	0.277	0	2.42	0.133	1.48	3.45	0.0314	1.09	0.289	0.0000377	13.2

Table 7-2. Relative error from the verification table.

Relative Error %											
Specific Dissipation Rate [s^-1]	Turbulence Kinetic Energy [m^2 s^-2]	Velocity [m s^-1]	Specific Dissipation Rate [s^-1]	Turbulence Kinetic Energy [m^2 s^-2]	Velocity [m s^-1]	Specific Dissipation Rate [s^-1]	Turbulence Kinetic Energy [m^2 s^-2]	Velocity [m s^-1]	Specific Dissipation Rate [s^-1]	Turbulence Kinetic Energy [m^2 s^-2]	Velocity [m s^-1]
0.848873	0.686051	-0.47357	0.670337	0.9999	0.006749	-10.6864	0.995181	-0.00337	-19.002	0.991283	-0.00337
0.559557	0.999858	-0.02296	0.771272	0.612401	0.464983	-11.6084	0.994625	-0.02411	-23.9522	0.984201	-0.02526
0.47762	0.999825	-0.0329	0.048108	0.999671	-0.04935	-50.2706	0.974169	-0.04818	-67.4898	0.964811	-0.04818
-0.56702	0.999422	-0.07479	-6.98406	0.996585	-0.076	-8.49348	0.995827	-0.076	-69.7046	0.962674	-0.076
-0.38091	-0.66397	0.143921	-32.7055	0.983102	-0.1067	0.325889	0.996879	-0.10918	-29.2328	0.985085	-0.1067
0.892484	0.999784	-0.33163	0.807315	0.999937	-0.19078	0.89122	0.999966	-0.20871	-38.2116	0.979523	-0.14213
0.891255	0.976848	-0.59151	0.876624	0.99996	-0.20159	0.888416	0.999424	-0.5252	-19.5699	0.989656	-0.18302
0.615825	0.957531	-0.2942	0.796697	0.999887	-0.34928	-10.8116	0.993871	-0.29275	-26.4411	0.984589	-0.29275
0.856281	0.921321	-0.68453	0.916038	0.683444	0.376723	0.898892	0.999962	-0.89893	-23.3061	0.985814	-0.366
0.885369	0.919206	-1.05255	0.900509	-0.00124	0.46798	0.904024	0.972515	-1.31527	-29.5502	0.98067	-0.4647
-10.8026	0.989495	0.783154	0.619366	-3.65898	0.249104	0.223978	0.999552	0.664875	-33.5226	0.975716	-0.59857
0.717418	-3.24022	-0.75252	0.769429	0.878235	-1.83702	-24.343	0.980976	-0.79477	-55.3177	0.954423	-0.79477
-3.14606	-2.14247	1	0.75602	-3.69564	0.508475	-19.3316	0.982235	-1.15981	-155.673	0.831876	-1.15981
-0.67973	0.386629	1	0.656294	-8.27042	0.323232	-25.7758	0.967744	-2.00337	-1.3117	-20.0807	-1.74074
0	0	0	0	0	0	0	0	0	0	0	0

Chapter 8 Conclusion and Recommendation.

The aims of the research as defined in the beginning of the programme, were achieved in the majority. The theoretical background and the numerical model, which were the principal elements to be considered to estimate the wind pattern in urban areas, were developed covering the initial thoughts of the author and business partner, O-innovation. Urban wind energy consists of the utilization of wind energy technology in applications to the urban and sub-urban built environment. Bowland Tower building and environs were considered for this research and in extension; buildings of different heights, various urban areas configurations and different roof shapes were also considered.

The research also indicated that while substantial progress has been made in the wind engineering fields, there is a strong need for additional comprehensive research, especially in area of urban aerodynamics and wind resource assessment, to optimize the generation and utilization of urban wind energy. It has been well established that mean wind speeds in urban areas are lower than in suburbs or rural areas. Tall buildings of different heights and shapes, which form most urban buildings, provide form and frictional drag to the wind flow. This drag tends to create turbulence, which produces local rapid changes in the direction and the speed of the wind. Furthermore, pressure gradients across the buildings (between windward and leeward sides) and along their height induce strong wind eddies. The Urban configuration is very important because besides building geometry, spacing of the buildings can also influence the aerodynamics of urban environment. Apparently, closely spaced buildings can create higher form drag causing winds to move quickly over the top and form eddies between them. Also, such building configurations may act as channels for the flow, in which the wind moves at faster speeds, particularly near ground level, as was indicated by (van Hooff and Blocken, 2012)

8.1 Conclusion

This research presents the feasibility assessment for the Bowland tower and environment. At the first step, the wind speed and wind direction data in Lancaster university (Hazelrigg weather centre) and from CEDA were evaluated by means of a wind data analysis. Subsequently, the wind data analysis results, in conjunction with the statistical analysis results of the long-term meteorological data measurement from CEDA, were adopted to predict the anticipated wind velocity and windrose outputs of these building. The main outcomes of this study are summarized as follows:

I. The development of a windrose using the huge data from CEDA and Lancaster, and sixteen directions were equally divided into in a circle, in which each direction contains 45◦ with 22.5◦ to the left and right of the direction point.
II. Based on the provided weather data, wind direction distributions are calculated by self-programmed statistical methods and a windrose was developed. For Hazelrigg weather station, the prevailing wind direction is the South-Southeast, and other dominant directions are East-southeast (ESE) and Northeast (NE), as demonstrated on the windrose in Fig. 3-2.
III. For the CEDA data, the prevailing wind direction is the South- Southwest, and over 50% wind flows from the direction (see Table 1). Less wind blows from the North and West-Southwest, and it could be as a result of the meteorological station having a rough terrain which could affect the local wind direction and wind speed distributions.

In this study, CFD simulations and field measurements have been conducted to evaluate the wind resources available in an urban area. By taking into account the details of the local urban topography and boundary conditions of the micro-environment, the predicted wind speed, direction and turbulence level are compared with the manual computed method and historical data to validate the

computational model in order to improve the accuracy of the estimates of the wind power by using CFD-based evaluation procedures to determine potential mounting sites and urban wind power production. The main conclusions are summarized below:

I. The simulated results by using the SST k—e model indicate that the calculated velocities agree well with the measured data in the windward region with differences less than 10%, whereas the discrepancies could be up to approximately 20% in the leeward region. The predicted wind direction matches well with the measured results in general. Besides, the SST k—e model provides more reasonable predictions of turbulence intensity for simulations of the swirling and separating flows around buildings than those with the use of the standard and RNG k–e models.

II. The simulated results clearly show the effects of geometric details of the surrounding structures on the wind pattern around the objective building in determining potential mounting sites for the O-Wind turbine implementation in a complex urban terrain. In essence, the high-rise building (Building A as depicted in Fig. 3-4) and as indicated on Table 3-1; in the upstream direction of the studied site tend to block the incoming wind and induce higher turbulence intensity over certain areas of the objective building.

III. It is also found to be favourable to increase the hub height and install turbines on the windward side of the building to acquire higher wind power production. The proposed CFD evaluation procedures used in this research would be useful for conducting design models with the factors of lowest mounting height, power density, turbulence intensity and cost so as to optimize potential mounting sites and wind power estimates.

IV. Finally, the major objective of the research was established. The impact of wind pattern in urban areas are dependent on several factors such as the urban configurations of the areas, roof shapes and height of the buildings, and the wind effect generated by these buildings. These established points will guide the decision making of implementation of the bladeless wind turbine or any other systems of similar potentials in an urban area settlement.

8.2 Recommendation for Potential Improvements of the Project

It is suggested that to improve understanding of the issues highlighted above that further research includes but is not limited to the following areas:

I. There should be full development of the objective buildings either in 3D printing or a prototype and it should be subjected to wind tunnel test in order to facilitate good experimental data.

II. The building of interest should have an attached bladeless wind turbine to run simulations. Although, this research has successfully studied the impact of wind pattern on any wind turbine implementation with great focus on the urban configuration, it is important that any product of the O-wind bladeless turbine should be subjected to these findings.

III. The study was largely on SST and RNG turbulence modelling with few studies on the realization k-epsilon turbulence model, it's highly recommended that there should be studies of comparison with other turbulence modelling such as the LES; although, previous work suggested SST, RNG and Realization turbulence model as the best.

IV. Simulation is expensive and running complex geometries is even more expensive. It's recommended that there should be full implementation of machine learning algorithm to make subsequent output predictions. Even though, some machine learning algorithms were used for this study in making the CFD results more relatable and the field measurement data more usable.

References

Faro, A.A *et al.* (2021) 'Study of the Stress Distribution Due to the Effect of Transient Analysis on a Vertical Pressure Vessel and Validation using the Mesh Independence Study', *Journal of Advanced Mechanical Engineering Applications*, 02(01), pp. 1–12. doi:10.30880/jamea.2021.02.01.001.

Al-Mulali, U. *et al.* (2013) 'Exploring the relationship between urbanization, energy consumption, and CO2 emission in MENA countries', *Renewable and Sustainable Energy Reviews*, 23, pp. 107–112. doi:10.1016/j.rser.2013.02.041.

Allen SR, Hammond GP, M.M. (2008) 'Energy analysis and environmental life cycle assessment of a micro-wind turbine.', *The Institution of Mechanical Engineers, Part A: Journal of Power and Energy.*, 22(7), pp. 669–684.

ANSYS (2017) 'Pressure-Velocity Coupling', *https://www.afs.enea.it/project/neptunius/docs/fluent/html/th/node373.htm*.

Bahaj, A.S., Myers, L. and James, P.A.B. (2007) 'Urban energy generation: Influence of micro-wind turbine output on electricity consumption in buildings', *Energy and Buildings*, 39(2), pp. 154–165. doi:10.1016/j.enbuild.2006.06.001.

Barbu, C. & Vyas, P. (2009) 'System and method for loads reduction in a horizontal-axis wind turbine using upwind information, US patent application', *20,090,047,116,* [Preprint].

Bauer. F et al. (2019) 'Control of a drag power kite over the entire wind speed range', *J. Guid. Control Dynam.*, pp. 1–16.

Bhandari, M., Shrestha, S. and New, J. (2012) 'Evaluation of weather datasets for building energy simulation', *Energy and Buildings*, 49, pp. 109–118. doi:10.1016/j.enbuild.2012.01.033.

Blocken, B. (2014) '50 years of Computational Wind Engineering: Past, present and future', *Journal of Wind Engineering and Industrial Aerodynamics*, 129, pp. 69–102. doi:10.1016/j.jweia.2014.03.008.

Burton, T. *et al.* (2011) *Wind Energy Handbook*. Wiley. doi:10.1002/9781119992714.

Carter, J. (2011) *The Effect of Wind Farms on Residential Property Values in Lee County, Illinois PLEASANT RIDGE EXHIBIT 33*.

Cavada, M., Hunt, D.V.L. and Rogers, C.D.F. (no date) *Smart Cities: Contradicting Definitions and Unclear Measures*. Available at: http://www.songdo.com.

Chandel, S.S., Ramasamy, P. and Murthy, K.S.R. (2014) 'Wind power potential assessment of 12 locations in western Himalayan region of India', *Renewable and Sustainable Energy Reviews*, 39, pp. 530–545. doi:10.1016/j.rser.2014.07.050.

Cook, K.R. & Gruenbacher, B. (2008) *Assessment of methodologies to forecast wind gust speed National Weather Service Weather Forecast Office.*

Csavina, J. *et al.* (2014) 'Effect of wind speed and relative humidity on atmospheric dust concentrations in semi-arid climates', *Science of the Total Environment*, 487(1), pp. 82–90. doi:10.1016/j.scitotenv.2014.03.138.

Dahbi, M., Benatiallah, A. and Sellam, M. (2013) 'The analysis of wind power potential in Sahara site of Algeria-an estimation using the "Weibull" density function', *Energy Procedia*, 36, pp. 179–188. doi:10.1016/j.egypro.2013.07.021.

Davidovic, D. *et al.* (2014) 'Airflow study for a cluster of of campus buildings using different turbulence modeling approaches', *Built*, 3(January), pp. 33–56.

Department for Business, E.& I.S. (2022) 'Digest of UK Energy Statistics (DUKES): electricity', *https://www.gov.uk/government/statistics/electricity-chapter-5-digest-of-united-kingdom-energy-statistics-dukes*.

Department for Energy Security and Net Zero (2022) 'Energy Trends: UK weather', *https://www.gov.uk/government/statisticsDepartment for Energy Security and Net Zero (2022) 'Energy Trends: UK weather', https://www.gov.uk/government/statistics/energy-trends-section-7-weather./energy-trends-section-7-weather*.

Department of business, energy and industrial strategy (2022) *UK ENERGY IN BRIEF 2022*.

Dutton, A. G., Bonnet, P. A., Hogg, P., & Lleong, Y.L. (2005) 'The feasibility of building mounted/integrated wind turbines (BUWTs): achieving their potential for carbon emission reductions', *Final Report, Under Contract of Carbon Trust (2002-07-028-1-6), Energy Research Reference, CCLRC*.

European Wind Energy Association. (2009) *Wind energy – the facts, part I: Technology, The annual variability of wind speed*.

FEA (2022) *FEA Tips*. Available at: https://featips.com/2021/05/07/how-to-verify-mesh-quality-in-ansys-workbench/#:~:text=If you look under Mesh,statistics for the selected metric.

Gao, C.F. and Lee, W.L. (2011) 'Evaluating the influence of openings configuration on natural ventilation performance of residential units in Hong Kong', *Building and Environment*, 46(4), pp. 961–969. doi:10.1016/j.buildenv.2010.10.029.

Georgiadis, N.J. *et al.* (2006) 'Aerodynamic design and analysis of high performance nozzles for mach 4 accelerator vehicles', *Collection of Technical Papers - 44th AIAA Aerospace Sciences Meeting*, 1(January), pp. 202–215. doi:10.2514/6.2006-16.

Georgiadis, N.J., Yoder, D.A. and Engblom, W.A. (2006) 'Evaluation of modified two-equation turbulence models for jet flow predictions', *Collection of Technical Papers - 44th AIAA Aerospace Sciences Meeting*, 8(January), pp. 5896–5911. doi:10.2514/6.2006-490.

Grant, A., Johnstone, C. and Kelly, N. (2008) 'Urban wind energy conversion: The potential of ducted turbines', *Renewable Energy*, 33(6), pp. 1157–1163. doi:10.1016/j.renene.2007.08.005.

Haas, T. (2019) 'Struggles in European Union energy politics: a gramscian perspective on power in energy transitions', *Energy Res. Social Sci.,* pp. 66-74,.

Hassanm, Y.H. & Hill, D.R. (1986) 'Islamic Technology: An Illustrated History', *Cambridge University Press* [Preprint].

Hassid, S. and Galperin, B. (2004) 'Comments on "An improved model for the turbulent PBL"', *Journal of the Atmospheric Sciences*, 61(10), pp. 1197–1199. doi:10.1175/1520-0469(2004)061<1197:COAIMF>2.0.CO;2.

Heintzelman, M.D. and Tuttle, C.M. (no date) *Values in the Wind: A Hedonic Analysis of Wind Power Facilities*. Available at: http://www.eia.doe.

Hemida, H. *et al.* (2020) 'On the flow over high-rise building for wind energy harvesting: An experimental investigation of wind speed and surface pressure', *Applied Sciences (Switzerland)*,

10(15). doi:10.3390/APP10155283.

Hinman, J.L. (2010) *WIND FARM PROXIMITY AND PROPERTY VALUES: A POOLED HEDONIC REGRESSION ANALYSIS OF PROPERTY VALUES IN CENTRAL ILLINOIS*.

Hoen, B. *et al.* (2009) *The Impact of Wind Power Projects on Residential Property Values in the United States: A Multi-Site Hedonic Analysis*. Berkeley, CA (United States). doi:10.2172/978870.

Hoen, B. *et al.* (2015) 'Spatial Hedonic Analysis of the Effects of US Wind Energy Facilities on Surrounding Property Values', *Journal of Real Estate Finance and Economics*, 51(1), pp. 22–51. doi:10.1007/s11146-014-9477-9.

van Hooff, T. and Blocken, B. (2012) 'Full-scale measurements of indoor environmental conditions and natural ventilation in a large semi-enclosed stadium: Possibilities and limitations for CFD validation', *Journal of Wind Engineering and Industrial Aerodynamics*, 104–106, pp. 330–341. doi:10.1016/j.jweia.2012.02.009.

Hub, R.E. (2022) 'No Title', *https://www.renewableenergyhub.co.uk/main/wind-turbines/how-much-does-a-wind-turbine-cost/*.

IRENE (2022) *Wind Power*, *IRENA - International Renewable Energy Agency*. Available at: https://www.irena.org/costs/Power-Generation-Costs/Wind-Power#:~:text=The global weighted-average cost,%2FkWh%2C without financial support.

Jackson, T.O. (2001) *The Effects of Environmental Contamination on Real Estate: A Literature Review*, *Source: Journal of Real Estate Literature*.

Jae-ho Jeong and Kwangtae Ha (2020) 'Evaluation of Wind Flow Characteristics by RANS-Based Numerical Site Calibration (NSC) Method with Met-Tower Measurements and Its Application to a Complex Terrain', *Energies;MDPI*, pp. 2–15.

James, P. and Earthscan, J. (2004) '" Wind Power " by Paul Gipe', pp. 629–631.

Kaldellis, J.K. and Zafirakis, D. (2011) 'The wind energy (r)evolution: A short review of a long history', *Renewable Energy*, 36(7), pp. 1887–1901. doi:10.1016/j.renene.2011.01.002.

Karanikas, N. *et al.* (2021) 'Occupational health hazards and risks in the wind industry', *Energy Reports*, 7, pp. 3750–3759. doi:10.1016/J.EGYR.2021.06.066.

Khaheshi, A. *et al.* (2021) 'Against the wind: A load-bearing, yet durable, kite inspired by insect wings', *Materials & Design*, 198, p. 109354. doi:10.1016/J.MATDES.2020.109354.

Kiel, K.A. and K.T.M. (1995) 'House Price during Siting Decision Stages—The Case of an Incinerator from Rumor through Operation.', *Journal of Environmental Economics and Management,* pp. 28, 241–55.

L. Ledo, P.B. Kosasih, P.C. (2011) 'Roof mounting site analysis for micro-wind turbines', pp. 1379–1391.

Landberg, L. *et al.* (2003) 'Wind resource estimation - An overview', *Wind Energy*, 6(3), pp. 261–271. doi:10.1002/we.94.

Lang, C., Opaluch, J.J. and Sfinarolakis, G. (2014) *The Windy City: Property Value Impacts of Wind Turbines in an Urban Setting*. Available at: https://digitalcommons.uri.edu/enre_facpubs.

M.S. Nazir, A.J. Mahdi, M. Bilal, H.M. Sohail, N. Ali, H.M.N.I. (2019) 'Environmental impact and

pollution-related challenges of renewable wind energy paradigm–A review', *Sci. Total Environ.,* pp. 436–444.

Margo Huxley, A.I. (2020) 'Urban Planning', *International Encyclopedia of Human Geography* [Preprint]. Available at: https://doi.org/10.1016/B978-0-08-102295-5.10228-8.

McKenna, R. *et al.* (2022) 'High-resolution large-scale onshore wind energy assessments: A review of potential definitions, methodologies and future research needs', *Renewable Energy*, 182, pp. 659–684. doi:10.1016/j.renene.2021.10.027.

Menter, F.R. (1994) 'Two-equation eddy-viscosity turbulence models for engineering applications', *AIAA Journal*, 32(8), pp. 1598–1605. doi:10.2514/3.12149.

Mertens, S. (2002) 'Wind energy in urban areas: Concentrator effects for wind turbines close to buildings', *Refocus*, 3(2), pp. 22–24. doi:10.1016/S1471-0846(02)80023-3.

Millward-hopkins, J. (2013) 'Predicting the Wind Resource Available to Roof-Mounted Wind Turbines in Urban Areas'.

Moravec. D et al. (2018) 'Wind turbine impact on near-ground air temperature', *Renew. Energy,* pp. 627–633.

Müller, G., Jentsch, M.F. and Stoddart, E. (2009) 'Vertical axis resistance type wind turbines for use in buildings', *Renewable Energy*, 34(5), pp. 1407–1412. doi:10.1016/j.renene.2008.10.008.

Olaofe, Z.O. and Folly, K.A. (2013) 'Wind energy analysis based on turbine and developed site power curves: A case-study of Darling City', *Renewable Energy*, 53, pp. 306–318. doi:10.1016/j.renene.2012.11.003.

Park, J. and Law, K.H. (2015) 'Layout optimization for maximizing wind farm power production using sequential convex programming', *Applied Energy*, 151, pp. 320–334. doi:10.1016/j.apenergy.2015.03.139.

Pasquay, T. (2004) 'Natural ventilation in high-rise buildings with double facades, saving or waste of energy', *Energy and Buildings*, 36(4), pp. 381–389. doi:10.1016/j.enbuild.2004.01.018.

Programme, U.E. (2022) 'RENEWABLE ENERGY DATA IN PERSPECTIVE', *https://www.ren21.net/gsr-2022/*.

Razak, A.A. *et al.* (no date) *Numerical investigation of urban geometry impact on pedestrian wind environment*.

Ready, R.C. (2005) *Do Landfills Always Depress Nearby Property Values? 'Contributing to the well-being of small towns and rural communities.'*

Ren, Z. *et al.* (2021) 'Vibration behavior and excitation mechanism of ultra-stretchable triboelectric nanogenerator for wind energy harvesting', *Extreme Mechanics Letters*, 45, p. 101285. doi:10.1016/J.EML.2021.101285.

Ricardo Gasparini (2020) *How to Set up an Atmospheric Boundary Layer in CFD Simulations?* Available at: https://www.simscale.com/knowledge-base/atmospheric-boundary-layer-abl/#turbulence-dissipation-rate-epsilon.

Roache, P.J. (1998) 'Verification of codes and calculations', *AIAA Journal*, 36(5), pp. 696–702. doi:10.2514/2.457.

Rushdi, M.A. *et al.* (no date) 'Towing Test Data Set of the Kyushu University Kite System'. doi:10.4121/uuid:c3cee766-2804-4c00-924f-8a9f6c8122fc.

Saidur, R. *et al.* (2011) 'Environmental impact of wind energy', *Renewable and Sustainable Energy Reviews*, 15(5), pp. 2423–2430. doi:10.1016/j.rser.2011.02.024.

Schmidt, E. *et al.* (2020) 'In-Flight Estimation of the Aerodynamics of Tethered Wings for Airborne Wind Energy', *IEEE Transactions on Control Systems Technology*, 28(4), pp. 1309–1322. doi:10.1109/TCST.2019.2907663.

Schöll, E.M. and Nopp-Mayr, U. (2021) 'Impact of wind power plants on mammalian and avian wildlife species in shrub- and woodlands', *Biological Conservation*, 256, p. 109037. doi:10.1016/J.BIOCON.2021.109037.

Shi, T. *et al.* (2021) 'Performance of an omnidirectional piezoelectric wind energy harvester', *Wind Energy*, 24(11), pp. 1167–1179. doi:10.1002/we.2624.

Siddiqi A H, Khan S and Rehman S (2005) 'Wind speed simulation using wavelets', *American Journal of Applied Sciences*, pp. 557–564.

Simons, R. and Saginor, J. (2006) 'A Meta-Analysis of the Effect of Environmental Contamination and Positive Amenities on Residential Real Estate Values', *Journal of Real Estate Research*, 28(1), pp. 71–104. doi:10.1080/10835547.2006.12091168.

Sims, S., Dent, P. and Oskrochi, G.R. (2008) 'Modelling the impact of wind farms on house prices in the UK', *International Journal of Strategic Property Management*, 12(4), pp. 251–269. doi:10.3846/1648-715X.2008.12.251-269.

Sinden, G. (2007) 'Characteristics of the UK wind resource: Long-term patterns and relationship to electricity demand', *Energy Policy*, 35(1), pp. 112–127. doi:10.1016/j.enpol.2005.10.003.

Sommerfeld, M. *et al.* (2019) 'Improving mesoscale wind speed forecasts using lidar-based observation nudging for airborne wind energy systems', *Wind Energy Science*, 4(4), pp. 563–580. doi:10.5194/wes-4-563-2019.

SPRA (2019) 'TECHNICAL GUIDANCE WIND LOADING PROTOCOL FOR CALCULATIONS'.

Stankovic, N.S.C. and S. (2001) *Final Report of the Project WEB (Wind Energy for the Built Environment)*.

Stankovic, S., Campbell, N. (Neil S. and Harries, A. (no date) *Urban wind energy*.

Toja-Silva, F., Colmenar-Santos, A. and Castro-Gil, M. (2013) 'Urban wind energy exploitation systems: Behaviour under multidirectional flow conditions - Opportunities and challenges', *Renewable and Sustainable Energy Reviews*. Elsevier Ltd, pp. 364–378. doi:10.1016/j.rser.2013.03.052.

UN Climate Change (2022) 'What is the Kyoto Protocol?', *https://unfccc.int/kyoto_protocol#:~:text=In%20short%2C%20the%20Kyoto%20Protocol,accordance%20with%20agreed%20individual%20targets.*

Venditti, B. (2022) *This chart shows the impact rising urbanization will have on the world*. Available at: https://www.weforum.org/agenda/2022/04/global-urbanization-material-consumption/ (Accessed: 24 January 2022).

Vyn, R.J. and Mccullough, R.M. (2014) 'The Effects of wind turbines on property values in Ontario:

Does public perception match empirical evidence?', *Canadian Journal of Agricultural Economics*, 62(3), pp. 365–392. doi:10.1111/cjag.12030.

WINEUR, P. (2005) *WINEUR, Wind energy integration in the urban environment.*

Wolsink, M. (2007) 'Wind power implementation: The nature of public attitudes: Equity and fairness instead of "backyard motives"', *Renewable and Sustainable Energy Reviews*, 11(6), pp. 1188–1207. doi:10.1016/J.RSER.2005.10.005.

Yang, A.S. *et al.* (2016) 'Estimation of wind power generation in dense urban area', *Applied Energy*, 171, pp. 213–230. doi:10.1016/j.apenergy.2016.03.007.

Appendices

Appendix A. Wind Data Cleaning with Python

The Wind data obtained from 2010 to 2021, for the Centre for Environmental Data Analysis (CEDA) data without surrounding obstacles, represent the wind conditions in United Kingdom; while the weather data from Jan. 2021 to Dec. 2021, for the Hazlerigg weather data, Lancaster University campus was cleaned using the python language.

```
# New Section

import warnings

warnings.filterwarnings('ignore')

import pandas as pd

import numpy as np

df = pd.read_csv("/content/RNG_V2.csv")

df.head()

# headers = ["OB_END_TIME", "ID_TYPE", "ID", "OB_HOUR_COUNT", "MET_DOMAIN_NAME", "VERSION_NUM", "SRC_ID", "REC_ST_IND", "MEAN_WIND_DIR",

#             "MEAN_WIND_SPEED", "MAX_GUST_DIR", "MAX_GUST_SPEED", "MAX_GUST_CTIME", "MEAN_WIND_DIR_Q", "MEAN_WIND_SPEED_Q", "MAX_GUST_DIR_Q",

#                         "MAX_GUST_SPEED_Q", "MAX_GUST_CTIME_Q", "METO_STMP_TIME", "MIDAS_STMP_ETIME", "MEAN_WIND_DIR_J", "MEAN_WIND_SPEED_J", "MAX_GUST_DIR_J",

#       "MAX_GUST_SPEED_J"]

df.columns

df.head()


df.describe()


# df['OB_END_TIME'] = pd.to_datetime(df['OB_END_TIME']).dt.strftime("%Y-%m-%d")

# #df['OB_END_TIME'] = pd.to_datetime(df['OB_END_TIME'], format = '%Y-%m-%d') #for daily aggregation

# df['OB_END_TIME'] = pd.to_datetime(df['OB_END_TIME'], format = '%Y-%m') #for monthly aggregation

# df['OB_END_TIME'] = pd.to_datetime(df['OB_END_TIME']).dt.strftime("%Y-%m")


col_interest = ['Node Number', ' X [ m ]', ' Y [ m ]', ' Z [ m ]',
```

```
    ' Force [ N ]', ' Mass Flow [ kg s^-1 ]', ' Pressure [ Pa ]',
    ' Specific Dissipation Rate [ s^-1 ]',
    ' Turbulence Kinetic Energy [ m^2 s^-2 ]', ' Velocity [ m s^-1 ]',
    ]

df_interest = df[col_interest]

df_interest.head()

#df_interest[' Wall Yplus'] = df_interest[' Wall Yplus'].str.replace(r'\D', '').replace('', np.nan).astype(float)

df_interest.isna().sum()

df_interest.mean()

df_final = df_interest.sample(n=15).sort_values(by='Node Number')
df_final

# df_interest.replace(" ", np.nan, inplace=True) #clean data

# df_interest['MEAN_WIND_DIR'] = df_interest['MEAN_WIND_DIR'].astype("float")
# df_interest['MEAN_WIND_SPEED'] = df_interest['MEAN_WIND_SPEED'].astype("float")
# df_interest['MAX_GUST_DIR'] = df_interest['MAX_GUST_DIR'].astype("float")
# df_interest['MAX_GUST_SPEED'] = df_interest['MAX_GUST_SPEED'].astype("float")

# df_final = df_interest.groupby("OB_END_TIME", as_index=False).mean()

df_final
```

```
df_final.to_csv("data.csv", index=False)
```

Appendix B. CFD results analysed with python programming

The computational fluid dynamics results are analysed for clarification purposes using the python programming.

```
import warnings

warnings.filterwarnings('ignore')


import pandas as pd

import numpy as np


df = pd.read_csv("/content/exportS.csv")


df.head()


# headers = ["OB_END_TIME", "ID_TYPE", "ID", "OB_HOUR_COUNT", "MET_DOMAIN_NAME", "VERSION_NUM", "SRC_ID", "REC_ST_IND", "MEAN_WIND_DIR",

#               "MEAN_WIND_SPEED", "MAX_GUST_DIR", "MAX_GUST_SPEED", "MAX_GUST_CTIME", "MEAN_WIND_DIR_Q", "MEAN_WIND_SPEED_Q", "MAX_GUST_DIR_Q",

#                                "MAX_GUST_SPEED_Q", "MAX_GUST_CTIME_Q", "METO_STMP_TIME", "MIDAS_STMP_ETIME", "MEAN_WIND_DIR_J", "MEAN_WIND_SPEED_J", "MAX_GUST_DIR_J",

#         "MAX_GUST_SPEED_J"]


df.columns


df.head()


df.describe()


# df['OB_END_TIME'] = pd.to_datetime(df['OB_END_TIME']).dt.strftime("%Y-%m-%d")

# #df['OB_END_TIME'] = pd.to_datetime(df['OB_END_TIME'], format = '%Y-%m-%d') #for daily aggregation
```

```
# df['OB_END_TIME'] = pd.to_datetime(df['OB_END_TIME'], format = '%Y-%m') #for monthly aggregation
# df['OB_END_TIME'] = pd.to_datetime(df['OB_END_TIME']).dt.strftime("%Y-%m")

col_interest = ['Node Number', ' X [ m ]', ' Y [ m ]', ' Z [ m ]',
    ' Specific Dissipation Rate [ s^-1 ]',
    ' Turbulence Kinetic Energy [ m^2 s^-2 ]', ' Velocity [ m s^-1 ]',
    ]

df_interest = df[col_interest]

df_interest.head()

#df_interest[' Wall Yplus'] = df_interest[' Wall Yplus'].str.replace(r'\D', '').replace('', np.nan).astype(float)

df_interest.isna().sum()

df_interest.mean()

df_final = df_interest.sample(n=15).sort_values(by='Node Number')
df_final

# df_interest.replace(" ", np.nan, inplace=True) #clean data

# df_interest['MEAN_WIND_DIR'] = df_interest['MEAN_WIND_DIR'].astype("float")
# df_interest['MEAN_WIND_SPEED'] = df_interest['MEAN_WIND_SPEED'].astype("float")
# df_interest['MAX_GUST_DIR'] = df_interest['MAX_GUST_DIR'].astype("float")
# df_interest['MAX_GUST_SPEED'] = df_interest['MAX_GUST_SPEED'].astype("float")
```

```
# df_final = df_interest.groupby("OB_END_TIME", as_index=False).mean()


df_final

df_final.to_csv("data.csv", index=False)
```

Appendix C. Scatter graphical method with Matplotlib to capture the turbulence model and wind velocity pattern adequately

```
import matplotlib.pyplot as plt


# line 1 points

x1 = [4.5, 10, 30, 60, 120]

y1 = [1.39724, 1.489668, 1.060977, 2.09641, 2.096409]

# plotting the line 1 points

plt.scatter(x1, y1, marker = "o", label = "SST")


# line 2 points

x2 = [4.5, 10, 30, 60, 120]

y2 = [1.554861, 1.87, 1.701511, 7.57e+3, 2.27e+4]

# plotting the line 2 points

plt.scatter(x2, y2, marker = "x", label = "RNG")


# line 3 points

#x3 = [4.5,30,4.5,120,10,60,10]

#y3 =
[122.3385381,250.4526564,144.7151369,96.32967179,177.6338599,72.47432554,146.8981901]

# plotting the line 2 points

#plt.plot(x3, y3, label = "line 3")


# naming the x axis

plt.xlabel('Height[m]')

# naming the y axis
```

```
plt.ylabel('TKE[m^2 s^-2]')
# giving a title to my graph
plt.title('TKE vs Height')

# show a legend on the plot
plt.legend()

# function to show the plot
plt.show()

import matplotlib.pyplot as plt

# line 1 points
x1 = [4.5, 10, 30, 60, 120]
y1 = [5.845465, 6.203042, 7.422323, 2.45573, 5.171425]
# plotting the line 1 points
plt.scatter(x1, y1, marker = "o", label = "SST")

# line 2 points
x2 = [4.5, 10, 30, 60, 120]
y2 = [7.323176, 8.474327, 5.514901, 4.57, 1.26]
# plotting the line 2 points
plt.scatter(x2, y2, marker = "x", label = "RNG")

# line 3 points
#x3 = [4.5,30,4.5,120,10,60,10]
#y3 =
[122.3385381,250.4526564,144.7151369,96.32967179,177.6338599,72.47432554,146.8981901]
# plotting the line 2 points
#plt.plot(x3, y3, label = "line 3")
```

```
# naming the x axis
plt.xlabel('Height[m]')
# naming the y axis
plt.ylabel('Wind Velocity[m s^-1]')
# giving a title to my graph
plt.title('Wind Velocity vs Height')

# show a legend on the plot
plt.legend()

# function to show the plot
plt.show()

import matplotlib.pyplot as plt

# Gabbled shape
x1 = [4.5, 30, 60, 120]
y1 = [1.450165, 1.81199, 2.071199, 2.453571]
# plotting the line 1 points
plt.scatter(x1, y1, marker = "o", label = "SST")

# line 2 points
x2 = [4.5, 30, 60, 120]
y2 = [1.499159, 1.53556, 1.64159, 2.108]
# plotting the line 2 points
plt.scatter(x2, y2, marker = "x", label = "RNG")

# line 3 points
```

```
#x3 = [4.5,30,4.5,120,10,60,10]
#y3 = [122.3385381,250.4526564,144.7151369,96.32967179,177.6338599,72.47432554,146.8981901]
# plotting the line 2 points
#plt.plot(x3, y3, label = "line 3")

# naming the x axis
plt.xlabel('Height[m]')
# naming the y axis
plt.ylabel('TKE[m^2 s^-2]')
# giving a title to my graph
plt.title('TKE vs Height')

# show a legend on the plot
plt.legend()

# function to show the plot
plt.show()

import matplotlib.pyplot as plt

# Gabbled shape
x1 = [4.5, 30, 60, 120]
y1 = [6.182099, 5.24636, 5.478936, 5.397815]
# plotting the line 1 points
plt.scatter(x1, y1, marker = "o", label = "SST")

# line 2 points
x2 = [4.5, 30, 60, 120]
y2 = [6.053203, 5.86554, 5.85303, 5.4006]
```

```
# plotting the line 2 points
plt.scatter(x2, y2, marker = "x", label = "RNG"
# line 3 points
#x3 = [4.5,30,4.5,120,10,60,10]
#y3 = [122.3385381,250.4526564,144.7151369,96.32967179,177.6338599,72.47432554,146.8981901]
# plotting the line 2 points
#plt.plot(x3, y3, label = "line 3")

# naming the x axis
plt.xlabel('Height[m]')
# naming the y axis
plt.ylabel('Wind Velocity[m s^-1]')
# giving a title to my graph
plt.title('Wind Velocity vs Height')

# show a legend on the plot
plt.legend()

# function to show the plot
plt.show()
```

Appendix D. Some Post-processing output on visuals

The velocity streamline contours of the plane views around the Bowland tower depicted for SST k—∈ turbulence model effect and Renormalization Group (RNG) k −ε turbulence model effect, which shows how impactful is the wind turbulence model not for just the objective building, Bowland tower but also at height, roof, size, and arrangement variation which are depicted at the pressure contour and velocity contour.

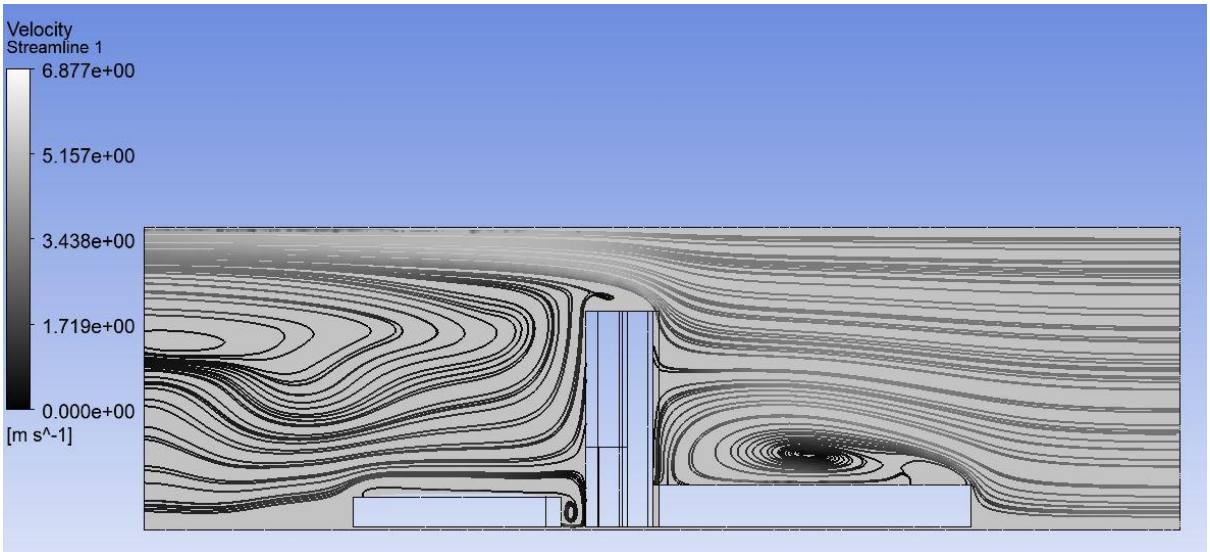

Figure 0-1: Bowland tower depicted for SST k—∈ turbulence model effect

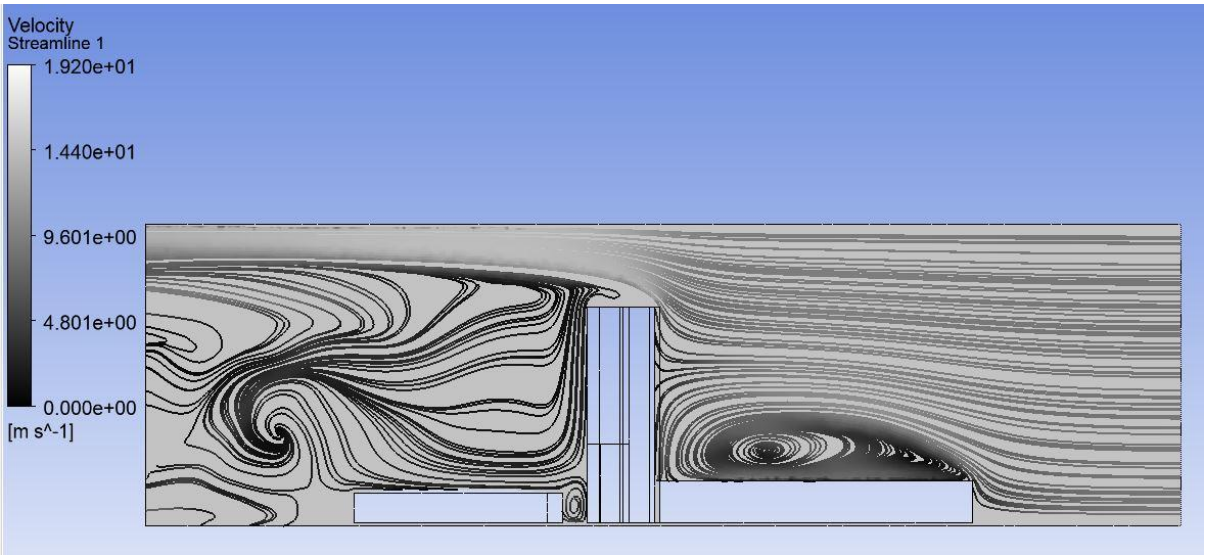

Figure 0-2: Bowland tower depicted for Renormalization Group (RNG) k −ε turbulence model effect.

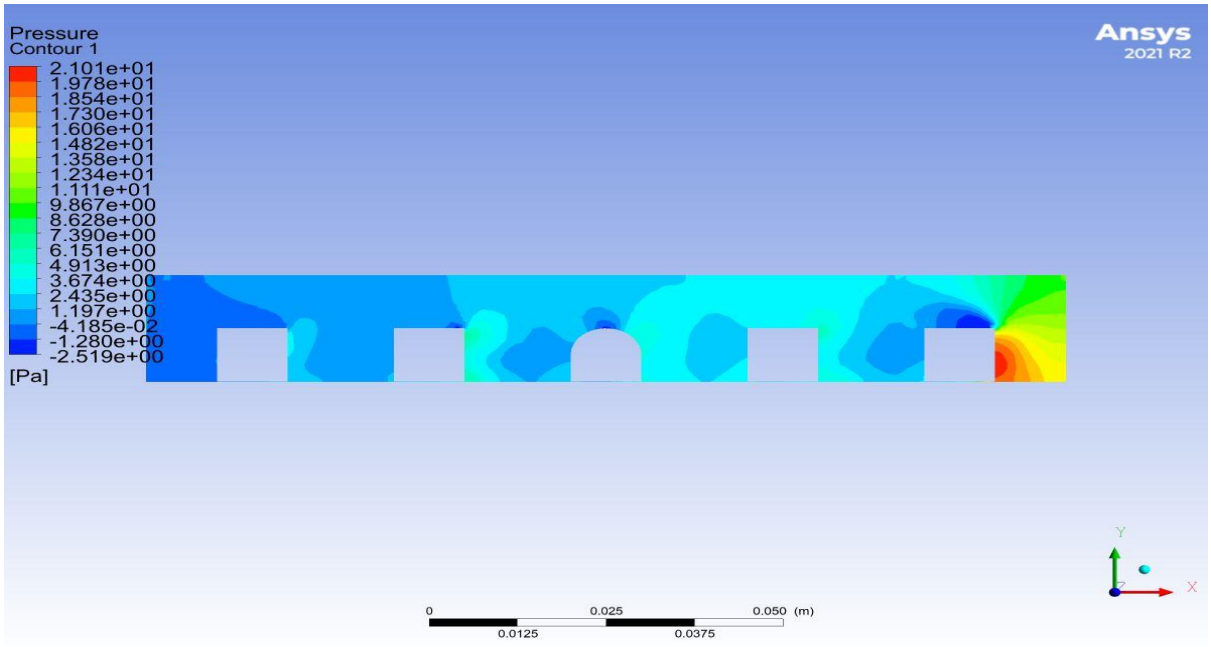

Figure 0-3: Pressure contour of a 6m gabled roof building.

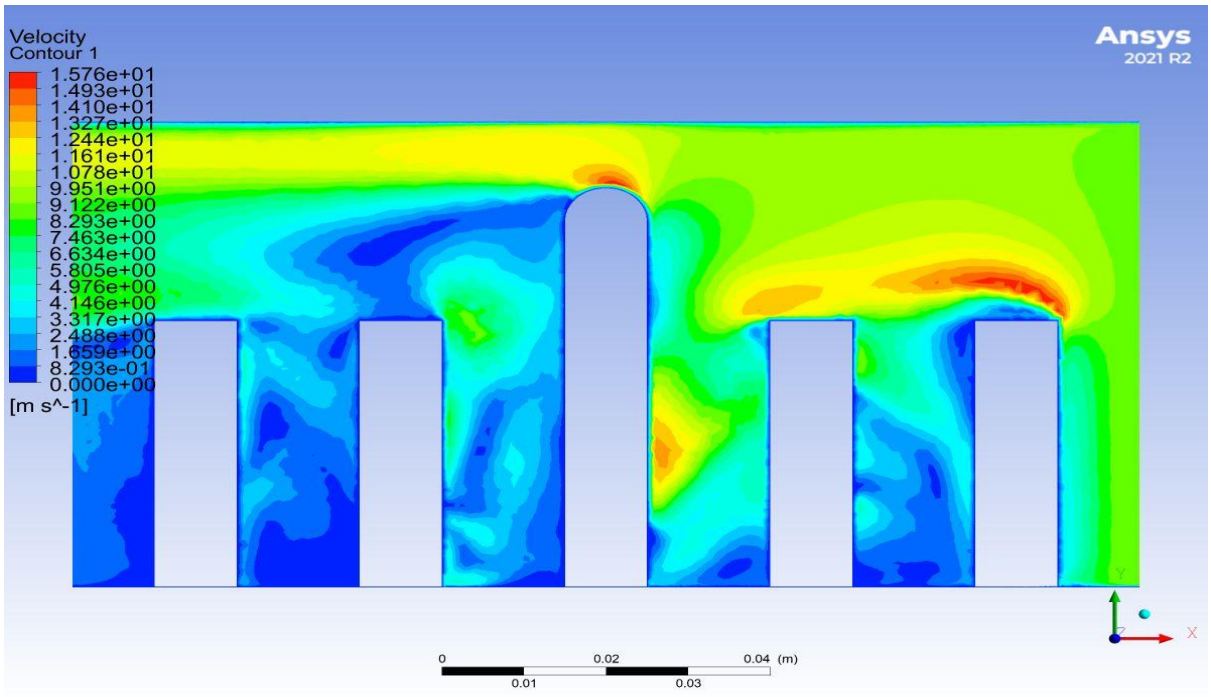

Figure 0-4: Velocity contour of a 60m gabled roof building.

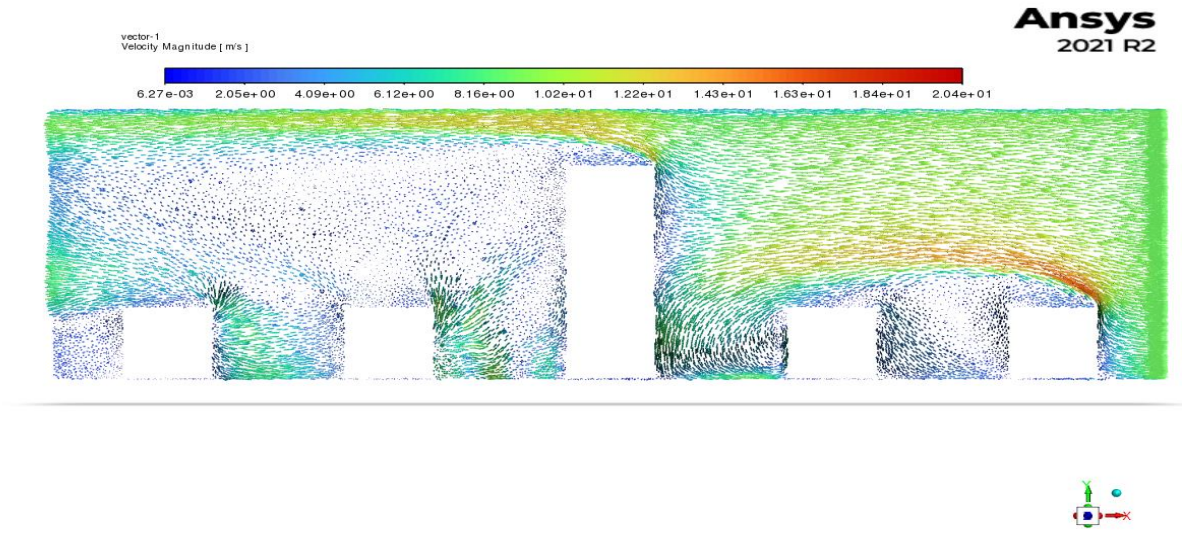

Figure 0-5: Velocity magnitude of flat roof at 60m building around 10m buildings.

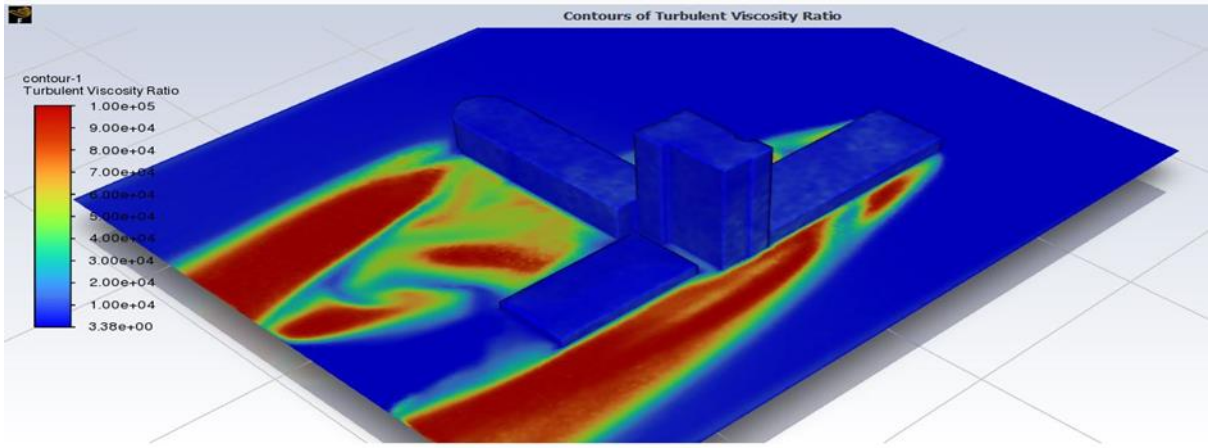

Figure 0-6: Turbulent viscosity ratio contour around the Bowland tower building

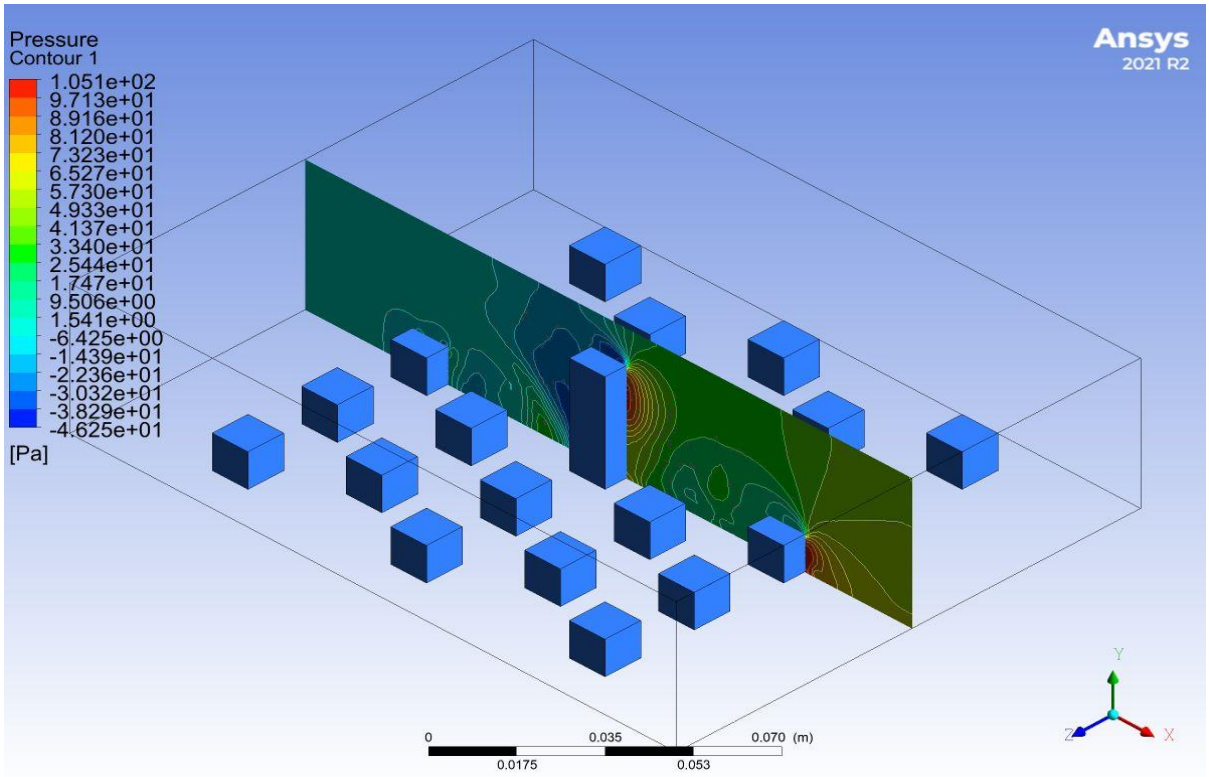

Figure 0-7 Wind Effects Generated by Buildings

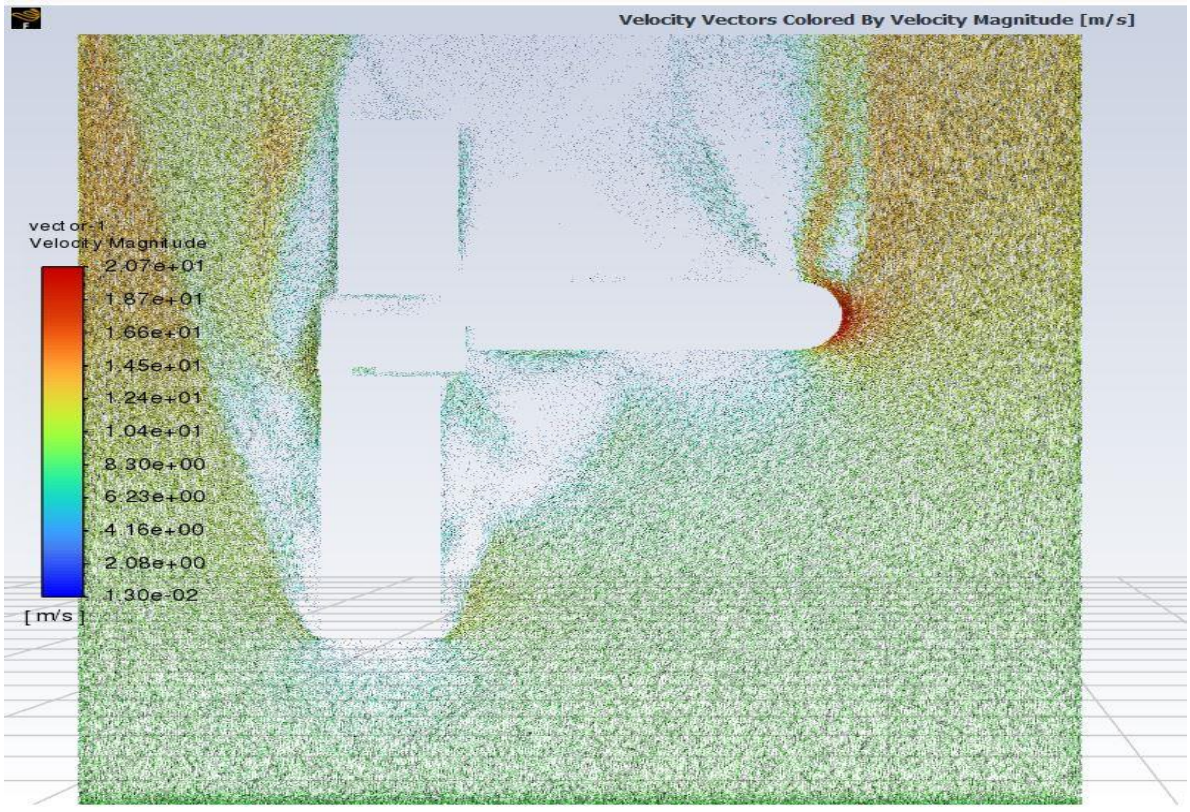

Figure 0-8 Recirculation zone on the Bowland tower

Appendix E. Some bullet points for the Rule of thumb.

These are some identified the rule of thumb to find the locations with the biggest power potential; detailed information on the thesis:

a. Height from ground level: I reported the recirculation zones on page 50 of the thesis; from these zones we can tell the following:
    i. Wind velocity increases with height from ground level.
    ii. Buildings have a huge impact on the wind flows over the buildings e.g., the windward topside east wing of Bowland tower is full of high speeds as illustrated in Fig. 6-1a and Fig. 6-1b where wind power is highly enhanced and building integrated wind turbines like the O-wind could be installed.
b. Lateral/vertical distance from the centre of the façade
    i. Using 6-2b as a case study and the velocity vectors around the centre of the façade for the slaidburn house, the thickness of the velocity magnitude 4.16m/s is about 10 m and the thickness of that below 1.45e+01 m/s is about 16 m
    ii. Therefore, the heights of 10 m or higher are suitable for small wind turbine installation, while those of 16 m or higher would be applicable for moderate wind turbine installation.
    iii. In a nutshell, for small or moderate wind turbine installation under the dominant wind direction, about a quarter of the windward roof has high potential of wind source
    iv. Low installation height is acceptable and feasible. However, the installation height of the wind turbine should avoid the low-speed areas.
c. Amplification Factor: As reported on page 48 and 61;
    i. While the wind energy over the roof normally falls somewhat slowly with larger corner separation in diverging inlet mode, it generally increases considerably with larger corner separation in converging inlet mode.
    ii. As the assessment altitude increases, the general amplification factor increases and then decreases. This means there should have an optimum altitude for wind energy development over the roof. More altitudes can be evaluated for some specific cases if necessary.
    iii. With respect to Figure 3.3 and Table below, 45◦ is the best inlet direction in most cases. Some cases show that 30◦/60◦ can also be a good choice, but hardly show any great advantage over 45◦

Urban Aerodynamics: Impact of urban configuration and height on wind pattern.										
Configurations	**Roof Shapes**	**Height (m)**	**Turbulence Model**	**Specific Dissipation Rate [s^-1]**	**Turbulence Eddy Dissipation [m^2 s^-3]**	**Turbulence Kinetic Energy [m^2 s^-2]**	**Velocity [m s^-1]**	**Density**	**Wind Power, PA**	**Anplification Factor**
Urban Canyon	Flat	4.5	SST k-ω	20614.3158	0	1.39724	5.845465	1.225	122.33854	0.281424971
		4.5	RNG k-epsilon	0	3531.230555	1.554861	7.323176	1.225	240.54953	0.553355018
		10	SST k-ω	141377.456		1.489668	6.203042	1.225	146.19087	0.336294374
		10	RNG k-epsilon	0	2.16E+06	1.87E+02	8.47E+00	1.225	372.75352	0.857474259
		30	SST k-ω	51018.7582		1.060977	7.422323	1.225	250.45266	0.576135964
		30	RNG k-epsilon	0	3299.257486	1.701511	5.514901	1.225	102.7352	0.236329861
		60	SST k-ω	25632.4915		2.09641	2.45573	1.225	9.0708491	0.020866388
		60	RNG k-epsilon			7.57E+03	4.57E+00	1.225	5.85E+01	0.134478866
		120	SST k-ω	30632.4915		2.096409	5.171425	1.225	84.71041	0.194866026
		120	RNG k-epsilon	0	3.54E+09	2.27E+04	1.26E+00	1.225	1.2252303	0.002818494
	Gabled	4.5	SST k-ω	100644.27		1.450165	6.182099	1.225	144.71514	0.332899623
		4.5	RNG k-epsilon	0	3383.815377	1.499159	6.053203	1.225	135.85068	0.31250801
		30	SST k-ω	48162.5506		1.81199	5.24636	1.225	88.44644	0.20346031
		30	RNG k-epsilon	0	3783.815377	1.53556	5.86554	1.225	123.60331	0.284334422
		60	SST k-ω	48162.5506		2.071199	5.478936	1.225	100.73834	0.231736327
		60	RNG k-epsilon	0	3663.815377	1.64159	5.85303	1.225	122.81413	0.282519017
		120	SST k-ω	31251.6106	0.00E+00	2.45E+00	5.40E+00	1.225	96.329672	0.221594728
		120	RNG k-epsilon	0	2.77E+06	2.11E+00	5.40E+00	1.225	96.478852	0.2219379
	Barrel Vaulted	10	SST k-ω	124279.476	0	1.376366	6.619216	1.225	177.63386	0.408625154
		10	RNG k-epsilon	99711.1174	0	0.144877	2.235889	1.225	6.846314	0.015749115
		60	SST k-ω	208629.386	0	2.023183	4.909373	1.225	72.474326	0.166718397
		60	RNG k-epsilon	0	2.44E+08	4.37E+03	3.75E+00	1.225	32.251612	0.074190921
	Pyramidal	10	SST k-ω	113248.766		1.510638	6.21303	1.225	146.89819	0.337921472
		10	RNG k-epsilon	109818.834	0	0.15119	2.116249	1.225	5.8050557	0.013353827
Staggared Urban	Flat	4.5	SST k-ω	67132.6717	0	1.510369	7.598137	1.225	268.67512	0.618054534
		4.5	RNG k-epsilon	4005.4788	0	1.632911	7.739565	1.225	283.95907	0.653213411
		30	SST k-ω	36867.812		2.019413	6.688568	1.225	183.27597	0.42160415
		30	Realizable k-epsilon	0	1782.367143	1.514787	6.612561	1.225	177.09862	0.40739389
	Gabled	10	SST k-ω	41580.0428	0	1.272071	7.061329	1.225	215.65793	0.496094916
		10	RNG k-epsilon	0	1650.224185	1.153228	7.03369	1.225	213.13549	0.490292339
		60	SST k-ω	27191.7149		2.010068	6.053872	1.225	135.89573	0.312611636
		60	Realizable k-epsilon	0	133806.8859	126.860673	9.048222	1.225	453.72827	1.043746854

Figure 0-9 Urban Aerodynamics tables with the amplification factor